Institute for Clinical and Experimental Surgery

Saarland University, Homburg/Saar

(Director: Prof. Dr. med. M. D. Menger)

Adipose tissue-derived microvascular fragments: A novel prevascularization strategy in skin tissue engineering

Dissertation with the aim of achieving the doctoral degree

Doktor der Medizin und der Naturwissenschaften (MD-PhD)

at the Medical Faculty of Saarland University

2019

by Dr. med. Florian Samuel Früh

born on May 31 1983 in Winterthur, Switzerland

MD PhD Promotion

Adipose tissue-derived microvascular fragments: A novel prevascularization strategy in skin tissue engineering

Tag der mündlichen Promotion

26.06.2020

Dekan

Prof. Dr. med. Michael D. Menger

Berichterstatter

1. Prof. Dr. med. Matthias W. Laschke, PhD
2. Prof. Dr. Gerald Thiel
3. Univ.-Prof. Dr. med. Hans-Günther Machens

Table of Contents

1. Summary

Full-thickness skin defects after burns, infection, trauma or tumor resection are a frequent challenge in reconstructive surgery. Most defects can be treated by means of autologous split-thickness skin grafts (STSG), which are the gold standard for the reconstruction of extensive skin loss. However, wounds above bradytrophic structures, such as tendons and bones, commonly do not exhibit a sufficient vascularization capacity to be covered with STSG alone. Moreover, STSG coverage is prone to restrictive scarring with subsequent functional and esthetic restrictions. Consequently, off-the-shelf dermal skin substitutes have been introduced for the restoration of the dermal layer. For instance, the clinically established Integra is characterized by an engineered collagen-glycosaminoglycan matrix, which provides guidance for infiltrating host cells with subsequent formation of a microvascular network. Stable revascularization of the implant requires ~ 21 days, and only after this period, STSG coverage can be performed. Importantly, this delayed vascularization kinetics is associated with high costs, two surgeries and an increased risk of infection with implant loosening. One approach to overcome this problem is prevascularization, i.e. the induction of a functional microvascular network within the matrix before implantation into a host organism. In the present thesis, adipose tissue-derived microvascular fragments (ad-MVF) are introduced as a novel prevascularization strategy for dermal skin substitutes. In contrast to adipose tissue-derived single cell isolates, ad-MVF consist of intact arteriolar, capillary and venular fragments and only have to reconnect to each other and the host microvasculature for the formation of a functional microvascular network. This work is based on three original articles investigating the isolation process of ad-MVF, their *in vitro* characterization and the *in vivo* application of ad-MVF-prevascularized Integra in two murine wound models.

In the first study of this thesis, a standardized protocol for the enzymatic isolation of ad-MVF from epididymal fat pads of mice is reported. The fat pads of transgenic green fluorescence protein (GFP)[+] C57BL/6 mice were harvested for the isolation of ad-MVF, which were subsequently characterized by means of microscopy, histology, immunohistochemistry and flow cytometry. The total time required for the isolation process was ~ 120 min. It was possible to isolate ~ 40,000 ad-MVF per mL adipose tissue. Individual fragments exhibited a mean length of 42 ± 1 µm. Moreover, they were characterized by a typical microvessel morphology with hierarchical vessel segments as indicated by immunohistochemical analyses. Flow cytometry revealed that ad-MVF contain 26 ± 2 % CD31^{+} endothelial cells, 17 ± 2 % α-smooth muscle actin (SMA)[+] perivascular cells and 9 ± 1 % cells positive for the mesenchymal stem cell marker CD117. Pilot experiments with ad-MVF-seeding onto Integra

indicated that the fragments were mainly localized on the implant's surface and only a few capillary vessel segments could be detected within its pores immediately after the seeding process.

In the second study of this thesis, Integra seeded with GFP$^+$ ad-MVF was investigated after implantation into full-thickness skin defects in a modified dorsal skinfold chamber model of wild-type C57BL/6 mice. Non-seeded implants served as controls. The *in vivo* experiments consisted of a 14 days-observation period with repetitive intravital fluorescence microscopy and stereomicroscopy for the assessment of the implants' vascularization and epithelialization. After 14 days, histological and immunohistochemical analyses of vascularization, lymphangiogenesis, epithelialization and collagen content were performed. The GFP$^+$/GFP$^-$ crossover approach allowed the identification of ad-MVF-derived blood and lymphatic vessels in the implants as well as in the surrounding skin. The ad-MVF rapidly reassembled into microvascular networks within the implants and inosculated to the host microvasculature between day 3 and 6 after transplantation. Accordingly, the vascularization of the implants was markedly accelerated, as indicated by a significantly higher microvessel density when compared to controls. Moreover, dense lymphatic networks originating from the GFP$^+$ ad-MVF developed within the implants. The GFP$^+$ blood and lymphatic vessels even invaded the surrounding skin. Finally, enhanced vascularization and lymphangiogenesis resulted in an increased implant integration and epithelialization.

In the third study of this thesis, ad-MVF-based prevascularization of Integra was analyzed in a novel animal model. In a first set of experiments, Integra seeded with GFP$^+$ ad-MVF was implanted into full-thickness skin defects on the skull of CD1 nu/nu mice for 21 days. Non-seeded implants served as controls. The implants were assessed *in situ* by means of photo-acoustic imaging. At the end of the *in vivo* experiments, vascularization, lymphangiogenesis as well as incorporation of the implants were analyzed using trans-illumination stereomicroscopy, histology and immunohistochemistry. In a second set of experiments, early autologous STSG coverage was performed 10 days after implantation of prevascularized and non-seeded Integra. The survival rate of STSG was assessed by planimetry and 5 days after STSG transplantation, the implants and the STSG were excised for histological and immunohistochemical analyses. After 21 days, the density of microvascular and lymphatic networks was markedly higher in prevascularized matrices when compared to controls. This was associated with an improved integration of the implants. Moreover, prevascularization with ad-MVF allowed successful STSG coverage already at day 10. In contrast, skin grafting of non-seeded controls resulted in STSG necrosis.

In summary, ad-MVF-seeding represents a novel and promising prevascularization strategy for the dermal skin substitute Integra. Murine ad-MVF enhance the vascularization and lymphangiogenesis of Integra and also result in a faster integration and epithelialization of the implant. Key advantages of ad-MVF prevascularization are the short isolation time and the intact microvascular characteristics, which are prerequisites for an intraoperative one-staged application. However, from a translational perspective, it has to be proven that ad-MVF harvested from subcutaneous adipose tissue of humans exhibit an equally high vascularization capacity compared with murine ad-MVF. If this holds true, ad-MVF may soon be taken from bench to bedside.

2. Zusammenfassung

Ausgedehnte Hautdefekte sind ein häufiges Problem in der rekonstruktiven Chirurgie. Der Goldstandard für die Behandlung der meisten Hautdefekte ist die autologe Spalthauttransplantation. Gewisse Defekte sind aber einer Spalthautdeckung nicht zugänglich. So sind die dünnen Hauttransplantate nicht geeignet für die Deckung von Wunden mit schlecht vaskularisiertem Wundgrund, zum Beispiel bei freiliegenden Sehnen oder Knochen. Ein weiteres relevantes Problem ist die Ausbildung von funktionellen und kosmetisch invalidisierenden Narbenkontrakturen. Biosynthetische dermale Ersatzmatrizen, wie das klinisch oft verwendete Integra, stellen eine Möglichkeit dar, diese Probleme zu umgehen. Integra besteht aus einer Kollagen-Glycosaminoglycan Matrix, in welche ein mikrovaskuläres Gefäßnetzwerk aus dem umgebenden Empfängergewebe vor einer Spalthautdeckung einsprossen muss. Dieser Prozess benötigt ungefähr 3 Wochen. Danach kann die Matrix mit Spalthaut gedeckt werden. Diese verzögerte Vaskularisierung resultiert in zwei operativen Eingriffen, in einem erhöhten Infektionsrisiko mit möglichem Implantatverlust sowie in hohen Kosten. Ein möglicher Lösungsansatz für dieses Problem basiert auf dem Prinzip der Prävaskularisierung. Der Begriff stammt aus dem Tissue Engineering und bedeutet die Induktion eines funktionellen Gefäßnetzwerkes in einem Gewebekonstrukt vor Implantation in einen Empfängerorganismus. In der vorliegenden Arbeit werden aus Fettgewebe isolierte mikrovaskuläre Fragmente (ad-MVF) als vielversprechende Prävaskularisierungs-Strategie für dermale Matrizen eingeführt. ad-MVF bestehen aus intakten arteriolären, kapillären und venulären Gefäßfragmenten, welche sich nach Implantation in einen Empfängerorganismus lediglich wieder zu einem mikrovaskulären Netzwerk verbinden müssen. Dies unterscheidet sie wesentlich von Einzelzell-basierten Isolaten aus Fettgewebe, wie zum Beispiel der stromal vascular fraction, die ebenfalls häufig für die Prävaskularisierung von Implantaten verwendet wird. Diese Arbeit beruht auf drei Originalarbeiten, welche die Isolation von ad-MVF, deren *in vitro* Charakterisierung sowie die *in vivo* Anwendung von mit ad-MVF prävaskularisiertem Integra in zwei Mausmodellen beschreiben.

In der ersten Studie wird ein ein standardisiertes Protokoll für die Isolation von ad-MVF aus epididymalem Fettgewebe von Mäusen beschrieben. Hierfür wurden ad-MVF von transgenen, green fluorescent protein (GFP)⁺ C57BL/6 Mäusen enzymatisch isoliert und mittels Mikroskopie, Histologie, Immunhistochemie und Durchflusszytometrie charakterisiert. Die Gesamtzeit für die Isolation betrug ~ 120 Minuten. Es konnten ~ 40,000 ad-MVF pro ml Fettgewebe gewonnen werden. Die einzelnen Fragmente wiesen eine durchschnittliche

Länge von 42 ± 1 µm und eine typische mikrovaskuläre Morphologie auf. Durchflusszytometrische Analysen zeigten, dass ad-MVF 26 ± 2 % CD31^{+} Endothelzellen, 17 ± 2 % α-smooth muscle actin (SMA)[+] perivaskuläre Zellen und 9 ± 1 % mesenchymale Stammzellen charakterisierende CD117^{+} Zellen enthalten. In Pilotversuchen wurden ad-MVF auf Integra gesiedelt. Auf diese Weise konnte histologisch gezeigt werden, dass der überwiegende Anteil der ad-MVF auf der Oberfläche des Implantates lokalisiert war und nur wenige kapilläre ad-MVF in die Poren von Integra eindringen konnten.

In der zweiten Studie wurde prävaskularisiertes Integra in Hautdefekten in einer modifizierten Rückenhautkammer an C57BL/6 Mäusen untersucht. Hierfür wurden die Implantate mit GFP[+] ad-MVF besiedelt. So konnte nach Implantation in GFP[-] C57BL/6 Tiere zwischen GFP[-] Empfängergefäßen und GFP[+] Gefäßen, die sich aus den ad-MVF entwickelten, unterschieden werden. Die Kontrollgruppe bestand aus unbesiedelten Implantaten. Während eines 14-tägigen *in vivo* Versuches wurden die Vaskularisierung und Epithelialisierung der Implantate mittels intravitaler Fluoreszenzmikroskopie sowie stereomikroskopischer Planimetrie erfasst. Nach 14 Tagen wurden die Implantate für die histologische und immunhistochemische Analyse der Vaskularisierung, Lymphangiogenese und Epithelialisierung sowie für die Quantifizierung des Kollagengehaltes entnommen. Interessanterweise bildeten die ad-MVF in kurzer Zeit innerhalb des Integra ein funktionelles Gefäßnetzwerk aus, welches über Inoskulation nach 3 - 6 Tagen Anschluss an die Gefäße des Empfängergewebes fand. Entsprechend konnte in den prävaskularisierten Implantaten eine deutlich verbesserte Vaskularisierung mit signifikant höherer mikrovaskulärer Dichte im Vergleich zu den nicht-besiedelten Implantaten der Kontrollgruppe nachgewiesen werden. Weiterhin wiesen die ad-MVF-besiedelten Implantate auch ein deutlich dichteres Lymphgefäßnetzwerk auf. GFP[+] Blut- und Lymphgefäße waren nicht nur in den Implantaten, sondern auch im umliegenden Empfängergewebe nachweisbar. Die verbesserte Vaskularisierung und Lymphangiogenese führten letztlich zu einer verstärkten Integration und Epithelialisierung der dermalen Matrizen.

In der dritten Studie wurde ad-MVF-prävaskularisiertes Integra hinsichtlich einer vorzeitigen Spalthautdeckung in einem neuen Mausmodell untersucht. Die Hypothese dieser Studie lautete, dass durch die Prävaskularisierung eine Spalthautdeckung früher möglich ist. Hierfür wurden in einem ersten Studienabschnitt besiedeltes und unbesiedeltes Integra in einen Hautdefekt auf dem Schädel von CD1 nu/nu Mäusen über 21 Tage implantiert. Während des *in vivo* Versuches wurde die Vaskularisierung der Implantate mittels Photoakustik analysiert. Nach Entnahme der Implantate wurden Vaskularisierung, Lymphangiogenese sowie die Gewebeintegration mittels Transilluminations-Stereomikroskopie, Histologie und Immunhistochemie erfasst. In einem zweiten Studienabschnitt wurden prävaskularisiertes

und nicht-prävaskularisiertes Integra 10 Tage nach Implantation mit autologen Spalthauttransplantaten gedeckt und für 5 weitere Tage mittels stereomikroskopischer Planimetrie untersucht. So konnte die prozentuale Überlebensrate der Transplantate objektiviert werden. Die Präparate wurden anschließend histologisch und immunhistochemisch ausgewertet. Nach 21 Tagen wiesen die prävaskularisierten Implantate analog zur zweiten Studie ein signifikant dichteres Blut- und Lymphgefäßnetzwerk im Vergleich zu den nicht-besiedelten Implantaten der Kontrollgruppe auf. Dies ging mit einer verbesserten Integration in das Gewebe einher. Die vorzeitige Spalthauttransplantation war nur auf den prävaskularisierten Implantaten möglich, wohingegen die Hauttransplantate auf den unbesiedelten Implantaten der Kontrollgruppe nekrotisch wurden.
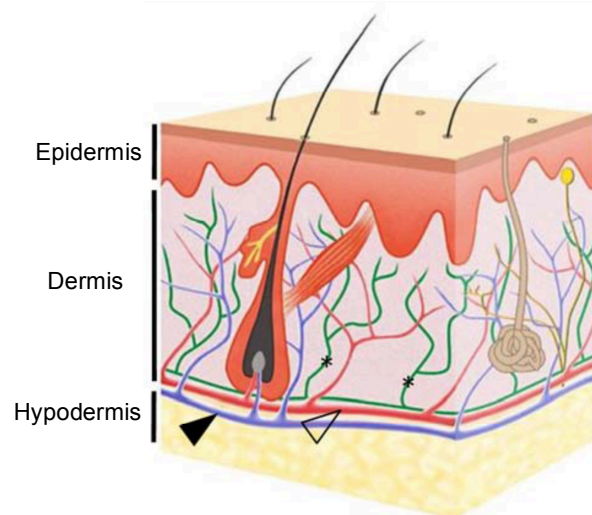
Abschließend kann festgehalten werden, dass murine ad-MVF eine vielversprechende Prävaskularisierungs-Strategie für dermale Ersatzmatrizen darstellen. Sie verbessern nicht nur die Ausbildung von Blut- und Lymphgefäßen innerhalb von Integra, sondern sind auch mit einer schnelleren Integration und Epithelialisierung der Implantate assoziiert. Von grosser Bedeutung sind die kurze Isolationszeit sowie die erhaltene mikrovaskuläre Morphologie der ad-MVF. Diese Punkte stellen eine *conditio sine qua non* für eine einzeitige intraoperative Anwendung dar. Aus der Perspektive des Klinikers müssen zukünftige Versuche zeigen, ob ad-MVF aus humanem Fettgewebe ein vergleichbar hohes Vaskularisierungspotential aufweisen. Dann wären ad-MVF-prävaskularisierte dermale Ersatzmatrizen in der Tat ein interessanter Therapieansatz für therapie-refraktäre chronische Wunden.

3. Introduction

The skin is the largest organ of the human body and provides a first line of defense against microbial pathogens and physical or chemical insults [NESTLE et al., 2009]. Moreover, it is critically involved in the regulation of body temperature and tissue fluid homeostasis [CUENI and DETMAR, 2006; ROMANOFSKY, 2014]. From a morphological point of view, the skin consists of two main structural compartments: The epidermis and the dermis (**Figure 1**). The epidermal layer is a continuously self-renewing epithelium protecting the skin from hazardous environmental threats [BARONI et al., 2012]. An intimate cooperation between epithelial cells, growth factors, chemokines and inflammatory cells is the prerequisite for the regeneration of wounded skin [TOULON et al., 2009; HAVRAN and JAMESON, 2010]. In contrast, the dermis is characterized by a papillary layer and a lower reticular layer. The extracellular matrix of these layers is built on collagen and elastin fibers and the main cellular component are fibroblasts, which continuously produce collagen and proteoglycan matrix [KAMEL et al., 2013]. Furthermore, the dermis contains a dense microvascular and lymphatic plexus nourishing and draining the avascular epidermis. In addition, sweat and sebaceous glands as well as hair follicles are part of the dermal compartment. Finally, the loose connective tissue and subcutaneous fat of the hypodermis is involved in mechanical shock protection and is active in energy metabolism and storage [BARONI et al., 2012]. Together, the dermis and hypodermis are responsible for mechanical support and protection [HUSSAIN et al., 2013]. Extensive full-thick-

Figure 1. The structure of human skin. This illustration shows the two main layers of skin: The epidermis and the lower, much thicker, dermis. The epidermal barrier is relatively thin (0.1 – 0.2 mm) and is secured to the underlying dermis by a specialized basement membrane. The dermis varies in thickness and is well vascularized with an arterial (empty arrowhead), venous (black arrowhead) and lymphatic (asterisks) network. Reproduced with permission from Frueh et al., 2018a. Copyright © 2018 Karger Publishers, Basel, Switzerland.

ness skin injury may lead to life-threatening systemic complications due to massive fluid loss, decrease of body temperature or infection. The most common etiologies for significant skin loss include burns, necrotizing infections, trauma and tumor resection [AKHTAR et al., 2006; PHAM et al., 2007; TUFARO et al., 2007; FRUEH et al., 2016]. Particularly burn injuries affecting ~ 20 % or more of the total body surface can result in a fatal systemic response,

known as burn shock [Rowan et al., 2015]. Beside these injuries, chronic wounds are a socio-economically highly relevant problem. In the United States of America, approximately 6.5 million patients suffer from chronic wounds and the burden is constantly growing due to an aging population and a rising incidence of diabetes, obesity and vasculopathies [Sen et al., 2009]. For both acute and chronic wounds, a rapid and stable reconstruction is crucial to prevent potentially fatal complications. In clinical practice, many skin defects can be successfully treated using split-thickness skin grafts (STSG).

The principle of autologous skin grafting goes back to Reverdin [1869] and has been the gold standard in the treatment of extensive skin defects in the last 150 years. STSG are easy to harvest and exhibit a low donor-site morbidity. They contain the epidermis and a variably thick part of the dermis and are revascularized within 72 hours after transplantation [Frueh et al., 2018a]. Graft revascularization is characterized by a complex combination of angiogenesis, vasculogenesis and inosculation. Briefly, the majority of a graft's microvasculature regresses and is replaced by ingrowing microvessels from the wound bed and after inosculation within 48 - 72 hours, the graft is re-oxygenated [Capla et al., 2006; Lindenblatt et al., 2010]. This process requires an intact microvascular network at the recipient site. However, chronic wounds and skin defects above bradytrophic structures, such as tendons and bones, commonly do not exhibit a sufficient vascularization capacity to be covered with STSG alone. Moreover, in case of full-thickness skin loss including the hypodermal layer, STSG coverage is prone to restrictive scarring with subsequent functional and esthetic restrictions [Shevchenko et al., 2010]. Finally, skin loss involving the majority of the body's surface precludes STSG harvesting. These limitations are the clinical background for the discipline of skin tissue engineering and led to the development of a multitude of artificial skin substitutes.

Tissue engineering is a rapidly expanding field of science. In 1987 the National Science Foundation defined it as "an interdisciplinary field that applies the principles of engineering and the life sciences towards the development of biological substitutes that restore, maintain or improve tissue function" [Langer and Vacanti, 1993]. Importantly, vascularization is the key challenge in tissue engineering and the re-establishment of a functional macro- and microvascular network is the major hurdle for clinical translation of engineered tissues or organs [Laschke et al., 2006; Novosel et al., 2011]. However, epidermal skin substitutes have been among the first for human application because they do not require an extensive internal vasculature [Gallico et al., 1984; MacNeil, 2007]. In contrast, skin substitutes that are thicker than 100-200 µm need a vascular system because every cell in a tissue needs to be close enough to capillaries to absorb oxygen and nutrients [Khademhosseini et al., 2009].

Accordingly, insufficient vascularization may result in infection, loosening and partial or complete necrosis of an implanted skin substitute [HENDRICKX et al., 2011]. Hence, the engineering of complex multi-layer skin substitutes is challenging and crucially depends on the integration of a functional microvascular network.

Several strategies have been developed to engineer a functional microvascular network within artificial skin. They can be classified into angiogenesis approaches and prevascularization approaches [LASCHKE and MENGER, 2016a; FRUEH et al., 2017a]. Vascularization strategies based on angiogenesis try to stimulate the ingrowth of blood vessels into skin substitutes. This can be achieved by modification of the structure [SCHNEIDER et al., 2009], by surface activation with plasma treatment [RING et al., 2010], by combination of different biomaterials [WANG et al., 2013; ZHAO et al., 2015], or by incorporation of angiogenic growth factors, such as vascular endothelial growth factor (VEGF) or platelet-derived growth factor (PDGF) [MARGOLIS et al., 2004; RECKHENRICH et al., 2011]. However, angiogenic approaches are clearly limited by a slow average growth rate of newly developing microvessels of only ~ 5 µm/h [UTZINGER et al., 2015], which precludes the vascularization of large skin substitutes by angiogenesis alone. To overcome this problem, the concept of prevascularization has emerged in the last decade. It aims at the generation of a preformed microvascular network inside engineered tissues prior to their implantation with subsequent connection to the recipient's microvasculature through inosculation [LASCHKE et al., 2009; LASCHKE and MENGER, 2016a]. Hence, in contrast to mainly angiogenesis-dependent vascularization, prevascularization should significantly shorten the hypoxic time period after implantation, during which skin substitutes may undergo critical ischemic damage. In skin tissue engineering, one promising prevascularization strategy is based on the cultivation of artificial skin grafts with vessel-forming cells. For instance, MARINO et al. [2014] introduced dermo-epidermal skin grafts engineered from human keratinocytes, human dermal fibroblasts and human dermal microvascular endothelial cells (HDMEC). The co-culture of these cells in fibrin hydrogels yields bi-layer skin substitutes with a functional microvascular network. Even though convincing in the preclinical setting, this approach has not yet been implemented into clinical routine because it includes *in vitro* incubation over weeks and relevant cell manipulation. In theory, the ideal prevascularization strategy for a future clinical translation should i) minimize *in vitro* steps, ii) involve as few cell manipulation as possible, iii) be minimally invasive for the patient, and iv) be suitable for a one-step operative procedure. The enrichment of skin substitutes with adipose tissue-derived microvascular fragments (ad-MVF) basically complies with these requirements. In the present thesis the suitability of ad-MVF as a novel prevascularization approach in skin tissue engineering was investigated [FRUEH et al., 2017b, 2017c and 2018b].

Historically, ad-MVF were isolated for the first time from the epididymal fat pads of rats [WAGNER et al., 1972; WAGNER and MATTHEWS, 1975]. They initially served for the isolation of capillary endothelium as well as for *in vitro* sprouting assays in angiogenesis research. Moreover, ad-MVF-seeded collagen gels were investigated for *in vivo* modeling of sprouting angiogenesis, vascularization and vascular remodeling [SHEPHERD et al., 2004]. ad-MVF represent a randomized mixture of arteriolar, capillary and venular vessel segments with all their morphological characteristics [HOYING et al., 1996; LASCHKE and MENGER, 2015]. Importantly, these segments still contain a lumen, an intact endothelium and vessel-stabilizing perivascular cells. Therefore, they only have to interconnect with each other and with the surrounding microvasculature to form a functional, blood-perfused microvascular network [LASCHKE et al., 2012]. This complex process is characterized by three morphologically defined vascular phenotypes: i) The formation of angiogenic sprouts, which form immature vessel segments for subsequent inosculation to the surrounding microvasculature, ii) vascular remodeling of the new microvasculature and finally, iii) vascular maturation resulting in a hierarchical microvascular network [NUNES et al., 2010]. The remarkable vascularization capacity of ad-MVF can be explained by experimental findings: Under culture conditions, they release growth factors, such as VEGF or basic fibroblast growth factor (bFGF), indicating a pro-angiogenic paracrine activity [LASCHKE et al., 2012; PILIA et al., 2014]. Moreover, ad-MVF contain Sca-1$^+$/VEGF receptor-2$^+$ endothelial progenitor cells as well as mesenchymal stem cells, which further increase their potency as vascular building units [LASCHKE et al., 2012; MCDANIEL et al., 2014].

The suitability of ad-MVF as vascularization units in regenerative medicine was first investigated by NAKANO et al. [1998], who found an improved survival of random pattern skin flaps on the back of rats after injecting the distal flap area with ad-MVF. In a subsequent study, they reported ad-MVF inosculation and survival after injection into superficial rat myocardium [NAKANO et al., 1999]. Further evidence that ad-MVF exhibit a high regenerative potential was reported by SHEPHERD et al. [2007], who analyzed the role of ad-MVF in a murine model of acute myocardial infarction. Of interest, epicardial transplantation of ad-MVF-prevascularized collagen patches was associated with a smaller infarct size and an improved left ventricular function when compared to control animals, which were treated with non-prevascularized patches. In line with these findings, ad-MVF-derived microvascular networks also promoted the survival of transplanted pancreatic islets [HISCOX et al., 2008] and skeletal muscle regeneration [PILIA et al., 2014] in rodents. The idea of using ad-MVF as natural vascularization units for tissue engineering scaffolds was introduced by LASCHKE et al. who established a dynamic seeding procedure for porous polyurethane scaffolds [LASCHKE et al. 2012; LASCHKE et al., 2014]. For that purpose, they isolated GFP$^+$ ad-MVF

from transgenic donor mice. After the seeding process, the scaffolds were implanted into dorsal skinfold chambers of wild-type mice for subsequent analyses by means of intravital fluorescence microscopy, histology and immunohistochemistry. The experimental GFP$^+$/GFP$^-$ crossover approach revealed that > 90 % of the microvessels within the scaffolds were GFP$^+$, hence originated from the transplanted ad-MVF. In summary, the scaffolds vascularized primarily through external inosculation, i.e. the interconnection of outgrowing GFP$^+$ microvessels with the host microvasculature [LASCHKE et al., 2012]. Based on the findings of these studies, it was hypothesized in the present thesis that ad-MVF may also be promising vascularization units for skin tissue engineering.

For the experiments of the present work the dermal skin substitute Integra (Integra Life Sciences, Plainsboro, NJ, USA) was chosen as scaffold for ad-MVF seeding. There are two FDA-approved and clinically established implants available: 1) Integra$^®$ Dermal Regeneration Template (bilayer Integra), which is made of a porous matrix of fibers of cross-linked bovine tendon collagen and shark chondroitin-6-sulfate [BURKE et al., 1981]. The artificial dermis is manufactured with a defined degradation rate and a controlled porosity, exhibiting pore sizes of 20 – 125 µm. In contrast, the superficial layer consists of a thin polysiloxane (silicone) layer to prevent moisture loss from the wound. In clinical practice, bilayer Integra is used to cover wounds with impaired vascularization, such as exposed bones or tendons, or for critically ill patients who are not eligible for reconstructive flap surgery. In a first step, the wound is debrided and covered with bilayer Integra. The dermal skin substitute should be well secured to the underlying wound to allow revascularization by ingrowing host microvessels, which takes approximately 21 days. After this interval, the silicone layer is removed and the revascularized neo-dermis can be covered with a STSG. 2) In contrast, Integra$^®$ Dermal Regeneration Template Single Layer (single layer Integra) only consists of a thin porous matrix without silicone layer. It is used in a one-staged procedure with immediate STSG coverage. However, its application is limited to smaller defects and, therefore, is less frequently used in clinical skin reconstruction.

The main drawback of both Integra implants is the long time period until a stable microvascular network is established. This delay of vascularization bears the risk of wound infection and is associated with extended patient hospitalization and the perioperative risk of two surgeries [FRUEH et al., 2017b]. Accordingly, numerous approaches have been suggested to enhance the slow vascularization kinetics of Integra [FRUEH et al., 2017a]. Prevascularization based on adipose tissue-derived angiogenic cells is particularly appealing from a translational perspective, because human adipose tissue is commonly available in abundant amounts, expendable and easily accessible by means of liposuction. In the

preclinical setting, different adipose tissue-based cellular isolates have been shown to enhance the vascularization of Integra. For instance, the stromal vascular fraction (SVF) is an uncultured heterogeneous cell population mainly composed of endothelial cells, immune cells, pericytes and hematopoietic stem cells [KLAR et al., 2017]. The implantation of SVF-loaded Integra in porcine full-thickness burn wounds resulted in a higher blood vessel density and maturation compared with non-loaded controls [FOUBERT et al., 2015]. Furthermore, adipose tissue-derived mesenchymal stem cells (ADSC) markedly enhanced implant vascularization and remodeling [MERUANE et al., 2012; CHERUBINO et al., 2016]. The prevascularization of Integra with ad-MVF may exhibit an even faster vascularization when compared to dermal substitutes enriched with single cell-isolates, such as the SVF or ADSC. To test the suitability of ad-MVF for this purpose, three experimental studies were performed between 2015 and 2018 for the present thesis. For all *in vitro* and *in vivo* experiments, male transgenic C57BL/6-Tg(CAG-EGFP)1Osb/J mice were used as adipose tissue donors for the isolation of ad-MVF. This transgenic mouse line is transfected with enhanced GFP cDNA under the transcriptional control of a chicken β-actin promoter and cytomegalovirus enhancer. Accordingly, all tissues of these animals except red blood cells and hair appear green under blue light excitation [OKABE et al., 1997], enabling a reliable identification of ad-MVF-derived microvascular networks after transplantation into GFP$^-$ C57BL/6 wild-type mice.

In the first study of this thesis, a standardized protocol for the enzymatic isolation of ad-MVF from epididymal fat pads of mice is reported [FRUEH et al., 2017c]. The fat pads of GFP$^+$ C57BL/6 mice were harvested and the amount of adipose tissue was quantified. Subsequently, ad-MVF were isolated by means of mechanical mincing and enzymatic digestion with collagenase for approximately 10 minutes. The time required for adipose harvesting and for the entire isolation process was recorded. Thereafter, the amount of isolated ad-MVF per mL adipose tissue as well as the mean length of individual fragments was evaluated by means of microscopy and histology. Furthermore, immunohistochemical analyses were performed to assess the microvascular morphology of isolated ad-MVF. Finally, the cellular composition of ad-MVF was characterized by means of flow cytometry. For this purpose, they were further digested in cell detachment solution into single cells. In additional pilot experiments, freshly isolated ad-MVF were seeded onto single layer Integra with subsequent histological and immunohistochemical analyses of the prevascularized implants.

After the first promising *in vitro* experiments, the *in vivo* performance of ad-MVF-prevascularized single layer Integra was evaluated **in the second study** using a modified dorsal skinfold chamber model [FRUEH et al., 2017b]. This versatile animal model is suitable

for non-invasive microcirculatory analyses of skin tissue throughout an observation period of up to two weeks [SORG et al., 2009; LASCHKE and MENGER, 2017b]. Technically, circular full-thickness skin defects were created in the chamber observation window on the back of C57BL/6 wild-type mice and single layer Integra seeded with GFP$^+$ ad-MVF isolated from transgenic C57BL/6 mice was implanted. Non-seeded implants served as controls. The *in vivo* experiments consisted of a 14 days-observation period with repetitive intravital fluorescence microscopy and stereomicroscopy for the assessment of the implants' vascularization and epithelialization. After 14 days, the implants were excised and processed for histological and immunohistochemical quantification of epithelialization, microvessel density and collagen content. There is increasing evidence that, beside a blood vascular network, the restoration of a functional lymphatic network is critical for the integration of skin substitutes [MARINO et al., 2014; FRUEH et al., 2018a]. Hence, the lymphatic vessel density of implanted Integra was also analyzed by means of immunohistochemistry. Of special interest, the GFP$^+$/GFP$^-$ crossover approach allowed the identification of ad-MVF-derived blood and lymphatic vessels in the implants as well as in the surrounding skin. Finally, flow cytometry of isolated ad-MVF was performed for a detailed analysis of their cellular composition.

The ultimate goal of Integra prevascularization is to shorten the timeframe until STSG coverage. This would reduce the risk of infection as well as the hospitalization time in the inpatient setting, presumably leading to a lower patient morbidity and to lower healthcare costs. Therefore, **in the third study** of this thesis, the value of ad-MVF-based prevascularization was investigated in a novel mouse model [FRUEH et al., 2018b]. In a first set of experiments, bilayer Integra seeded with ad-MVF was implanted into 8 mm-sized full-thickness skin defects on the skull of CD1 nu/nu mice for 21 days. Non-seeded implants served as controls. From the clinician's perspective, these wounds mimic scalp defects with exposed bone after oncological tumor resection. The implants were assessed *in situ* by means of photo-acoustic imaging. At the end of the *in vivo* experiments, vascularization, lymphangiogenesis as well as incorporation of the implants were analyzed using trans-illumination stereomicroscopy, histology and immunohistochemistry. In a second set of experiments, early (i.e., at day 10 after Integra implantation) STSG coverage of prevascularized and non-seeded implants was performed. For this purpose, autologous STSG were excised from the groin of CD1 nu/nu mice and fixed on the Integra implants on the skull of the animals. The survival rate of STSG was assessed by planimetry. At day 5 after STSG transplantation the implants and the STSG were excised for histological and immunohistochemical analyses.

4. Aim of the Study

The original articles of the present thesis represent a cumulative investigation on the novel application of ad-MVF-based prevascularization of the dermal skin substitute Integra. Each study addresses specific hypotheses.

In the first study, published 2017 in the *Journal of Visualized Experiments*, the standardized isolation of ad-MVF from mouse epididymal fat is reported. The following questions were addressed:

- What are the most critical technical steps of ad-MVF isolation?
- Do ad-MVF-seeded Integra matrices exhibit the potential for *in vivo* application?

In the second study, published 2017 in the *Journal of Investigative Dermatology*, the *in vivo* performance of ad-MVF-seeded Integra skin substitutes was investigated for the first time in the dorsal skinfold chamber of mice. The following questions were addressed:

- Does prevascularized Integra exhibit a faster vascularization and a higher microvessel density when compared to non-seeded implants?
- Does prevascularized Integra exhibit a higher lymphatic vessel density when compared to non-seeded implants?
- Does improved vascularization and lymphangiogenesis of prevascularized Integra lead to faster integration of the implants?
- Does improved vascularization and lymphangiogenesis of prevascularized Integra lead to faster epithelialization of the implants?

In the third study, published 2018 in *Scientific Reports*, ad-MVF-prevascularization of Integra was taken to the next level and a proof-of-concept study with autologous skin grafting was performed in a novel mouse wound model. The goal of this study was to investigate whether the time-consuming two-staged skin reconstruction using Integra may be shortened with ad-MVF-seeding. The following questions were addressed:

- Is the harvesting of murine STSG possible?
- Do the mice tolerate the dermal skin substitutes on the skull for 21 days?
- Does ad-MVF-based prevascularization allow one-stage STSG coverage in mice?
- Does ad-MVF-based prevascularization allow early STSG coverage in mice?
- Do the STSG exhibit GFP$^+$ (i.e. ad-MVF-derived) microvessels 5 days after transplantation?
- Do the STSG exhibit GFP$^+$ (i.e. ad-MVF-derived) lymphatic vessels 5 days after transplantation?

5. Original Articles

Video Article

Isolation of Murine Adipose Tissue-derived Microvascular Fragments as Vascularization Units for Tissue Engineering

Florian S. Frueh[1,2], Thomas Später[1], Claudia Scheuer[1], Michael D. Menger[1], Matthias W. Laschke[1]

[1]Institute for Clinical and Experimental Surgery, Saarland University

[2]Division of Plastic Surgery and Hand Surgery, University Hospital Zurich, University of Zurich

Correspondence to: Florian S. Frueh at florian.frueh@usz.ch

Abstract

A functional microvascular network is of pivotal importance for the survival and integration of engineered tissue constructs. For this purpose, several angiogenic and prevascularization strategies have been established. However, most cell-based approaches include time-consuming *in vitro* steps for the formation of a microvascular network. Hence, they are not suitable for intraoperative one-step procedures. Adipose tissue-derived microvascular fragments (ad-MVF) represent promising vascularization units. They can be easily isolated from fat tissue and exhibit a functional microvessel morphology. Moreover, they rapidly reassemble into new microvascular networks after *in vivo* implantation. In addition, ad-MVF have been shown to induce lymphangiogenesis. Finally, they are a rich source of mesenchymal stem cells, which may further contribute to their high vascularization potential. In previous studies we have demonstrated the remarkable vascularization capacity of ad-MVF in engineered bone and skin substitutes. In the present study, we report on a standardized protocol for the enzymatic isolation of ad-MVF from murine fat tissue.

Video Link

The video component of this article can be found at https://www.jove.com/video/55721/

Introduction

Tissue engineering focuses on the fabrication of tissue and organ substitutes that maintain, restore or augment the function of inoperable *in vivo* counterparts[1,2]. The fate of engineered tissue constructs crucially depends on an adequate vascularization[3]. Microvascular networks within these constructs should be hierarchically organized with arterioles, capillaries, and venules to allow efficient blood perfusion after inosculation to the recipient's vasculature[4]. The generation of such networks is among the key challenges in tissue engineering. For this purpose, a broad spectrum of experimental vascularization strategies has been introduced over the last two decades[5,6].

Angiogenic approaches stimulate the ingrowth of recipient microvessels into engineered tissues by means of structural or physicochemical scaffold modification, such as the incorporation of growth factors[7]. However, for the vascularization of large three-dimensional constructs, angiogenesis-dependent strategies are markedly limited by slow growth rates of developing microvessels[8].

In contrast, the concept of prevascularization aims for the generation of functional microvascular networks within tissue constructs prior to their implantation[9]. Conventional prevascularization involves the co-culture of vessel-forming cells, such as endothelial cells, mural cells or stem cells[10], within scaffolds. After microvascular network formation, the prevascularized constructs can then be implanted into tissue defects. Noteworthy, this prevascularization approach is difficult to apply in a clinical setting, because it is based on complex and time-consuming *in vitro* procedures, which are restricted by major regulatory hurdles[9]. Accordingly, there is still a need for the development of novel prevascularization strategies that are more suitable for a broad clinical application.

Such a prevascularization strategy may be the application of adipose tissue-derived microvascular fragments (ad-MVF). ad-MVF represent potent vascularization units that can be harvested in large amounts from the fat tissue of rats[11,12] and mice[13]. They consist of arteriolar, capillary, and venular vessel segments, which exhibit a physiological microvessel morphology with a lumen and stabilizing perivascular cells[14,15]. This unique feature allows the immediate implantation of ad-MVF-seeded scaffolds into tissue defects without precultivation. There, the ad-MVF rapidly reassemble into functional microvascular networks. Furthermore, ad-MVF represent a rich source of mesenchymal stem cells[16], which may additionally contribute to their striking regenerative capacity. Accordingly, ad-MVF are increasingly used in different fields of tissue engineering[14,15,17,18,19,20,21].

The isolation of ad-MVF has originally been established in rats[11,12]. Herein, we describe a protocol, which allows the standardized isolation of murine ad-MVF from epididymal fat pads. This may provide further insights into molecular mechanisms underlying ad-MVF function by using transgenic mouse models.

Protocol

All procedures were performed according to the National Institute of Health guidelines for the use of experimental animals and followed institutional guidelines (Landesamt für Soziales, Gesundheit und Verbraucherschutz, Abt. Lebensmittel- und Veterinärwesen, Zentralstelle, Saarbrücken, Germany).

1. Preparation of Surgical Instruments

1. Keep ready the dissection scissors, surgical forceps, small preparation scissors, fine forceps and a sterile Petri dish with 15 mL Dulbecco's modified Eagle medium (DMEM; 10% fetal calf serum (FCS), 100 U/mL penicillin, 0.1 mg/mL streptomycin) for harvesting epididymal fat pads.
2. Expose the surgical instruments to a disinfecting solution for 5 min. Alternatively, sterilize them (steam sterilization; 121 °C, 20 min).

2. Animals and Anesthesia

1. Choose carefully the strain of the mice as indicated for the study and the subject under investigation.
   NOTE: In this study we used male wild-type C57BL/6 mice as donors for the harvesting of epididymal fat. Of interest, ad-MVF may be also isolated from transgenic green fluorescent protein (GFP)-positive donor animals (C57BL/6-Tg(CAG-EGFP)1Osb/J)[22]. This bears the major advantage that the fragments are easily detectable by immunohistochemical staining of GFP after implantation into GFP-negative wild-type mice[14].
2. Anesthetize the animals with an intraperitoneal injection of xylazine (15 mg/kg) and ketamine (75 mg/kg). Make sure that the animals are deeply anesthetized by performing a toe pinch with no response. Eye lubricant is not indicated as the donor animals are sacrificed after fat harvesting.
   NOTE: Ensure that analgesia and surgical sterility are in agreement with the respective guidelines of the country and institution where the experiments are planned.

3. Harvesting of Epididymal Fat Pads

1. Transfer the animal to an operation table. Place the animal in a supine position under a surgical stereomicroscope and confirm deep anesthesia using toe pinch.
2. Immobilize the paws by taping them to a surgical drape and disinfect the abdomen with disinfecting solution.
3. Separate the abdominal skin free of the underlying muscle layer with the dissection scissors.
4. Perform a midline laparotomy with the dissection scissors and laterally unfold the flaps of the abdominal wall.
5. Bilaterally identify testis, epididymis and the epididymal fat pad using the fine forceps (**Figure 1**). **Do not harm the intestinal structures to prevent fecal contamination of the fat pads.**
6. Harvest the epididymal fat pads with the small preparation scissors and the fine forceps under the stereomicroscope. **Keep a safety margin of several mm between the epididymis and the fat to reduce the risk of accidental epididymal harvesting.**
   NOTE: This procedure can also be performed without a stereomicroscope. However, this may further increase the risk of accidental injury of the epididymis and spermatic cords.
7. Transfer the epididymal fat pads into a Petri dish containing 15 mL of DMEM pre-heated at 37 °C for the transport to the cell laboratory.
8. Sacrifice the animal by incision of the abdominal aorta or cervical dislocation.

4. Isolation of ad-MVF

1. Prepare three sterile Petri dishes with 15 mL of phosphate-buffered saline (PBS), sterile 14-mL polypropylene (PP) tubes, a sterile 50-mL Erlenmeyer flask, sterile 1.5-mL conical microcentrifuge tubes and sterilized fine scissors.
2. Wash the fat pads thrice in Petri dishes with 15 mL of PBS under a laminar flow hood.
3. Transfer the fat into a 14-mL PP tube. Determine the volume of harvested fat tissue (in mL) by means of the tube scale. Mince the fat tissue mechanically with the fine scissors until a homogeneous tissue suspension is obtained.
4. Transfer the minced tissue with two volumes of collagenase NB4G (0.5 U/mL PBS) into a 50-mL Erlenmeyer flask by means of 10-mL measuring pipette. The total volume becomes thrice the volume of fat tissue measured in step 4.3. Perform tissue digestion in an incubator for 10 min under vigorous stirring by means of an automated stirrer (size of magnetic stir bar: 25 mm) at 37 °C and humidified atmospheric conditions with 5% CO_2.
5. Observe a small fraction (10 µL) of the digested tissue under a microscope to judge whether the digestion can be stopped. Ascertain that the digestate mainly contains "free" ad-MVF next to single cells, indicating the appropriate point to stop the enzymatic digestion process (**Figure 2**).
   NOTE: This step requires experience with the procedure and is critical for the quality of isolated ad-MVF. Prolonged fat digestion results in a single-cell suspension without ad-MVF.
6. Neutralize the enzyme with two volumes of PBS/20% FCS. The total volume becomes thrice the volume of the cell-vessel suspension in step 4.4. Transfer the cell-vessel suspension back into new PP tubes.
7. Incubate the suspension for 5 min at 37 °C to separate ad-MVF from remaining fat by gravity. Then carefully remove the main fat supernatant with a 1-mL precision pipette. Repeat this cycle several times with a 100-µL precision pipette until the suspension appears to be fat-free.

8. Put a 500-µm filter on top of a 50-mL conical centrifuge tube. Transfer the cell-vessel suspension with a 10-mL measuring pipette from the 14-mL PP tubes onto the filter membrane to remove remaining fat clots. Transfer the filtered suspension into new 14-mL PP tubes according to the number of individual ad-MVF isolates for the planned experiments.
   NOTE: For *in vitro* assays focusing on microvascular network formation, it may be beneficial to further purify the cell-vessel suspension to improve the imaging quality during microscopic analyses. For this purpose, the suspension may be additionally filtered once with a 20-µm filter to remove single cells from the ad-MVF collected on the filter.
9. Centrifuge the cell-vessel suspension (600 x g, 5 min, room temperature) to obtain a pellet containing ad-MVF.
10. After centrifugation, remove the supernatant until 1 mL is left. Resuspend the pellet with ad-MVF in this 1 mL and transfer the suspension into a 1.5-mL conical microcentrifuge tube.
11. Centrifuge the ad-MVF suspension in the microcentrifuge tube (600 x g, 5 min) to obtain a pellet.
12. Remove the supernatant to resuspend the pellet in the required final volume of PBS / 20% FCS.
    NOTE: The number of ad-MVF per isolate can be assessed by microscopic counting. For this purpose, 1/10 of the final cell-vessel suspension is diluted 1:10 in PBS and 100 µL of this dilution are transferred into a well of a 96-well plate. The entire number of ad-MVF exhibiting a vessel-like morphology is then counted and extrapolated to the whole isolate. The required ad-MVF concentration and purification can be individually adapted to the respective *in vitro* or *in vivo* application of the ad-MVF. This can include the embedding of ad-MVF in collagen gels for the *in vitro* analysis of microvascular network formation or the seeding of ad-MVF on scaffolds for *in vivo* implantation into tissue defects.

Representative Results

In the present study we performed six ad-MVF isolation procedures with fat tissue from 7- to 12-month-old male wild-type C57BL/6 mice (mean body weight: 35 ± 1 g). **Figure 1** illustrates the harvesting of murine epididymal fat pads with subsequent mechanical and enzymatic ad-MVF isolation. The time required for the harvesting of fat was 30 min and for the isolation of ad-MVF was 120 min. In total, the procedure took 150 min.

We harvested 1.2 ± 0.1 mL of adipose tissue per donor animal. This amount of fat allowed the isolation of 42,000 ± 2,000 ad-MVF per mL. The mean length of the isolated ad-MVF was 42 ± 1 µm (**Figure 2A**). The duration of enzymatic digestion was determined by means of microscopic control as shown in **Figure 2B**. ad-MVF exhibited a typical microvessel morphology with hierarchical vessel segments (**Figure 2C**).

We additionally characterized the ad-MVF by means of flow cytometry. For this purpose, ad-MVF were further digested in cell detachment solution for 30 min into single cells[15]. The flow cytometric analyses revealed that ad-MVF contain 26 ± 2% CD31-positive endothelial cells, 17 ± 2% α-smooth muscle actin (SMA)-positive perivascular cells, and 9 ± 1% cells positive for the mesenchymal stem cell marker CD117 (**Figure 3A-C**). After seeding on a dermal skin substitute, which was fixed and sectioned immediately for histological analyses, larger ad-MVF were mainly localized on the implant's surface (**Figure 3D**). However, capillary vessel segments could also be detected within its pores. Immunohistochemical staining of seeded ad-MVF further revealed physiological microvessel configuration with arteriolar, venular and capillary-like fragments (**Figure 3E**).
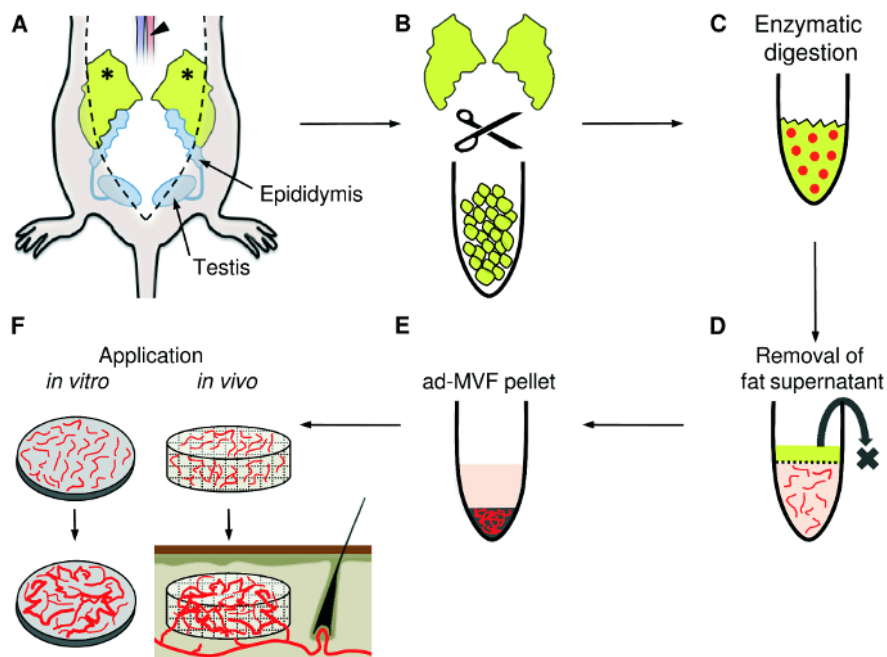
Figure 1: ad-MVF Isolation. A) Following midline laparotomy, the epididymal fat pads (asterisks) are identified. The adipose tissue is harvested with a small preparation scissors and the animal is sacrificed by incision of the abdominal aorta (arrowhead). **B)** Mechanical mincing of the fat pads with fine scissors until the tissue suspension appears homogeneous. **C)** For enzymatic digestion, collagenase is added to the tissue suspension. **D)** The cell-vessel suspension is incubated and the supernatant fat layer is discarded. **E)** After centrifugation, the pellet containing ad-MVF is resuspended and can be used for different applications, such as the *in vitro* analysis of microvascular network formation or the seeding of ad-MVF on scaffolds for *in vivo* implantation into tissue defects **(F)**. Please click here to view a larger version of this figure.
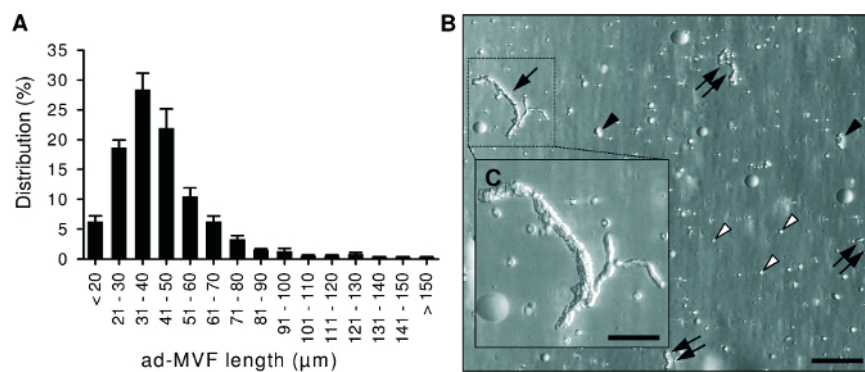
Figure 2: Morphological Characteristics of ad-MVF. A) Length distribution of freshly isolated ad-MVF. Mean ± standard error of the mean (n = 6). **B)** Microscopic image of a cell-vessel suspension smear with large (arrow), medium-sized (double arrows) and small (black arrowheads) ad-MVF as well as single cells (white arrowheads). Scale bar = 110 µm. Higher magnification reveals that ad-MVF exhibit a mature microvessel morphology with hierarchical microvessel segments **(C, inset of B)**. Scale bar: C = 50 µm. Please click here to view a larger version of this figure.
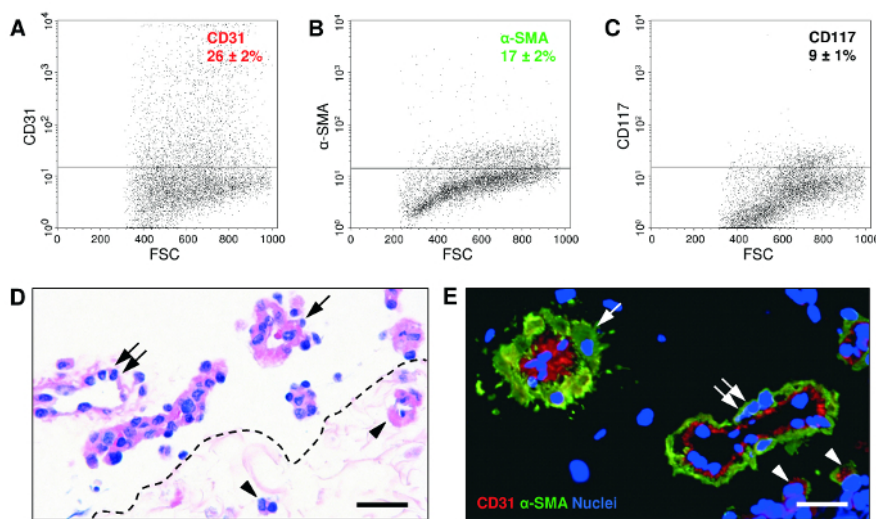
Figure 3: Flow Cytometric, Histological and Immunohistochemical Characteristics of ad-MVF. A-C) Flow cytometric analyses of freshly isolated ad-MVF illustrating CD31-positive endothelial cell **(A)**, α-SMA-positive perivascular cell **(B)** and CD117-positive mesenchymal stem cell **(C)** fractions. Appropriate isotype-identical controls were used to adjust threshold levels. Mean ± standard error of the mean (n = 6). **D)** Hematoxylin and eosin-stained section of a seeded dermal skin substitute. A few capillary vessel segments are located in the implant's pores (arrowheads). Larger microvessels with venular (double arrow) or arteriolar (arrow) morphology are localized on its surface. Scale bar = 40 μm. Broken line = implant border. **E)** Characterization of ad-MVF by means of immunohistochemical detection of the endothelial cell marker CD31 (red) and the perivascular cell marker α-SMA (green). Cell nuclei were stained with a DNA-binding fluorescent dye (blue). Arteriolar ad-MVF (arrow) are characterized by a thicker α-SMA-positive cell layer when compared to venular fragments with a larger lumen (double arrow). Arrowheads = capillary ad-MVF. Scale bar = 25 μm. Please click here to view a larger version of this figure.

Discussion

In this study we present a well-established protocol for the isolation of ad-MVF. Obtaining ad-MVF from murine adipose tissue is a straightforward procedure with a few critical steps. Mice exhibit different subcutaneous and intraabdominal fat deposits. As previously described for rats, the most suitable fat source for the isolation of ad-MVF are the epididymal fat pads due to their size, homogeneous structure and minimal contamination with larger blood vessels[11,12]. In contrast, subcutaneous fat deposits in mice are much smaller and more adherent to the surrounding tissue. However, the excision of epididymal fat pads bears the risk of accidental injury of the epididymis and spermatic cords, resulting in contamination of the harvested tissue with sperms. Therefore, the identification of epididymis, testis and spermatic cords is of major importance in this procedure. Moreover, the fat pads should be rapidly processed after harvesting to minimize *ex vivo* tissue damage. Finally, it should be considered that there are major age-dependent variations in the vascularization of murine epididymal fat pads[23]. In our experience, the use of 6- to 12-month-old male donor mice provides sufficient amounts of ad-MVF for *in vitro* and *in vivo* studies. However, it may also be possible to isolate ad-MVF from younger mice, which exhibit smaller but highly vascularized fat pads[24].

The enzymatic digestion of the harvested epididymal fat pads crucially determines the final quality of isolated ad-MVF. Too short exposure to collagenase leads to incomplete separation of ad-MVF from surrounding adipocytes. On the other hand, prolonged digestion results in the destruction of ad-MVF to a single cell suspension, the so-called stromal vascular fraction (SVF). The SVF is a heterogeneous cell population containing mesenchymal stem cells, endothelial cells, pericytes, macrophages and many other cell types with regenerative potential through paracrine and differentiation mechanisms[25]. The use of ad-MVF exhibits considerable advantages when compared to SVF-based approaches. The fully functional microvessel morphology of ad-MVF allows their immediate implantation for *in vivo* experiments without time-consuming and complex *in vitro* cultivation. Moreover, the isolation of the SVF usually requires the digestion of the tissue with collagenase up to 90 min[26]. In contrast, tissue degradation should not exceed 10 min for the isolation of ad-MVF. This supports the idea of intraoperative one-step applications of ad-MVF[9]. For this purpose, ad-MVF may be automatically isolated from autologous lipoaspirates and transferred back into a tissue defect of the patient without leaving the operation theatre. This is a realistic goal considering the fact that the automated isolation of SVF from lipoaspirates is already a clinically established procedure in plastic surgery[27,28,29].

Recently, we have demonstrated a strong effect of ad-MVF on the *in vivo* vascularization of bone[14] and skin[15] substitutes. Of interest, we found that it is beneficial not to remove single cells from the ad-MVF isolate, because they may provide a more physiological environment that contributes to the high vascularization capacity of ad-MVF[13]. Therefore, we only used a 500-μm filter during the isolation of ad-MVF for the removal of larger non-digested fat clots. Moreover, we found that ad-MVF induce lymphangiogenesis in implanted skin substitutes[15]. Hence, ad-MVF may also be promising building blocks for lymphatic tissue engineering and lymphedema therapy.

For the successful translation of these experimental findings into clinical practice, the next logical step is to clarify whether human adipose tissue is equally suited for the isolation of ad-MVF as rodent fat. In this context, a critical issue is the amount of fat required to isolate large amounts of ad-MVF. The herein described protocol resulted in approximately 40,000 ad-MVF per mL fat tissue. Accordingly, 3 mL fat tissue would be necessary to prevascularize 1 cm^2 of dermal skin substitute[15]. Hence, this approach may not be feasible for the treatment of larger wounds or severely ill patients due to a limited amount of available fat tissue for ad-MVF isolation.

Beside a broad spectrum of potential *in vivo* applications in tissue engineering and regenerative medicine, ad-MVF are also suitable for *in vitro* modeling of angiogenic processes. For instance, rat ad-MVF have been cultured in three-dimensional collagen hydrogels to study the formation of new microvascular networks[30]. Similar approaches have been used to evaluate sophisticated imaging techniques for the visualization of neovessel growth[13] or interstitial matrix remodeling during angiogenesis[31].

Taken together, these findings indicate that ad-MVF are not only promising vascularization and lymphangiogenic units for future therapeutic strategies, but also for basic research in the field of angiogenesis and vascular physiology.

Disclosures

The authors declare that they have no competing financial interests.

Acknowledgements

References

1. Langer, R., Vacanti, J.P. Tissue engineering. *Science.* **260** (5110), 920-926 (1993).
2. Khademhosseini, A., Langer, R. A decade of progress in tissue engineering. *Nat Protoc.* **11** (10), 1775-1781 (2016).
3. Novosel, E.C., Kleinhans, C., Kluger, P.J. Vascularization is the key challenge in tissue engineering. *Adv Drug Deliv Rev.* **63** (4-5), 300-311 (2011).
4. Rouwkema, J., Khademhosseini, A. Vascularization and Angiogenesis in Tissue Engineering: Beyond Creating Static Networks. *Trends Biotechnol.* **34** (9), 733-745 (2016).
5. Laschke, M.W., Menger, M.D. Vascularization in tissue engineering: angiogenesis versus inosculation. *Eur Surg Res.* **48** (2), 85-92 (2012).
6. Sarker, M., Chen, X.B., Schreyer, D.J.. Experimental approaches to vascularisation within tissue engineering constructs. *J Biomater Sci Polym Ed.* **26** (12), 683-734 (2015).
7. Frueh, F.S., Menger, M.D., Lindenblatt, N., Giovanoli, P., Laschke, M.W. Current and emerging vascularization strategies in skin tissue engineering. *Crit Rev Biotechnol.* **20**, 1-13 (2016).
8. Utzinger, U., Baggett, B., Weiss, J.A., Hoying, J.B., Edgar, L.T. Large-scale time series microscopy of neovessel growth during angiogenesis. *Angiogenesis.* **18** (3), 219-232 (2015).
9. Laschke, M.W., Menger, M.D. Prevascularization in tissue engineering: Current concepts and future directions. *Biotechnol Adv.* **34** (2), 112-121 (2016).
10. Baiguera, S., Ribatti, D. Endothelialization approaches for viable engineered tissues. *Angiogenesis.* **16** (1), 1-14 (2013).
11. Wagner, R.C., Kreiner, P., Barrnett, R.J., Bitensky, M.W. Biochemical characterization and cytochemical localization of a catecholamine-sensitive adenylate cyclase in isolated capillary endothelium. *Proc Natl Acad Sci U S A.* **69** (11), 3175-3179 (1972).
12. Wagner, R.C., Matthews, M.A. The isolation and culture of capillary endothelium from epididymal fat. *Microvasc Res.* **10** (3), 286-297 (1975).
13. Laschke, M.W., Menger, M.D. Adipose tissue-derived microvascular fragments: natural vascularization units for regenerative medicine. *Trends Biotechnol.* **33** (8), 442-448 (2015).
14. Laschke, M.W., *et al.* Vascularisation of porous scaffolds is improved by incorporation of adipose tissue-derived microvascular fragments. *Eur Cell Mater.* **24**, 266-277 (2012).
15. Frueh, F.S., *et al.* Adipose tissue-derived microvascular fragments improve vascularization, lymphangiogenesis and integration of dermal skin substitutes. *J Invest Dermatol.* **137** (1), 217-227 (2017).
16. McDaniel, J.S., Pilia, M., Ward, C.L., Pollot, B.E., Rathbone, C.R. Characterization and multilineage potential of cells derived from isolated microvascular fragments. *J Surg Res.* **192** (1), 214-22 (2014).
17. Nakano, M., *et al.* Effect of autotransplantation of microvessel fragments on experimental random-pattern flaps in the rat. *Eur Surg Res.* **30** (3), 149-160 (1998).
18. Nakano, M., *et al.* Successful autotransplantation of microvessel fragments into the rat heart. *Eur Surg Res.* **31** (3), 240-248 (1999).
19. Shepherd, B.R., Hoying, J.B., Williams, S.K. Microvascular transplantation after acute myocardial infarction. *Tissue Eng.* **13** (12), 2871-2879 (2007).
20. Pilia, M., *et al.* Transplantation and perfusion of microvascular fragments in a rodent model of volumetric muscle loss injury. *Eur Cell Mater.* **28**, 11-23 (2014).
21. Laschke, M.W., *et al.* Adipose tissue-derived microvascular fragments from aged donors exhibit an impaired vascularisation capacity. *Eur Cell Mater.* **28**, 287-298 (2015).
22. Okabe, M., Ikawa, M., Kominami, K., Nakanishi, T., Nishimune, Y. 'Green mice' as a source of ubiquitous green cells. *FEBS Lett.* **407** (3), 313-319 (1997).
23. Honek, J., *et al.* Modulation of age-related insulin sensitivity by VEGF-dependent vascular plasticity in adipose tissues. *Proc Natl Acad Sci U S A.* **111** (41), 14906-14911 (2014).
24. Cho, C.H., *et al.* Angiogenic role of LYVE-1-positive macrophages in adipose tissue. *Circ Res.* **100** (4), e47-57. (2007).
25. Han, S., Sun, H.M., Hwang, K.C., Kim, S.W. Adipose-Derived Stromal Vascular Fraction Cells: Update on Clinical Utility and Efficacy. *Crit Rev Eukaryot Gene Expr.* **25** (2), 145-152 (2015).
26. Chen, Y.J., *et a*l. Isolation and Differentiation of Adipose-Derived Stem Cells from Porcine Subcutaneous Adipose Tissues. *J Vis Exp.* (109), e53886 (2016).
27. Guillaume-Jugnot, P., *et al.* Autologous adipose-derived stromal vascular fraction in patients with systemic sclerosis: 12-month follow-up. *Rheumatology (Oxford).* **55** (2), 301-306 (2016).

28. Tissiani, L.A., Alonso, N. A Prospective and Controlled Clinical Trial on Stromal Vascular Fraction Enriched Fat Grafts in Secondary Breast Reconstruction. *Stem Cells Int.* **2016**, 2636454 (2016).

29. Calcagni, M., *et al.* The novel treatment of SVF-enriched fat grafting for painful end-neuromas of superficial radial nerve. *Microsurgery.* in press (2016).

30. Hoying, J.B., Boswell, C.A., Williams, S.K. Angiogenic potential of microvessel fragments established in three-dimensional collagen gels. *In Vitro Cell Dev Biol Anim.* **32** (7), 409-419 (1996).

31. Kirkpatrick, N.D., Andreou, S., Hoying, J.B., Utzinger, U. Live imaging of collagen remodeling during angiogenesis. *Am J Physiol Heart Circ Physiol.* **292** (6), H3198-206 (2007).

Adipose Tissue-Derived Microvascular Fragments Improve Vascularization, Lymphangiogenesis, and Integration of Dermal Skin Substitutes

Florian S. Frueh[1,2], Thomas Später[1], Nicole Lindenblatt[2], Maurizio Calcagni[2], Pietro Giovanoli[2], Claudia Scheuer[1], Michael D. Menger[1] and Matthias W. Laschke[1]

Full-thickness skin defects can be covered with dermal skin substitutes in combination with split-thickness skin grafts. However, slow vascularization of the matrices bears the risk of wound infection and extends the length of hospitalization. To overcome these problems, we describe a promising vascularization strategy. Green fluorescent protein[+] adipose tissue-derived microvascular fragments (ad-MVF) were isolated from epididymal fat pads of C57BL/6-Tg(CAG-EGFP)1Osb/J mice. ad-MVF were seeded on collagen-glycosaminoglycan matrices, which were implanted into full-thickness skin defects in the dorsal skinfold chamber of wild-type C57BL/6 mice. Nonseeded matrices served as controls. Vascularization, lymphangiogenesis, and integration of the implants were studied by using intravital fluorescence microscopy, histology, and immunohistochemistry over 14 days. ad-MVF rapidly reassembled into microvascular networks within the implants, which developed interconnections to the host microvasculature. Accordingly, vascularization of the implants was markedly accelerated, as indicated by a significantly higher microvessel density when compared with controls. Moreover, dense lymphatic networks originating from the green fluorescent protein[+] ad-MVF developed within the implants. This was associated with an improved implant integration. Hence, seeding ad-MVF on collagen-glycosaminoglycan matrices represents a potential strategy to reduce morbidity and hospitalization of patients undergoing the treatment of full-thickness skin defects.

INTRODUCTION

The treatment of large full-thickness skin wounds represents a major challenge in reconstructive surgery. Impaired skin integrity due to mechanical or thermal trauma, tumor resection, or systemic illness bears the risk of substantial fluid loss, infection, and ultimate death (Clark et al., 2007). Hence, the rapid re-establishment of the skin's life-saving barrier function is of pivotal importance. Autologous split-thickness skin grafts (STSGs) provide reliable coverage. However, they are prone to scarring and contracture (Shevchenko et al., 2010). In addition, dermal and subcutaneous layers are destructed in deep wounds, which aggravates the functional and esthetic disadvantages of STSGs. To overcome these problems, bioengineered off-the-shelf dermal skin substitutes, such as the U.S. Food and Drug Administration-approved Integra (Integra Life Sciences, Plainsboro, NJ), have been introduced (Burke et al., 1981).

Integra consists of a cross-linked bovine collagen and shark glycosaminoglycan matrix covered with a silicone pseudo-epidermis that protects the implant from exsiccation. In clinical routine, Integra is directly implanted into the debrided wound bed. After vascularization, the silicone pseudo-epidermis is removed, and the dermal scaffold is covered with STSG. A major drawback of this two-step procedure is the fact that host vessel ingrowth into Integra requires up to 3 weeks (Debels et al., 2015). This delay of vascularization bears the risk of wound infection and is associated with extended patient hospitalization. Accordingly, there is a need for an effective strategy that markedly accelerates the vascularization of the dermal substitute.

Various angiogenic and prevascularization strategies have been developed in the field of tissue engineering to improve the survival of tissue substitutes (Auger et al., 2013; Laschke et al., 2006; Laschke and Menger, 2016). Angiogenic approaches focus on the stimulation of blood vessel ingrowth into implants from the surrounding tissue. In line with this concept, Reckhenrich et al. (2011) showed that the vascularization of Integra is enhanced by incorporation of angiogenic growth factors. However, the vascularization process may still be too slow, because it is subject to the physiological kinetics of angiogenesis with an average vessel growth rate of only 5 μm/h (Utzinger et al., 2015). In contrast, prevascularization approaches aim at the establishment of preformed

---

---

microvascular networks within scaffolds before their implantation (Athanassopoulos et al., 2012; Egaña et al., 2009; Formigli et al., 2015; Meruane et al., 2012). These networks are then rapidly perfused by developing interconnections to the microvessels at the implantation site by inosculation (Laschke et al., 2009). Nonetheless, the cell-based generation of preformed microvascular networks requires time-consuming in vitro cultivation and, thus, is not suitable for intraoperative one-step procedures.

Recent studies indicate that adipose tissue-derived microvascular fragments (ad-MVF) may represent a promising solution to overcome the aforementioned problems (Laschke et al., 2012; Pilia et al., 2014). In fact, ad-MVF are functional vessel segments with a high vascularization capacity that can be harvested in large amounts from fat tissue and immediately transplanted without any further in vitro processing (Laschke and Menger, 2015). Hence, we speculated that ad-MVF may be suitable vascularization units for Integra implants.

To test this hypothesis, ad-MVF from transgenic green fluorescent protein (GFP)$^+$ donor mice were seeded on Integra. The prevascularized matrices and nonseeded controls were implanted into full-thickness skin defects in dorsal skinfold chambers of wild-type recipient animals to analyze their vascularization, lymphangiogenesis, and integration by means of intravital fluorescence microscopy, histology, and immunohistochemistry.

RESULTS

Isolation and cellular composition of ad-MVF
ad-MVF were enzymatically isolated from the epididymal fat pads of male C57BL/6-Tg(CAG-EGFP)1Osb/J mice (Figure 1a and b). This transgenic mouse line is transfected with enhanced GFP cDNA under the control of a chicken β-actin promoter and cytomegalovirus enhancer. Accordingly, all tissues of these animals except red blood cells (RBCs) and hair appear green under blue light excitation (Okabe et al., 1997). From each donor animal, approximately 0.75 ml of fat tissue was harvested for the isolation of approximately 30,000 ad-MVF.

The cellular composition of isolated ad-MVF was assessed by means of flow cytometry. This analysis showed that the ad-MVF contained $38.5 \pm 5.8\%$ CD31$^+$ endothelial cells, $7.0 \pm 1.1\%$ adipocyte-specific adhesion molecule$^+$ adipocytes, and $65.0 \pm 2.6\%$, $7.0 \pm 0.5\%$, and $5.8 \pm 0.4\%$ cells positive for the stromal/stem cell surface markers CD29, CD90, and CD117.

Implant seeding
ad-MVF from one donor animal were seeded on two 4-mm Integra samples, which were cut out of a 1.3-mm-thick Integra Dermal Regeneration Template Single Layer without silicone sheet (Integra GmbH, Ratingen, Germany) (Figure 1c). According to this protocol, approximately 120,000 ad-MVF isolated from approximately 3 ml of fat tissue would be needed to seed 1 cm^2 of Integra for the treatment of larger skin defects. Histological and immunohistochemical analyses showed that ad-MVF were mainly seeded on the matrices' surfaces (Figure 1d) and consisted of arteriolar, venular, and capillary vessel segments (Figure 1e).

Vascularization of the implants
For the in vivo analysis of prevascularized and nonseeded control matrices we used a modified dorsal skinfold chamber model, which was originally introduced by Sorg et al. (2007, 2009) for wound healing studies (Figure 1f−h). For this purpose, a 4-mm-sized full-thickness skin defect was created in the observation window of the chamber (Figure 1g). The defect included the skin and the underlying panniculus carnosus muscle while sparing the contralateral muscle layer (Figure 1h). Immediately after defect preparation, the matrices were implanted, and the observation window was sealed with a removable cover glass.

Repetitive intravital fluorescence microscopy showed that nonseeded Integra induced only a weak angiogenic host tissue response and did not show a significant vessel ingrowth except on the implants' outer periphery throughout an observation period of 14 days (Figure 2a−c). In contrast, seeding of Integra with ad-MVF resulted in the formation of dense microvascular networks in the border and center zones of the implants. These networks developed from the GFP$^+$ ad-MVF, which rapidly interconnected with each other and the surrounding host microvasculature, resulting in an early onset of blood perfusion within the implants between days 3 and 6 (Figure 2d−l). Accordingly, the prevascularized implants exhibited a significantly higher number of perfused regions of interest (ROIs) and functional microvessel density between days 6 and 14 compared with nonseeded controls (Figure 2k and l).

Microhemodynamic analyses of microvessels in prevascularized Integra showed typical signs of vascular maturation and remodeling. At day 6, first blood-perfused microvessels still presented with a rather large diameter of 33 μm, which progressively decreased to 17 μm at day 14 (Table 1). This was associated with a continuous increase of the centerline RBC velocity and the wall shear rate over time. In the nonseeded control group, microhemodynamic parameters could be assessed within only two implants at days 10 and 14, because the other implants did not exhibit perfused microvessels on their surface throughout the 2-week observation period (Figure 2k and l). Compared with prevascularized Integra, the measurements showed a lower centerline RBC velocity and wall shear rate (Table 1).

Additional histological analyses of the implants at day 14 confirmed our intravital microscopic findings. Hematoxylin and eosin (HE)-stained tissue sections showed that nonseeded control implants mainly contained invaded single cells (Figure 3a), whereas the pores of prevascularized Integra were completely filled with a well-vascularized granulation tissue (Figure 3b). Immunohistochemical detection of CD31$^+$ microvessels further showed a significantly increased microvessel density within the prevascularized matrices (Figure 3c−e). This microvessel density was comparable to that of the surrounding skin in the border zones of the implants (Figure 3e). CD31/GFP co-staining showed that more than 95% of the microvessels within the prevascularized Integra were GFP$^+$, indicating their origin from seeded ad-MVF (Figure 3g−j). The GFP$^+$ microvessels even invaded the surrounding skin tissue, resulting in 47% GFP$^+$ microvessels at the border of the implants (Figure 3j). In line with these findings, additional immunohistochemical analyses
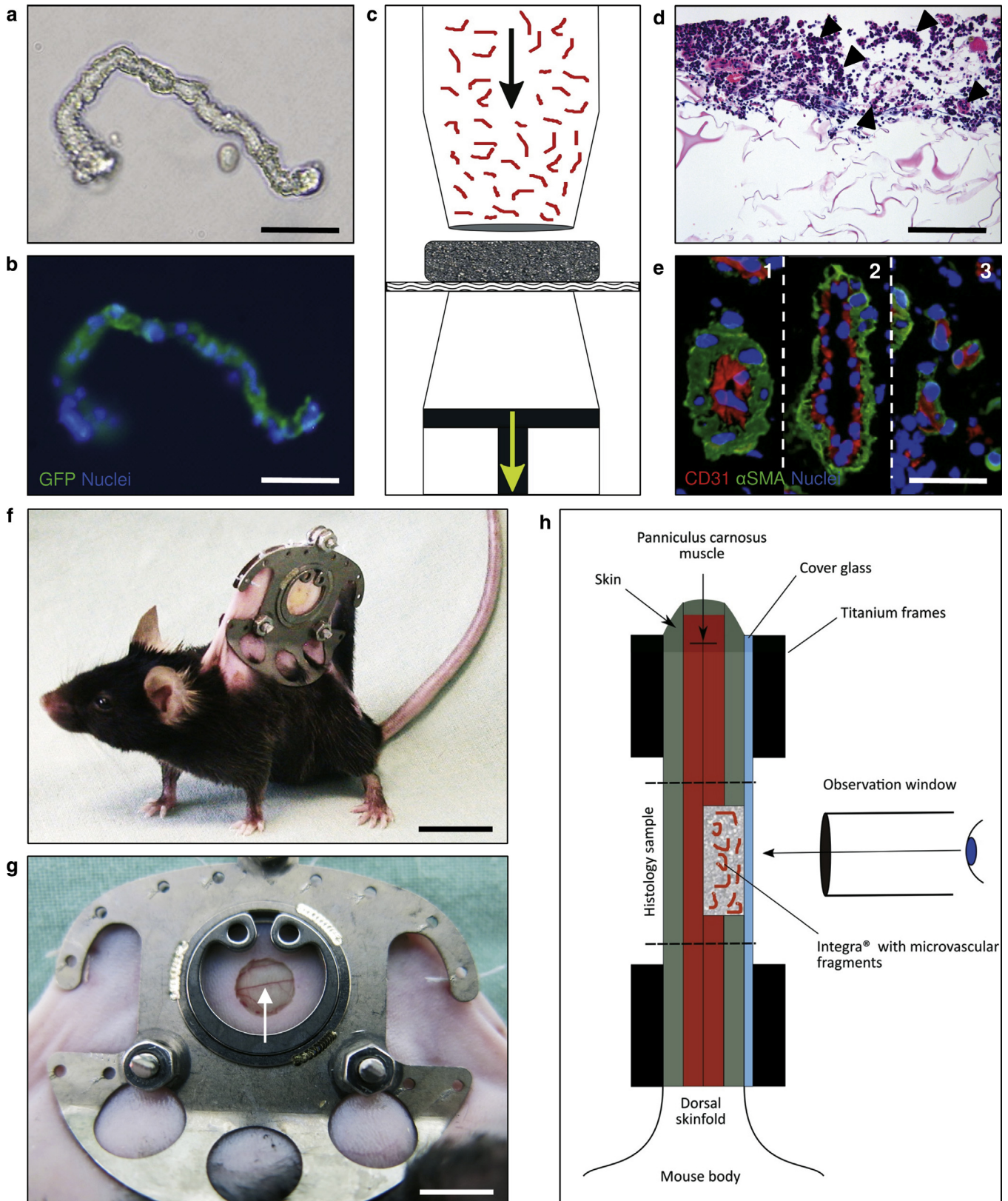
Figure 1. In vivo analysis of vessel-seeded Integra. (**a**) Brightfield and (**b**) multifluorescence microscopy of a GFP⁺ ad-MVF. Scale bars = 20 μm. (**c**) Seeding of Integra with ad-MVF. (**d**) Hematoxylin and eosin-stained cross-section of Integra after the seeding process. The ad-MVF (arrowheads) are mainly seeded on the implant's surface. Scale bar = 130 μm. (**e**) The ad-MVF include (1) arterioles, (2) venules, and (3) capillaries, as shown by immunohistochemical detection of CD31 and α-SMA. Scale bars in 1 and 3 = 35 μm; scale bar in 2 = 45 μm. (**f**) C57BL/6-mouse with a dorsal skinfold chamber. Scale bar = 20 mm. (**g**) Overview of the chamber observation window with a full-thickness skin defect (diameter = 4 mm). Arrow = vessel of the contralateral panniculus carnosus muscle. Scale bar = 5.8 mm. (**h**) Schematic cross-section of a dorsal skinfold chamber with implanted prevascularized Integra. ad-MVF, adipose tissue-derived microvascular fragments; GFP, green fluorescent protein; SMA, smooth muscle actin.
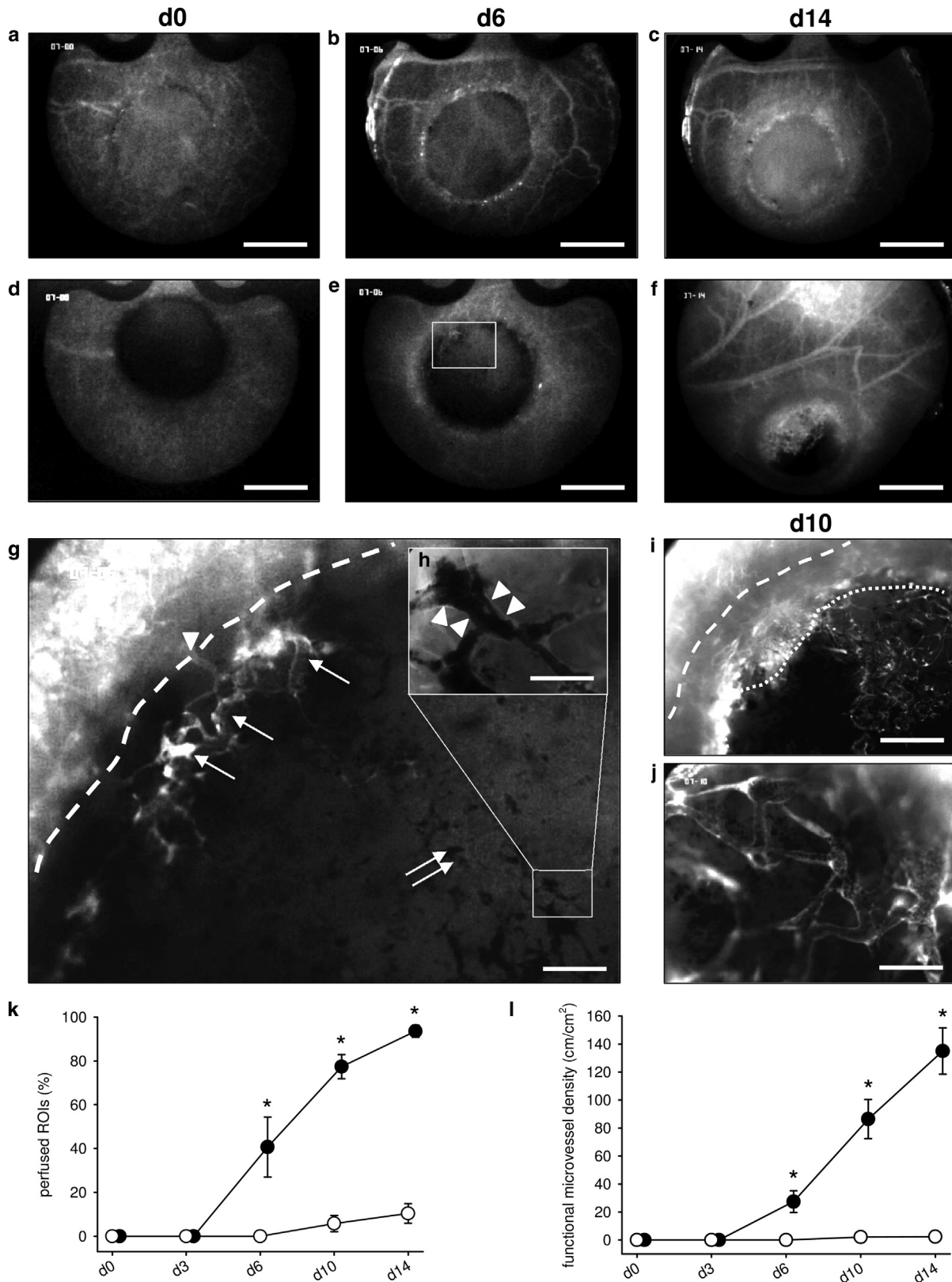
Figure 2. Intravital fluorescence microscopy. (**a–f**) Chamber observation window with (**a–c**) nonseeded and (**d–f**) prevascularized matrices after implantation (d0) and at days 6 and 14 (blue light epi-illumination, 5% FITC-labeled dextran, 150,000 intravenously). Scale bars = 2.5 mm. (**g**) Insert of **e** highlighting the onset of blood perfusion at day 6 (arrowhead = feeding vessel; arrows = perfused microvascular network; broken line = implant border; double arrow = nonperfused, RBC-filled microvessels). Scale bar = 250 μm. (**h**) Insert of **g** (arrowheads = GFP$^+$ endothelium of the microvessels). Scale bar = 80 μm. (**i, j**) At day 10, the center of the implant is also perfused (area between broken and dotted line = multilayered epithelium). Scale bars: **i** = 500 μm, **j** = 120 μm. (**k, l**) Perfused ROIs and functional microvessel density of nonseeded (white circles) and prevascularized Integra (black circles). Mean ± standard error of the mean, n = 8. *$P < 0.05$ versus nonseeded. d, day; GFP, green fluorescent protein; RBC, red blood cell; ROI, region of interest.

Table 1. Microhemodynamic parameters of the microvasculature within nonseeded (control) and prevascularized Integra (ad-MVF)

	d0	d3	d6	d10	d14
Diameter (μm)					
ad-MVF	—	—	33.0 ± 3.3	23.3 ± 1.5	17.2 ± 0.6
Control	—	—	—	29.1 ± 6.1	18.3 ± 1.3
Centerline RBC velocity (μm/s)					
ad-MVF	—	—	83.2 ± 16.2	374.3 ± 61.1	489.0 ± 73.1
Control	—	—	—	166.6 ± 102.6	167.3 ± 97.7
Wall shear rate (s^{-1})					
ad-MVF	—	—	21.4 ± 5.1	129.9 ± 20.1	230.2 ± 35.4
Control	—	—	—	53.9 ± 39.4	76.3 ± 47.9

ad-MVF (n = 8); control (n = 2); mean ± standard error of the mean.

Abbreviations: ad-MVF, adipose tissue-derived microvascular fragment; RBC, red blood cell.

showed that 9.5 ± 1.0% of the CD31$^+$ endothelial cells within the implants expressed the proliferation marker Ki67 (see Supplementary Figure S1 online).

Development of a lymphatic network within the implants
Additional immunohistochemical analyses included the detection of lymphatic vessel endothelial hyaluronan receptor (LYVE)-1$^+$ lymphatic vessels at the border and center of the implants. Both nonseeded and prevascularized Integra contained lymphatic vessels at day 14 after implantation. However, the lymphatic vessel density was significantly higher in prevascularized implants than in controls (Figure 3f). LYVE-1/GFP co-staining further showed that more than 60% of the lymphatic vessels within the prevascularized implants originated from seeded ad-MVF (Figure 3k—n). As already observed for microvessels, GFP$^+$ lymphatic vessels also invaded the surrounding host tissue at the border of the implants (Figure 3n).

Collagen content of the implants
At day 14, Sirius red-stained sections were analyzed for the visualization of mature collagen fibers (type I) within the implants. Under polarized light, these fibers appear reddish because of birefringence (Junqueira et al., 1979). Overall, both nonseeded and prevascularized Integra contained relatively low amounts of collagen fibers compared with healthy skin (Figure 4a—f). However, the collagen content was significantly higher in prevascularized matrices when compared with nonseeded controls (Figure 4f).

Epithelialization of the implants
In line with the improved vascularization and tissue integration, prevascularized Integra also exhibited an accelerated epithelialization compared with nonseeded control implants (Figure 5). Repetitive planimetric measurements of the epithelialized implant surface area throughout the observation period of 14 days showed a significantly enhanced epithelialization of prevascularized matrices at days 10 and 14 (Figure 5a—j). Vessel-seeded Integra exhibited slight hemorrhages after the onset of blood perfusion at day 6 after implantation (Figure 5e and h). However, these focal bleedings did not affect their epithelial coverage. These findings were confirmed by additional immunohistochemical quantification of cytokeratin$^+$ multilayered epithelium covering the implants at day 14 (Figure 5k—m).

Apoptotic cell death within the implants
Prevascularized Integra matrices were additionally analyzed after implantation to clarify whether cell death occurred within the implants. Immunohistochemical detection of the apoptosis marker cleaved caspase-3 showed that the implants contained 6.6 ± 0.5% and 1.4 ± 0.3% apoptotic cells at day 3 and day 14 (see Supplementary Figure S2 online).

DISCUSSION
The vascularization kinetics of implanted Integra determine the time interval during which the wound is prone to infection and until STSG coverage is possible. We herein introduce an approach that markedly reduces this critical phase and, thus, may contribute to a reduction of patient morbidity and hospitalization in the future treatment of full-thickness skin defects. Indeed, we showed that the seeding with ad-MVF rapidly results in blood perfusion of Integra within the initial 3—6 days after implantation.

For our in vivo analyses, we used the mouse dorsal skinfold chamber, as previously described by Michael et al. (2013a, 2013b). Contraction of the panniculus carnosus muscle, which represents a problem in loose-skinned animal models for wound healing (Griffin et al., 2015), is avoided in this model by fixation of the skin between the two titanium frames. Moreover, implanted matrices are protected from exsiccation and manipulation by the animal in the closed chamber (Michael et al., 2013b). Hence, it is not necessary to regularly change wound dressings, which may influence the healing process and jeopardize objective analyses. Accordingly, we herein could use single-layer Integra without a silicone sheet. This enabled us to study the vascularization of the matrices by means of repetitive intravital fluorescence microscopy over 14 days. In contrast to histological analyses, this technique additionally allows the assessment of microhemodynamic parameters. Thus, it is possible to determine microvascular blood perfusion and vascular remodeling as essential indicators for the functionality of the newly developing microvascular networks within the implants.

By harvesting ad-MVF from transgenic GFP$^+$ donor mice, we could analyze their fate after implantation into GFP$^-$ wild-type animals. Immunohistochemical analyses at the end of the 14-day observation period showed homogenously distributed GFP$^+$ microvessels within the implants, although ad-MVF were initially seeded mainly on the superficial layers of Integra. This indicates that they could rapidly invade the matrix, which may have been supported by its relatively loose architecture with pore sizes of 30—120 μm (Reiffel et al., 2012; van der Veen et al., 2010). In addition, we found that more than 95% of the microvessels within the implants stained positive for GFP. Furthermore, the matrices contained only low numbers of apoptotic cells at days 3 and 14 after implantation. These results confirm previous findings that ad-MVF survive the isolation and transplantation well and exhibit a unique capacity for rapidly reassembling into new microvascular networks (Laschke et al., 2012, 2014). Moreover, they release substantial amounts of angiogenic
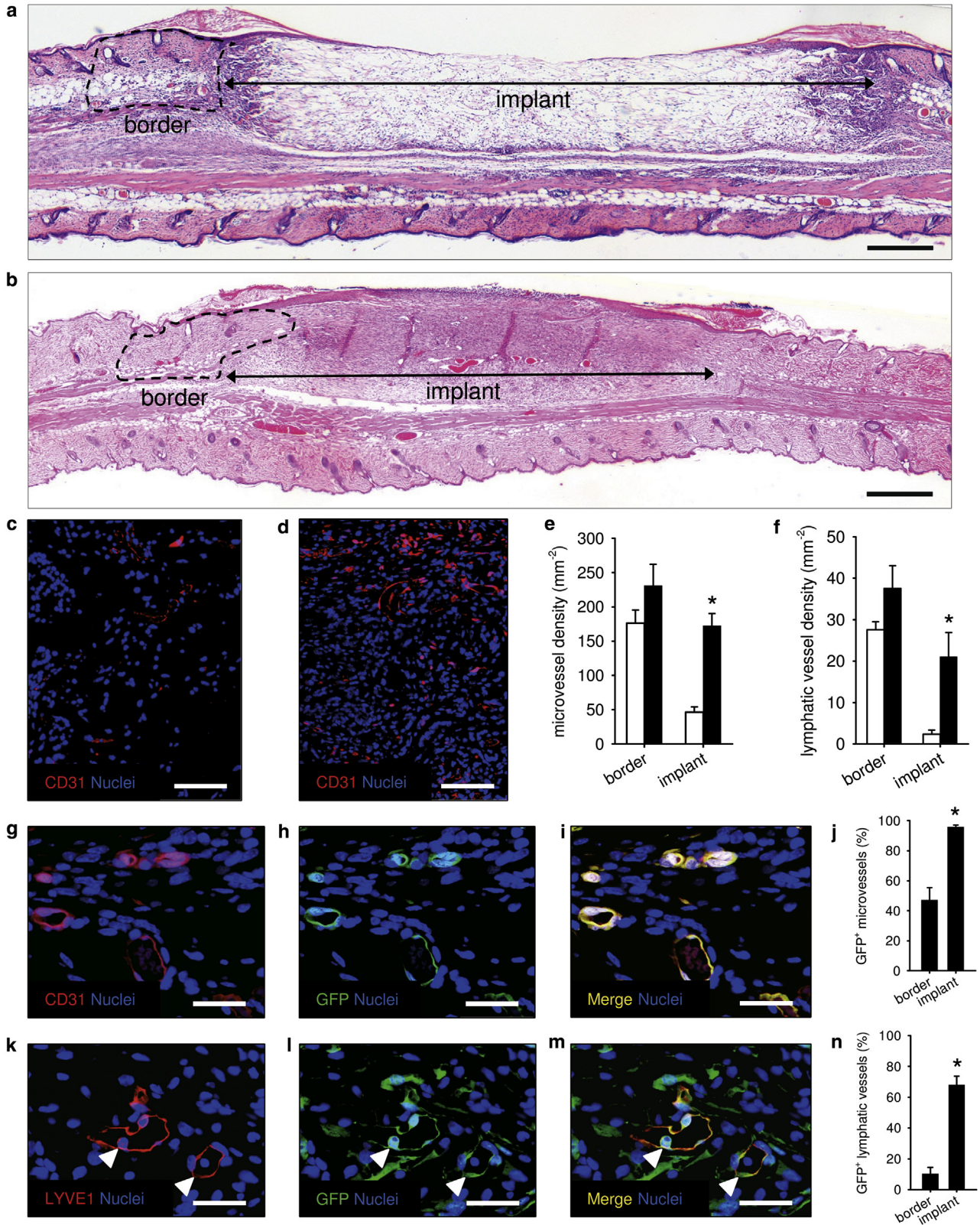
Figure 3. Vascularization and lymphatic network development. (**a, b**) Hematoxylin and eosin-stained sections of (**a**) nonseeded and (**b**) prevascularized matrices at day 14. Scale bars = 500 μm. (**c, d**) Immunohistochemical detection of CD31$^+$ microvessels in (**c**) nonseeded and (**d**) prevascularized matrices at day 14. Scale bars = 90 μm. (**e, f**) Microvessel density and lymphatic vessel density within nonseeded (white bars) and prevascularized (black bars) Integra and within the skin at the implants' border. Mean ± standard error of the mean, n = 8. *$P < 0.05$ versus nonseeded. (**g–i**) Microvessels and (**k–m**) lymphatic vessels within a prevascularized matrix at day 14 (arrowheads = LYVE-1$^+$/GFP$^+$ lymphatic vessels). Scale bars in **g–i** and **k–m** = 30 μm. (**j, n**) GFP$^+$ microvessels and lymphatic vessels within prevascularized Integra and the skin at the implants' border. Mean ± standard error of the mean, n = 8. *$P < 0.05$ versus border. GFP, green fluorescent protein; LYVE, lymphatic vessel endothelial hyaluronan receptor.
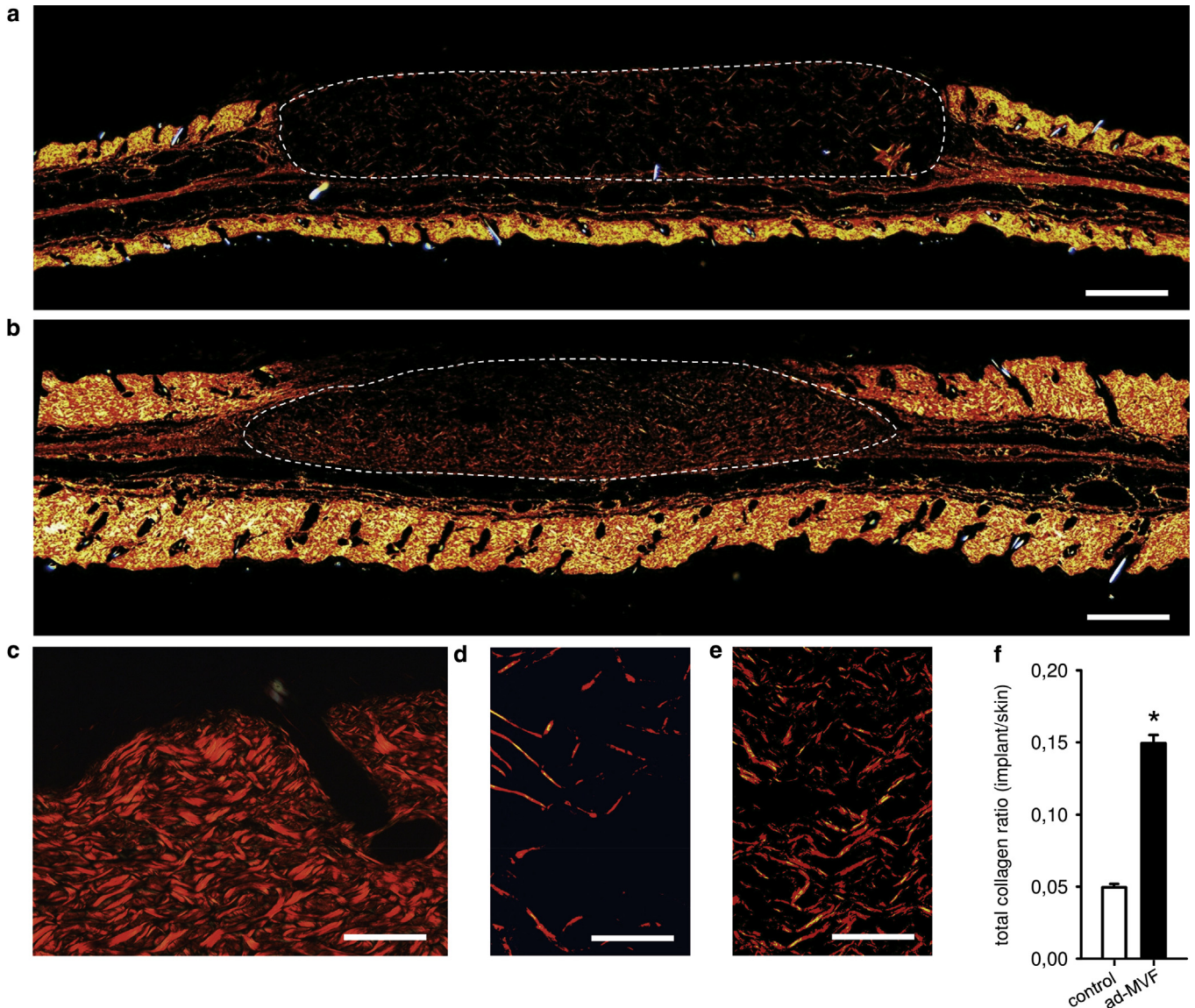
Figure 4. Collagen content of implanted Integra. (**a–e**) Polarized light microscopy of Sirius red-stained sections of (**a, d**) nonseeded and (**b, e**) prevascularized matrices and (**c**) adjacent skin at day 14 (**a, b** = overview; **d, e** = higher magnification of implant center; broken lines = implant borders). Scale bars: **a, b** = 500 μm; **c–e** = 70 μm. (**f**) Total collagen ratio within nonseeded (white bar) and prevascularized Integra (black bar). Mean ± standard error of the mean, n = 8. *$P < 0.05$ versus nonseeded. ad-MVF, adipose tissue-derived microvascular fragments.

growth factors, such as vascular endothelial growth factor and basic fibroblast growth factor (Laschke et al., 2012). Their high vascularization potential may have been further supported by mesenchymal stem cells, which are closely attached within their physiological niche to the fragments (McDaniel et al., 2014). Taken together, these factors may have also contributed to the strong angiogenic sprouting activity of the transplanted ad-MVF, which even grew out of the matrices into the surrounding skin tissue, where they developed interconnections with the host vessels by external inosculation (Laschke et al., 2009).

The lymphatic system is critically involved in the drainage of the interstitial space, and its failure leads to accumulation of lymph and seroma formation (Frueh et al., 2016). Marino et al. (2014) recently showed the importance of the lymphatic system for bioengineered dermal-epidermal skin grafts. They engineered a human lymphatic vascular network, which successfully inosculated to the host lymphatic system after transplantation into nude rats. However, so far there is only limited knowledge about lymphangiogenesis within implanted Integra (Cherubino et al., 2014). We found that only a few lymphatic vessels had grown into nonseeded Integra 14 days after implantation. In contrast, seeding of the matrix with ad-MVF resulted in the development of lymphatic networks, which consisted of 60% LYVE-1^{+}/GFP^{+} lymphatic vessels. This indicates that ad-MVF do not only represent effective vascularization units but may also be a source of lymphatic endothelial cells or entire lymphatic vessel fragments. In addition, it may be speculated that fragment-associated mesenchymal stem cells exhibit the capacity of rapidly differentiating into lymphatic vessels after transplantation. If this holds true, our findings may pave the way for applications of ad-MVF in the field of lymphatic tissue engineering and lymphedema therapy.
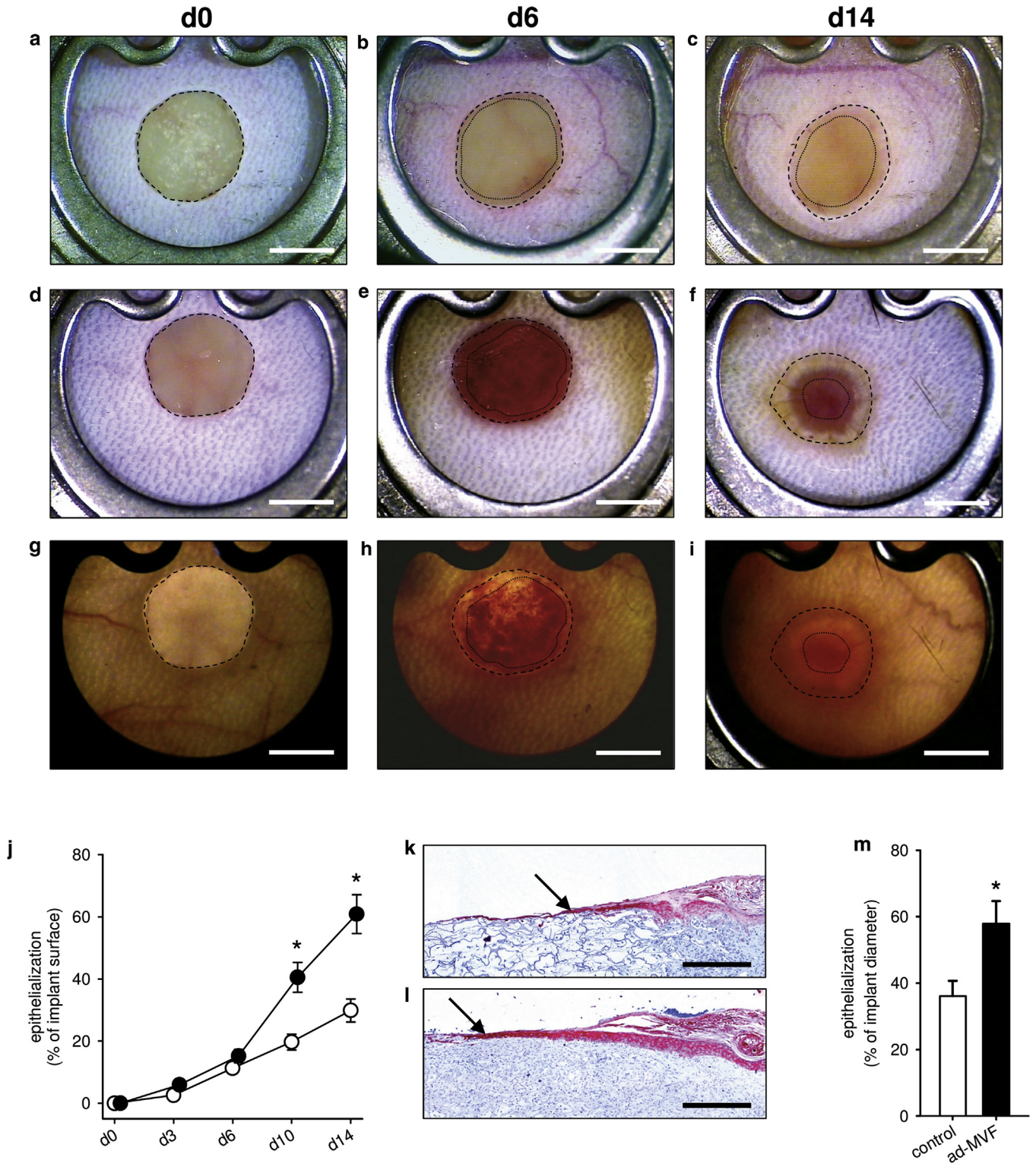
Figure 5. Epithelialization of implanted Integra. (**a−i**) Stereomicroscopy in (**a−f**) epi-illumination and (**g−i**) transillumination of the chamber observation window with (**a−c**) nonseeded and (**d−i**) prevascularized matrices after implantation (d0) and at days 6 and 14 (outer broken line = implant border; inner dotted line = border of nonepithelialized area). Scale bars = 2.5 mm. (**j**) Epithelialization of nonseeded (white circles) and prevascularized Integra (black circles). Mean ± standard error of the mean, n = 8. *$P < 0.05$ versus nonseeded. (**k−m**) Immunohistochemical detection of cytokeratin[+] multilayered epithelium (arrows) covering a (**k**) nonseeded and (**l**) prevascularized matrix at day 14 after implantation. Scale bars = 250 μm. (**m**) Epithelial coverage of nonseeded (white bar) and prevascularized Integra (black bar). Mean ± standard error of the mean, n = 8. *$P < 0.05$ versus nonseeded. ad-MVF, adipose tissue-derived microvascular fragments; d, day.

Finally, we could show that the improved vascularization of vessel-seeded Integra resulted in an enhanced tissue integration of the implants, as indicated by a significantly higher collagen content when compared with nonseeded controls. Moreover, the formation of a multilayered epithelium covering the implants was markedly accelerated. This further supports the idea of using ad-MVF to reduce the time period until coverage of the implants by STSG to a minimum. Under clinical conditions, this approach may have the advantage that ad-MVF could be harvested minimally invasively from lipoaspirated human fat tissue with low donor site morbidity. Because ad-MVF represent fully functional vascularization units, they could be directly seeded on Integra and retransferred to the patient in an intraoperative one-step procedure without the need of prolonged in vitro incubation procedures to stimulate blood vessel formation. In the future, this may be achieved by means of automated closed-system devices, as they are already available for the preparation of stem cell or platelet-rich plasma products (Cohn et al., 2015; Donnenberg et al., 2011).

This study shows that the seeding of Integra with ad-MVF markedly improves the vascularization, lymphangiogenesis, and integration of the dermal matrix during the initial 14 days after implantation. Hence, this approach may contribute in the future to reducing the infection risk and hospitalization of patients undergoing the treatment of full-thickness skin defects.

MATERIALS AND METHODS
Animals
Dorsal skinfold chambers were implanted in male wild-type C57BL/6 mice (Institute for Clinical & Experimental Surgery, Saarland University, Homburg/Saar, Germany) with an age of 4—6 months and a body weight of 24—28 g. Epididymal fat was harvested from male C57BL/6-Tg(CAG-EGFP)1Osb/J mice (The Jackson Laboratory, Bar Harbor, ME, USA) with an age of 12—18 months and a body weight of 30 g or greater.

The animals were housed one per cage under a 12-hour day/night cycle and were fed ad libitum with water and standard pellet food (Atromin, Lage, Germany). The local governmental animal care committee approved all experiments, which were conducted in accordance with the European legislation on the protection of animals (Directive 2010/63/EU) and the National Institutes of Health guidelines on the care and use of laboratory animals (National Institutes of Health publication #85-23 Rev. 1985).

Isolation of ad-MVF
GFP$^+$ donor mice were anesthetized by intraperitoneal injection of ketamine (75 mg/kg body weight; Ursotamin, Serumwerk Bernburg AG, Bernburg, Germany) and xylazine (15 mg/kg body weight; Rompun, Bayer, Leverkusen, Germany). After laparotomy, the animals were killed by incision of the abdominal aorta. The bilateral epididymal fat pads were transferred into 10% DMEM (100 U/ml penicillin, 0.1 mg/ml streptomycin; Biochrom, Berlin, Germany). The fat was washed three times in phosphate buffered saline. The tissue was minced with a fine scissors and digested in collagenase NB4G (0.5 U/ml; Serva, Heidelberg, Germany) for 9 minutes while being stirred under humidified atmospheric conditions (37 °C, 5% CO_2). After tissue digestion, the enzyme was neutralized with phosphate buffered saline mixed with 20% fetal calf serum and the

cell-vessel suspension was incubated for 5 minutes at 37 °C. This incubation cycle was repeated three to five times to remove the fat supernatants after each cycle. The suspension was further filtered once with a 500-μm mesh (pluriSelect Life Science, Leipzig, Germany) to remove remaining fat clots. The suspension contained GFP$^+$ ad-MVF that were enriched to a pellet by centrifugation for 5 minutes at 120g. Finally, the pellet was resuspended in phosphate buffered saline containing 20% fetal calf serum to prevent agglutination of individual ad-MVF.

Flow cytometry
The cellular composition of ad-MVF was characterized by means of flow cytometry. For this purpose, isolated ad-MVF from six male C57BL/6 donor mice (pooled in three separate assays) were digested in Accutase (BioLegend, Fell, Germany) for 30 minutes into single cells. The cells were analyzed for the expression of the monoclonal rat anti-mouse endothelial cell marker CD31-PE (BD Biosciences, Heidelberg, Germany) and the monoclonal stromal/stem cell surface markers rat anti-mouse CD117-FITC (BD Biosciences), mouse anti-mouse CD90-FITC (BioLegend), and hamster anti-mouse CD29-FITC (BioLegend). Isotype-identical rat IgG2aκ-PE or IgG2aκ-FITC (BD Biosciences), mouse Ig1κ-FITC (BD Biosciences) and hamster IgG-FITC (BioLegend) served as controls. In addition, the cells were analyzed for the expression of the polyclonal sheep anti-adipocyte marker adipocyte-specific adhesion molecule (Bio-Techne, Wiesbaden, Germany) followed by a secondary donkey anti-sheep IgG-Alexa488 antibody (Molecular Probes, Eugene, OR). Flow cytometric analyses were performed by means of a FACScan (BD Biosciences). Data were assessed using the software package CellQuest Pro (BD Biosciences).

Implant seeding
Integra matrices were placed on a 500-μm cell strainer (pluriSelect, Life Science), and 10 μl phosphate buffered saline containing ad-MVF were transferred on the samples with a 100-μl pipette (Eppendorf, Wesseling-Berzdorf, Germany). Negative pressure was applied with a syringe to facilitate seeding of central areas.

Dorsal skinfold chamber model
To mount the chamber, the mice were anesthetized as described. A detailed description of the implantation procedure is given in Laschke et al. (2011). To prevent postoperative alterations of the local microcirculation due to anesthesia and surgery, the animals were allowed to recover for 48 hours before defect preparation and matrix implantation.

Microscopy and microcirculatory analysis
The anesthetized animals were fixed on an acrylic glass stage, and the dorsal skinfold chamber was positioned horizontally under a stereomicroscope (Leica M651; Leica, Wetzlar, Germany) to quantify the epithelial coverage of the implants by planimetry. The chamber tissue was visualized by epi-illumination and transillumination to identify epithelialized and nonepithelialized areas. Epithelialization (given in percentage) was defined as (total implant area) − (nonepithelialized implant area)/(total implant area) × 100.

For intravital fluorescence microscopy, 0.1 ml of 5% FITC-labeled dextran (molecular weight = 150,000 Da; Sigma-Aldrich, Taufkirchen, Germany) were injected retrobulbarily for contrast enhancement by staining of the blood plasma. The observation window was positioned under a Zeiss Axiotech microscope (Zeiss, Oberkochen, Germany), and the images were transferred to a DVD system for offline analysis (Ehrmantraut et al., 2010).

Image analysis was performed with the software package CapImage (Zeintl, Heidelberg, Germany). The vascularization of the implants was assessed in 12 different ROIs. Perfused ROIs (in percentage of all ROIs) were defined as ROIs exhibiting either newly developed RBC-perfused microvessels or GFP$^+$ ad-MVF. We further assessed the functional microvessel density, that is, the length of all RBC-perfused microvessels per ROI in cm/cm^2. Finally, we measured the diameter (d, in µm) and the centerline RBC velocity (v, in µm/s) of 40 randomly selected microvessels in ROIs with established blood flow. To calculate the wall shear rate (y, in s^{-1}), we used the Newtonian definition $y = 8 \times v/d$ (Ehrmantraut et al., 2010).

Experimental protocol

ad-MVF were harvested from four male C57BL/6-Tg(CAG-EGFP)1Osb/J donor mice and seeded on eight Integra matrices. The prevascularized matrices and eight nonseeded control matrices were implanted into full-thickness skin defects in dorsal skinfold chambers of 16 wild-type C57BL/6 mice. Epithelialization and vascularization of the implants were analyzed using epi-illumination and transillumination stereomicroscopy and intravital fluorescence microscopy directly after implantation (day 0) and at days 3, 6, 10, and 14. Finally, the animals were killed with an anesthesia overdose and tissue specimens were further processed for histological and immunohistochemical analyses.

In addition, ad-MVF were harvested from four male wild-type C57BL/6 mice and seeded on eight Integra matrices. Four matrices were directly processed for the histological assessment of the seeding quality without in vivo implantation. The other four matrices were implanted into four wild-type C57BL/6 mice for the immunohistochemical analysis of apoptotic cell death at day 3.

Histology and immunohistochemistry

Formalin-fixed tissue samples were embedded in paraffin and cut into 3-µm—thick sections. Individual sections were stained with hematoxylin and eosin. To quantify the collagen content of the implants, additional sections were stained with Sirius red. Using a BX60 microscope (Olympus, Hamburg, Germany) and the imaging software cellSens Dimension 1.11 (Olympus), the collagen content in relation to normal skin was assessed in four ROIs of each sample.

For the immunohistochemical analysis of implant epithelialization, sections were stained with a polyclonal rabbit antibody against cytokeratin (1:100, Abcam, Cambridge, UK) followed by a biotinylated goat anti-rabbit IgG antibody (ready-to-use; Abcam). The biotinylated antibody was detected by peroxidase-labeled streptavidin (1:50; Sigma-Aldrich). 3-Amino-9-ethylcarbazole (Abcam) was used as chromogen. The length of the cytokeratin$^+$ multilayered epithelium and the diameter of the implants were measured to assess epithelialization as (length of epithelium)/(total diameter of implant) × 100.

Additional sections were stained with a monoclonal rat anti-mouse antibody against CD31 (1:100; dianova GmbH, Hamburg, Germany) and a polyclonal rabbit antibody against LYVE-1 (1:200; Abcam). A goat anti-rat IgG-Alexa555 antibody (1:100; Molecular Probes, Eugene, OR, USA) and a goat anti-rabbit IgG-Alexa555 antibody (1:200; Molecular Probes) served as secondary antibodies. On each section, cell nuclei were stained with Hoechst 33342 (1:500; Sigma-Aldrich) to merge the images exactly. Quantitative analyses of the sections included the determination of the microvessel density and lymphatic vessel density within the implants and the adjacent skin, that is, the border of the implants.

For the immunohistochemical differentiation between GFP$^+$ and GFP$^-$ blood and lymphatic vessels, sections were stained with the listed primary and secondary antibodies against CD31 and LYVE-1 and with a polyclonal goat anti-GFP antibody (1:100; Rockland, Limerick, PA) to enhance GFP fluorescence. As secondary antibody we used a biotin-labeled donkey anti-goat IgG antibody (1:15; Jackson ImmunoResearch, Baltimore, MD), which was detected by fluorescein labeled-streptavidin (1:50; Vector Labs, Burlingame, CA). For this purpose, the sections were placed in Coplin jars with 0.05% citraconic anhydride solution (pH 7.4) for 1 hour at 98 °C and then incubated overnight at 4 °C with the primary antibody, followed by the secondary antibody at 37 °C for 2 hours. The fractions of GFP$^+$ and GFP$^-$ blood and lymphatic vessels within the implants and the adjacent skin were assessed using the BX60 microscope.

For the characterization of freshly seeded ad-MVF, sections were stained with a monoclonal mouse anti-mouse antibody against α-smooth muscle actin (1:100; Sigma-Aldrich) followed by a secondary peroxidase-labeled goat anti-mouse antibody (1:200; dianova GmbH).

Statistics

Data were tested for normal distribution and equal variance. Differences between two groups were analyzed using the unpaired Student t test (SigmaStat; Jandel Corporation; San Rafael, CA). All values are expressed as mean ± standard error of the mean. Statistical significance was accepted for values of $P < 0.05$.

CONFLICT OF INTEREST

The authors declare no conflict of interest.

SUPPLEMENTARY MATERIAL

Supplementary material is linked to the online version of the paper at www.jidonline.org, and at http://dx.doi.org/10.1016/j.jid.2016.08.010.

REFERENCES

Athanassopoulos A, Tsaknakis G, Newey SE, Harris AL, Kean J, Tyler MP, et al. Microvessel networks [corrected] pre-formed in artificial clinical grade dermal substitutes in vitro using cells from haematopoietic tissues. Burns 2012;38:691—701.

Auger FA, Gibot L, Lacroix D. The pivotal role of vascularization in tissue engineering. Annu Rev Biomed Eng 2013;15:177—200.

Burke JF, Yannas IV, Quinby WC Jr, Bondoc CC, Jung WK. Successful use of a physiologically acceptable artificial skin in the treatment of extensive burn injury. Ann Surg 1981;194:413—28.

Cherubino M, Pellegatta I, Tamborini F, Cerati M, Sessa F, Valdatta L. Evaluation of lymphangiogenesis in acellular dermal matrix. Indian J Plast Surg 2014;47:318—24.

Clark RA, Ghosh K, Tonnesen MG. Tissue engineering for cutaneous wounds. J Invest Dermatol 2007;127:1018—29.

Cohn CS, Lockhart E, McCullough JJ. The use of autologous platelet-rich plasma in the orthopedic setting. Transfusion 2015;55:1812—20.

Debels H, Hamdi M, Abberton K, Morrison W. Dermal matrices and bioengineered skin substitutes: a critical review of current options. Plast Reconstr Surg Glob Open 2015;3:e284.

Donnenberg AD, Donnenberg VS, Griffin DL, Moore LR, Tekinturhan F, Kormos RL. Intra-operative preparation of autologous bone marrow-derived CD34-enriched cellular products for cardiac therapy. Cytotherapy 2011;13:441—8.

Egaña JT, Danner S, Kremer M, Rapoport DH, Lohmeyer JA, Dye JF, et al. The use of glandular-derived stem cells to improve vascularization in scaffold-mediated dermal regeneration. Biomaterials 2009;30:5918—26.

Ehrmantraut S, Laschke MW, Merkel D, Scheuer C, Willnecker V, Meyer-Lindenberg A, et al. Perioperative steroid administration inhibits angiogenic host tissue response to porous polyethylene (Medpor) implants. Eur Cell Mater 2010;19:107—16.

Formigli L, Paternostro F, Tani A, Mirabella C, Quattrini Li A, Nosi D, et al. MSCs seeded on bioengineered scaffolds improve skin wound healing in rats. Wound Repair Regen 2015;23:115—23.

Frueh FS, Gousopoulos E, Rezaeian F, Menger MD, Lindenblatt N, Giovanoli P. Animal models in surgical lymphedema research-a systematic review. J Surg Res 2016;200:208—20.

Griffin DR, Weaver WM, Scumpia PO, Di Carlo D, Segura T. Accelerated wound healing by injectable microporous gel scaffolds assembled from annealed building blocks. Nat Mater 2015;14:737—44.

Junqueira LC, Bignolas G, Bretani RR. Picrosirius staining plus polarization microscopy, a specific method for collagen detection in tissue sections. Histochem J 1979;11:447—55.

Laschke MW, Grässer C, Kleer S, Scheuer C, Eglin D, Alini M, et al. Adipose tissue-derived microvascular fragments from aged donors exhibit an impaired vascularisation capacity. Eur Cell Mater 2014;28:287—98.

Laschke MW, Harder Y, Amon M, Martin I, Farhadi J, Ring A, et al. Angiogenesis in tissue engineering: breathing life into constructed tissue substitutes. Tissue Eng 2006;12:2093—104.

Laschke MW, Kleer S, Scheuer C, Schuler S, Garcia P, Eglin D, et al. Vascularisation of porous scaffolds is improved by incorporation of adipose tissue-derived microvascular fragments. Eur Cell Mater 2012;24:266—77.

Laschke MW, Menger MD. Adipose tissue-derived microvascular fragments: natural vascularization units for regenerative medicine. Trends Biotechnol 2015;33:442—8.

Laschke MW, Menger MD. Prevascularization in tissue engineering: current concepts and future directions. Biotechnol Adv 2016;34:112—21.

Laschke MW, Vollmar B, Menger MD. Inosculation: connecting the life-sustaining pipelines. Tissue Eng Part B Rev 2009;15:455—65.

Laschke MW, Vollmar B, Menger MD. The dorsal skinfold chamber: window into the dynamic interaction of biomaterials with their surrounding host tissue. Eur Cell Mater 2011;22:147—64.

Marino D, Luginbühl J, Scola S, Meuli M, Reichmann E. Bioengineering dermo-epidermal skin grafts with blood and lymphatic capillaries. Sci Transl Med 2014;6:221ra14.

McDaniel JS, Pilia M, Ward CL, Pollot BE, Rathbone CR. Characterization and multilineage potential of cells derived from isolated microvascular fragments. J Surg Res 2014;192:214—22.

Meruane MA, Rojas M, Marcelain K. The use of adipose tissue-derived stem cells within a dermal substitute improves skin regeneration by increasing neo-angiogenesis and collagen synthesis. Plast Reconstr Surg 2012;130:53—63.

Michael S, Sorg H, Peck CT, Koch L, Deiwick A, Chichkov B, et al. Tissue engineered skin substitutes created by laser-assisted bioprinting form skin-like structures in the dorsal skin fold chamber in mice. PLoS One 2013a;8:e57741.

Michael S, Sorg H, Peck CT, Reimers K, Vogt PM. The mouse dorsal skin fold chamber as a means for the analysis of tissue engineered skin. Burns 2013b;39:82—8.

Okabe M, Ikawa M, Kominami K, Nakanishi T, Nishimune Y. 'Green mice' as a source of ubiquitous green cells. FEBS Lett 1997;407:313—9.

Pilia M, McDaniel JS, Guda T, Chen XK, Rhoads RP, Allen RE, et al. Transplantation and perfusion of microvascular fragments in a rodent model of volumetric muscle loss injury. Eur Cell Mater 2014;28:11—23.

Reckhenrich AK, Hopfner U, Krötz F, Zhang Z, Koch C, Kremer M, et al. Bioactivation of dermal scaffolds with a non-viral copolymer-protected gene vector. Biomaterials 2011;32:1996—2003.

Reiffel AJ, Henderson PW, Krijgh DD, Belkin DA, Zheng Y, Bonassar LJ, et al. Mathematical modeling and frequency gradient analysis of cellular and vascular invasion into integra and strattice: toward optimal design of tissue regeneration scaffolds. Plast Reconstr Surg 2012;129:89—99.

Shevchenko RV, James SL, James SE. A review of tissue-engineered skin bioconstructs available for skin reconstruction. J R Soc Interface 2010;7:229—58.

Sorg H, Krueger C, Schulz T, Menger MD, Schmitz F, Vollmar B. Effects of erythropoietin in skin wound healing are dose related. FASEB J 2009;23:3049—58.

Sorg H, Krueger C, Vollmar B. Intravital insights in skin wound healing using the mouse dorsal skin fold chamber. J Anat 2007;211:810—8.

Utzinger U, Baggett B, Weiss JA, Hoying JB, Edgar LT. Large-scale time series microscopy of neovessel growth during angiogenesis. Angiogenesis 2015;18:219—32.

van der Veen VC, van der Wal MB, van Leeuwen MC, Ulrich MM, Middelkoop E. Biological background of dermal substitutes. Burns 2010;36:305—21.

SCIENTIFIC REP✦RTS

Prevascularization of dermal substitutes with adipose tissue-derived microvascular fragments enhances early skin grafting

Florian S. Frueh [1,2], Thomas Später[1], Christina Körbel[1], Claudia Scheuer[1], Anna C. Simson[1], Nicole Lindenblatt[2], Pietro Giovanoli[2], Michael D. Menger[1] & Matthias W. Laschke[1]

Split-thickness skin grafts (STSG) are still the gold standard for the treatment of most skin defects. Hence, there is an ongoing need to improve this procedure. For this purpose, we herein analyzed dermal matrices seeded with adipose tissue-derived microvascular fragments (ad-MVF) in a bradythrophic wound model. In additional experiments, the matrices were covered with autologous STSG 10 days after implantation. Green fluorescence protein (GFP)+ ad-MVF were isolated from C57BL/6-Tg(CAG-EGFP)1Osb/J mice and seeded onto collagen-glycosaminoglycan matrices. Non-seeded and prevascularized matrices were implanted into full-thickness skin defects on the skull of CD1 nu/nu mice for 21 days. Vascularization, lymphangiogenesis and incorporation of the matrices were analyzed using photo-acoustic imaging, trans-illumination stereomicroscopy, histology, and immunohistochemistry. The survival rate of STSG was assessed by planimetry. After 21 days, the density of microvascular and lymphatic networks was significantly higher in prevascularized matrices when compared to controls. This was associated with an improved implant integration. Moreover, prevascularization with ad-MVF allowed successful autologous skin grafting already at day 10, while coverage of non-seeded controls at day 10 resulted in STSG necrosis. In conclusion, ad-MVF represent powerful vascularization units. Seeded on dermal substitutes, they accelerate and enhance the healing of full-thickness skin defects and allow early coverage with STSG.

Full-thickness skin defects with impaired vascularization are a reconstructive challenge. These wounds are typically encountered when treating diabetic ulcers, burn injuries, or after tumor resection[1]. In the United States, around 6.5 million patients are affected by chronic wounds and the burden is growing due to an aging population and rising incidence of diabetes and obesity[2]. Thus, there is an on-going need to develop innovative wound-healing strategies.

The treatment of bradytrophic wounds with split-thickness skin grafts (STSG) alone is rarely successful, because the underlying tissues do not exhibit a sufficient vascularization capacity. Moreover, STSG without dermal support are prone to extensive scarring and contraction[3]. To overcome these problems, bioengineered dermal substitutes have been introduced. The FDA-approved Integra (Integra Life Sciences, Plainsboro, NJ, USA) consists of a collagen-glycosaminoglycan matrix with a silicone pseudo-epidermis and is frequently used in clinical practice[4]. However, microvascular network formation within the matrix requires up to 3 weeks before STSG coverage can be performed[5]. This vascularization kinetics crucially determines the risk of wound infection, which is elevated as long as the physiological barrier of the skin is not re-established[6].

The vascularization of dermal substitutes can be improved by means of angiogenic or prevascularization approaches[7]. Prevascularization based on the seeding of adipose tissue-derived microvascular fragments (ad-MVF) is particularly suitable for intraoperative one-step procedures and, therefore, a promising strategy for future clinical application[8,9]. Ad-MVF are functional vessel segments that rapidly reassemble into microvascular networks after transplantation[10]. Recently, we demonstrated that the prevascularization of Integra with ad-MVF enhances incorporation and epithelialization as well as the development of microvascular and lymphatic

[1]Institute for Clinical and Experimental Surgery, Saarland University, 66421, Homburg/Saar, Germany. [2]Division of Plastic Surgery and Hand Surgery, University Hospital Zürich, University of Zürich, 8091, Zürich, Switzerland. Correspondence and requests for materials should be addressed to F.S.F. (email: florian.frueh@usz.ch)
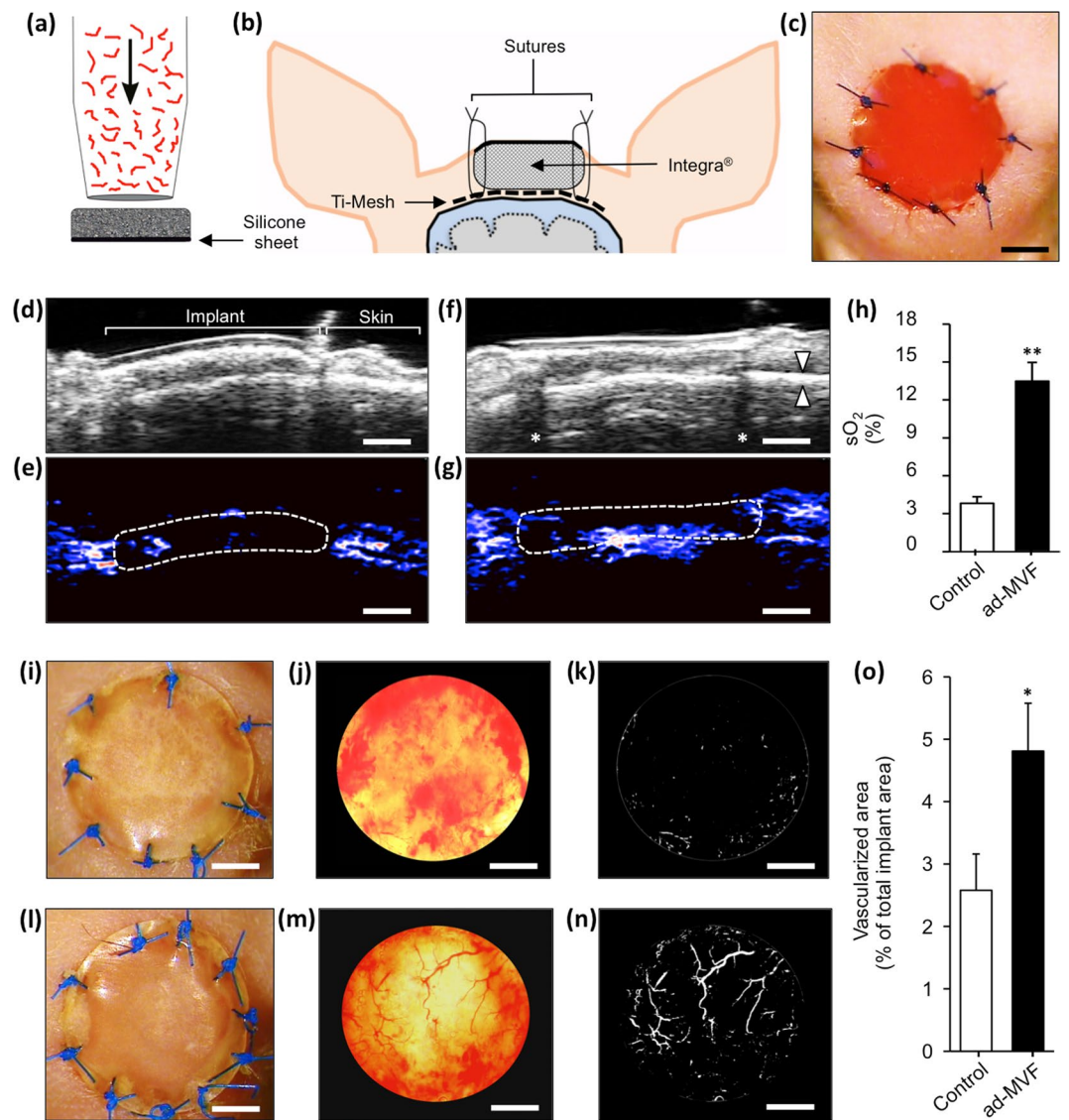
Figure 1. Animal model, photo-acoustic imaging and trans-illumination stereomicroscopy. (**a**–**c**) After the seeding process (**a**), the matrices were implanted into full-thickness skin defects on the skull of CD1 nu/nu mice (**b** and **c**). (**d**–**g**) B-mode ultrasound (**d** and **f**) and OxyHemo-mode photo-acoustic imaging (**e** and **g**) of non-seeded (**d** and **e**) and prevascularized (**f** and **g**) Integra 21 days after implantation. Red areas = high oxygenation, blue areas = low oxygenation, arrowheads in **f** = frontal calvaria, asterisks in **f** = dorsal acoustic attenuation (sutures), broken line in **e** and **g** = implants. (**h**) Quantification of sO$_2$ (%). Mean ± SEM, n = 8, **$P < 0.001$ vs. non-seeded control. (**i**–**n**) Epi-illumination (**i** and **l**) and trans-illumination (**j** and **m**) microscopy with digital segmentation images (**k** and **n**) of non-seeded (**i**–**k**) and prevascularized (**l**–**n**) Integra. (**o**) Quantification of vascularized area (% of total implant area). Mean ± SEM, n = 8, *$P < 0.05$ vs. non-seeded control. Scale bars: **c** = 2.5 mm, **d**–**g** = 1.8 mm, **i**–**n** = 2 mm.

networks within the matrix[11]. These results led to the hypothesis that ad-MVF seeding may also accelerate the integration and vascularization of Integra in bradytrophic wounds, which may then allow early skin grafting.

To test this hypothesis, we used a full-thickness skin defect model on the skull of mice, mimicking bradytrophic wounds after tumor resection on the human scalp. Implanted non-seeded and prevascularized Integra matrices were assessed for 21 days using stereomicroscopy, photo-acoustic imaging, histology and immunohistochemistry. In a subsequent proof-of-principle experiment, coverage with autologous STSG was performed 10 days after Integra implantation and the grafts' survival was analyzed.

Results

Full-thickness skin defect model. Ad-MVF were isolated from green fluorescent protein (GFP)$^+$ donor mice and seeded onto Integra as previously described[11,12] (Fig. 1a). Non-seeded Integra served as control. To analyze the vascularization and incorporation of the matrices, full-thickness skin defects were prepared on the skull of CD1 nu/nu mice. For this purpose, we modified the head punch model[13,14] and prepared an 8 mm skin defect
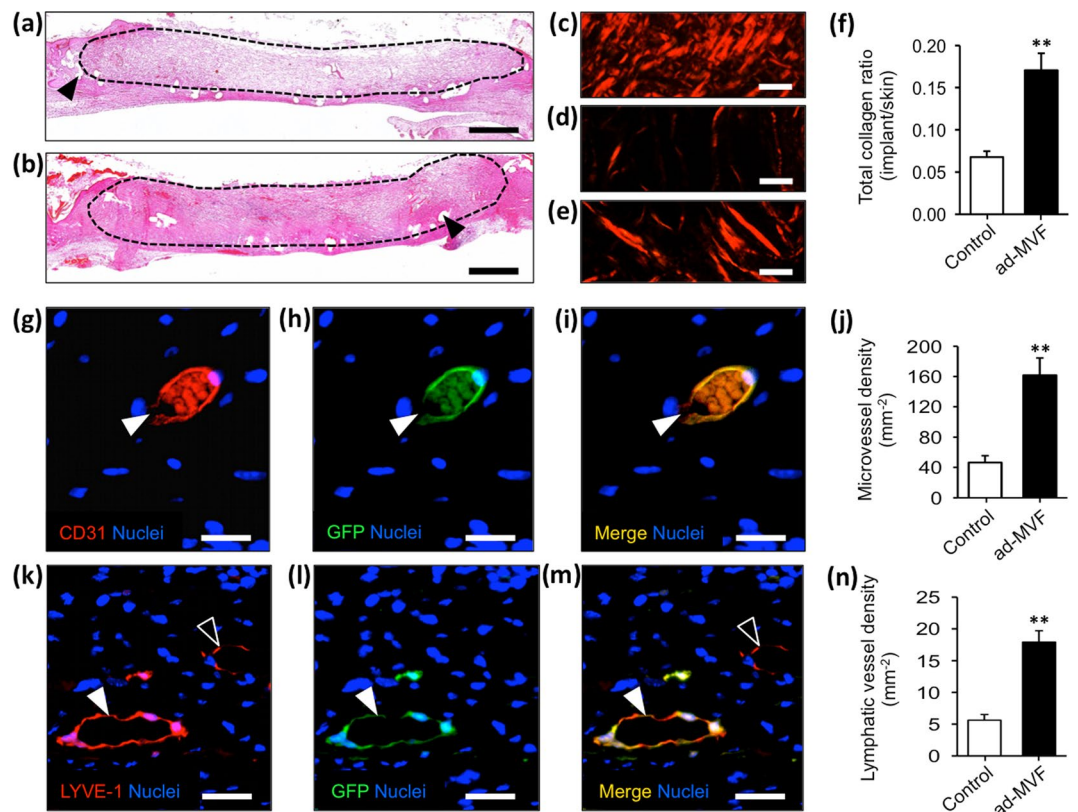
Figure 2. Histology and immunohistochemistry. (**a** and **b**) HE-stained sections of non-seeded (**a**) and prevascularized (**b**) implants. Broken line = implant border, arrowheads = mesh fibers. (**c–e**) Polarized light microscopy of Sirius red-stained sections of normal skin (**c**), non-seeded (**d**) and prevascularized (**e**) Integra. (**f**) Quantification of total collagen ratio (implant/skin). Mean ± SEM, n = 8, **$P < 0.001$ vs. non-seeded control. (**g–i** and **k–m**) Immunohistochemical staining of microvessels (**g–i**, white arrowhead = CD31$^+$/GFP$^+$ microvessel) and lymphatic vessels (**k–m**, white arrowhead = LYVE-1$^+$/GFP$^+$ lymphatic vessel, empty arrowhead = LYVE-1$^+$/GFP$^-$ lymphatic vessel) within prevascularized Integra 21 days after implantation. (**j** and **n**) Quantification of microvessel density (mm^{-2}) and lymphatic vessel density (mm^{-2}). Mean ± SEM, n = 8, **$P < 0.001$ vs. non-seeded control. Scale bars: **a** and **b** = 800 μm, **c–e** = 20 μm, **g–i** = 20 μm, **k–m** = 30 μm.

on the crown of the skull. The periosteum was resected to create a poorly vascularized, bradytrophic wound bed. To ensure implant immobilization, a titanized mesh was placed on the bone overlapping the wound edges according to a published model[15]. Subsequently, non-seeded and ad-MVF-seeded (prevascularized) Integra matrices were implanted and secured with sutures (Fig. 1b and c).

Photo-acoustic imaging and trans-illumination stereomicroscopy. Photo-acoustic imaging was performed to quantify *in situ* the oxygen saturation within the neo-dermis of non-seeded and prevascularized Integra 21 days after implantation. This approach revealed that prevascularized matrices were characterized by significantly higher oxygenation levels than non-seeded controls (Fig. 1d–h).

In a next step, the implants were excised and assessed using trans-illumination stereomicroscopy to objectify microvascular network formation. In line with the photo-acoustic results, this analysis revealed a significantly reduced vascularization in non-seeded controls when compared to matrices seeded with ad-MVF (Fig. 1i–o).

Histology and immunohistochemistry. Histological analyses of the implants showed that non-seeded Integra was characterized by a low cellular infiltration (Fig. 2a). In contrast, the neo-dermis of prevascularized Integra exhibited a dense granulation tissue (Fig. 2b). Accordingly, the integration of the prevascularized matrices was markedly enhanced, as indicated by significantly more mature Sirius red stained collagen fibers when compared to non-seeded controls (Fig. 2c–f).

Immunohistochemical detection of the endothelial cell marker CD31 demonstrated that the prevascularized matrices exhibited a 3.5-fold higher microvessel density 21 days after implantation when compared to non-seeded controls (Fig. 2g–j). GFP/CD31 co-staining further revealed that > 95% of the microvessels within the prevascularized implants were GFP$^+$. Moreover, the lymphatic vessel density of prevascularized implants was markedly increased (Fig. 2k–n). However, compared to the microvasculature, a lower fraction of lymphatic vessels exhibited a GFP$^+$ signal (88 ± 1%).

Autologous skin grafting.   In additional experiments, we analyzed the survival of autologous STSG, which were transplanted onto non-seeded and prevascularized Integra 10 days after implantation. Full-thickness skin grafts (Fig. 3a) were harvested from the groin of CD1 nu/nu mice and defatted to imitate STSG (Fig. 3b). The STSG were then transplanted onto the matrices and secured with sutures. To protect the STSG from exsiccation, a sterile plastic dressing (Fig. 3c) and a second titanized mesh were fixed to the previously implanted mesh (Fig. 3d and e).

Planimetric and histological analysis of STSG.   The survival of the STSG was assessed by planimetric analyses 5 days after transplantation. STSG on prevascularized Integra exhibited a survival rate of $40 \pm 11\%$. In contrast, skin grafting on non-seeded controls resulted in a significantly lower transplant survival of $5 \pm 5\%$ (Fig. 3f–j).

Histological analyses revealed that dermal thickness and hierarchical integrity of the STSG were more preserved in the prevascularized group when compared to controls (Fig. 3k and l). Moreover, the transplantation of STSG on prevascularized implants also resulted in a thicker cytokeratin+ epidermis (Fig. 3m and n). Finally, immunohistochemical GFP/CD31 co-staining was performed for a qualitative assessment of cell migration into the STSG. Of interest, we detected a few GFP+ cells, which were incorporated into the CD31+ endothelium of individual microvessels (Fig. 3o–q).

Discussion

The treatment of bradytrophic skin defects is a major challenge. In the last decade, skin tissue engineering has evolved dramatically with promising approaches to manage difficult wounds[16]. In fact, preconditioned hydrogels[17–19], microporous gels[20] or engineered cell sheets[21,22] exhibit a tremendous wound healing potential in the preclinical setting. However, the majority of these techniques involves complex *in vitro* steps and, thus, is not suitable for intraoperative one-step procedures. Hence, straightforward strategies need to be developed.

We have recently introduced ad-MVF-seeded Integra as a powerful strategy to treat full-thickness skin defects[11]. In the present study, we further evaluated this approach in a murine wound model with early STSG coverage. For this purpose, we used hairless CD1 nu/nu mice, because they enabled the application of compressive wound dressings and photo-acoustic imaging without the need for repetitive mechanical and chemical skin depilation, which may have markedly affected the incorporation of the implanted matrices and the engraftment of STSG. In addition, these immunoincompetent animals allowed the transplantation of ad-MVF from GFP+ donor mice without inducing a rejection reaction. Hence, it was possible to identify GFP+ ad-MVF-derived and GFP- host-derived blood and lymphatic vessels within the implanted matrices. On the other hand, it should be considered that CD1 nu/nu mice lack a thymus and, thus, are unable to produce T-cells. Importantly, epidermal and dermal T-cells are crucially involved in the regulation of murine wound healing by local production of epithelial growth factors and inflammatory cytokines[23–26]. Moreover, human epidermal T-cells have been shown to contribute to the effective healing of acute wounds and are functionally defective in patients with chronic wounds[27,28]. Accordingly, it can be assumed that the implantation of ad-MVF-seeded matrices into immunocompetent animals might have even resulted in an improved vascularization and incorporation of the implants when compared to the herein reported results. This further underlines the high potential of ad-MVF for applications in regenerative medicine.

To create full-thickness skin defects with a poorly vascularized wound bed, we combined two mouse models[13,15]. Even though the literature negates wound contraction in the head punch model[29] we observed implant loss without additional stabilization. Hence, we used a titanized mesh to secure the dermal substitute. Importantly, we did not observe significant foreign body reactions around the mesh. In our model, the surrounding skin margin represented the only site for ad-MVF inosculation or angiogenic ingrowth.

Photo-acoustic imaging and trans-illumination stereomicroscopy showed a significantly higher oxygenation and vascularization in the prevascularized matrices when compared to non-seeded controls. Accordingly, we also measured an increased microvessel density. Moreover, >95% of the microvessels within the prevascularized implants were GFP+, indicating that they originated from the seeded ad-MVF. This finding is important, because in contrast to previous studies[11,30,31] we herein used the double-layer Integra, which is covered with a silicone sheet. Hence, ad-MVF could only be seeded on the bottom side of the matrices and were implanted in direct contact to the bone of the mouse skull. Nonetheless, GFP+ microvessels were homogeneously distributed in deep and superficial layers of the matrices at day 21 after implantation. This suggests that the ad-MVF even survive in an initially poorly oxygenated environment and rapidly reassemble into new microvascular networks, most probably driven by hypoxia-induced secretion of angiogenic growth factors.

The two-staged treatment of bradytrophic skin defects with dermal substitutes and STSG is a common procedure in clinical practice. To further unravel the potential of prevascularization with ad-MVF, we assessed the fate of autologous STSG in a proof-of-principle experiment. The application of STSG in mice is technically demanding due to the small animal size and thin skin. Because conventional STSG harvesting is not feasible, we microsurgically removed the panniculus carnosus muscle and the deep dermal layer of excised skin samples. This resulted in skin grafts similar to STSG. The compression of these grafts was the major prerequisite for successful engraftment. For this purpose, we fixed them with a titanized mesh, which was well tolerated by the animals. No graft was lost due to manipulation. In pilot experiments, we performed STSG coverage already at day 0, i.e. immediately after the implantation of Integra. However, this one-step procedure was not effective with complete graft necrosis. This may be explained by the fact that the onset of blood perfusion in ad-MVF-derived microvascular networks requires 3–6 days[11]. Consequently, we decided to cover the implants at day 10. At this time point, the neo-dermis of the prevascularized matrices was stable and allowed STSG coverage. Importantly, graft survival in the prevascularized group was significantly improved when compared to non-seeded controls.
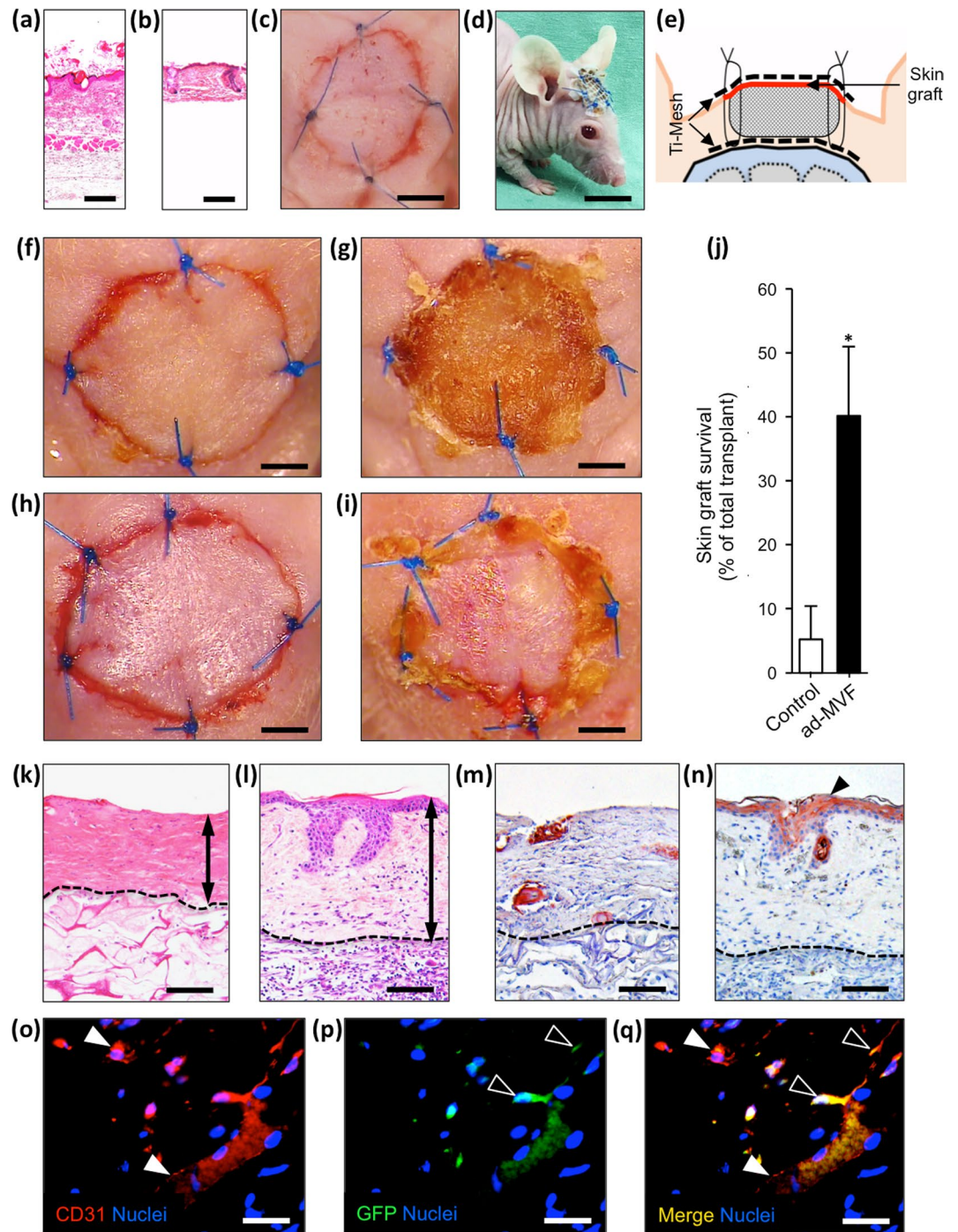
Figure 3. Autologous skin grafting. (**a**–**e**) HE-stained sections of a skin graft before (**a**) and after (**b**) defatting. The autologous grafts are transferred onto implanted Integra and are secured with sutures, a sterile plastic dressing (**c**) and a titanized mesh (**d** and **e**). (**f**–**i**) Stereomicroscopy of non-seeded (**f** and **g**) and prevascularized (**h** and **i**) implants immediately (**f** and **h**) and 5 days (**g** and **i**) after skin grafting. (**j**) Quantification of skin graft survival (% of total transplant) 5 days after transplantation. Mean ± SEM, n = 6, *$P < 0.05$ vs. non-seeded control. (**k** and **l**) HE-stained sections after skin grafting of non-seeded (**k**) and prevascularized (**l**) Integra. Double arrows = graft thickness. (**m** and **n**) Immunohistochemical detection of cytokeratin+ epithelium (**n**, arrowhead) after grafting of a non-seeded (**m**) and prevascularized (**n**) matrix. (**o**–**q**) Immunohistochemical detection of CD31+ microvessels (**o** and **q**, white arrowheads) within a skin graft 5 days after transplantation on prevascularized Integra. CD31/GFP co-staining reveals CD31+/GFP+ cells (**p** and **q**, empty arrowheads) involved in microvessel formation. Scale bars: **a** and **b** = 120 μm, **c** = 3 mm, **d** = 9 mm, **f**–**i** = 1.8 mm, **k**–**n** = 80 μm, **o**–**q** = 35 μm.

Previous experiments with full-thickness skin grafts in the dorsal skinfold chamber model revealed that blood vessel ingrowth from the wound bed crucially contributes to graft revascularization[32,33]. In these studies, reperfusion was established ~3 days after transplantation and subsequently, an angiogenic response was detected within the skin grafts' capillaries. Of interest, angiogenesis started in the center of the grafts, indicating that the hypoxic stimulus may be most prominent in this area[33]. Accordingly, our study also revealed graft survival mainly in the center of the transplants. This finding was consistent in all vital grafts and supports the theory of hypoxia-induced angiogenesis in central parts of STSG.

Ad-MVF are a rich source of regenerative cells. In fact, they contain a relevant fraction of Sca-1^{+}/VEGFR-2^{+} endothelial progenitor cells[10,34]. These cells boost wound revascularization and reoxygenation in mice[35]. To analyze cellular interactions between the wound bed and the skin grafts, co-staining with CD31/GFP was performed. Indeed, we could show that GFP^{+} cells incorporated into the CD31^{+} endothelium of individual microvessels within the STSG. Hence, it can be assumed that the revascularization of the grafts was achieved by external inosculation, i.e. the outgrowth of the grafts' microvessels into the surrounding skin[36], and by the ingrowth of GFP[+] ad-MVF-derived vascular sprouts from the prevascularized matrices. However, this conclusion may not completely explain the advantageous effect of prevascularized Integra on the survival rate of STSG. As indicated by photo-acoustic imaging, the prevascularized matrices exhibited a significantly higher oxygen level. Consequently, we speculate that the ~200 μm thick skin grafts on ad-MVF-enhanced neo-dermis were supplied by diffusion with life-sustaining oxygen and growth factors to bridge the critical 48–72 h after implantation.

Beside a sufficient vascularization, lymphatic vessel formation is essential to re-establish skin function. Dermal lymphatic vessels are crucially involved in the regulation of tissue fluid homeostasis and immune cell trafficking[37]. Adipose tissue-derived stem cells have shown potential to support lymphangiogenesis *in vitro*[38] and *in vivo*[39]. To assess lymphangiogenic effects within non-seeded and prevascularized Integra, we quantified the lymphatic vessel density 21 days after implantation. We found that prevascularized Integra contained >3-fold more lymphatic vessels than non-seeded controls. We hereby confirm the recently observed lymphangiogenic effect of ad-MVF[11]. Finally, lymphatic vessels play an important role in the engraftment of STSG. However, to observe lymphatic anastomoses between STSG and the wound bed, up to 14 days observation after grafting are required[18]. Accordingly, within the short observation period of 5 days, we were not able to detect lymphatic interconnections in the present study.

In conclusion, this study indicates that ad-MVF represent powerful vascularization units. Seeded on dermal substitutes, they enhance the vascularization and incorporation of dermal substitutes in skin defects exhibiting a bradytrophic wound bed. In addition, they allow the early coverage of Integra with STSG. Hence, they may markedly contribute to shorten the time frame needed for future skin reconstruction and, thus, to reduce the infection risk and hospitalization times for patients.

Methods

Animals.
Full-thickness skin defects were prepared in CD1 nu/nu mice (age: ~3 months, body weight: 30–32 g). Ad-MVF were isolated from C57BL/6-Tg(CAG-EGFP)1Osb/J mice (age: 7–12 months, body weight: >30 g; The Jackson Laboratory, Bar Harbor, ME, USA)[40]. The animals were housed under a 12 h light/dark cycle and received water and standard food pellets (Altromin, Lage, Germany) *ad libitum*.

All experiments were approved by the local governmental animal care committee (Landesamt für Verbraucherschutz, Saarbrücken, Germany; permit number: 25/2016) and conducted in accordance with the European legislation on the protection of animals (Directive 2010/63/EU) and the National Institutes of Health (NIH) guidelines on the care and use of laboratory animals (NIH publication #85–23 Rev. 1985).

Isolation of ad-MVF.
Epididymal fat pads were harvested from GFP[+] donor mice, transferred into 10% Dulbecco's modified eagle medium (DMEM; 100 U/mL penicillin, 0.1 mg/mL streptomycin; Biochrom GmbH, Berlin, Germany), and washed with phosphate-buffered saline (PBS; Biochrom GmbH). The fat was mechanically minced and digested for 10 min with collagenase NB4G (0.5 U/mL; Serva Electrophoresis GmbH, Heidelberg, Germany) while stirring under humidified atmospheric conditions (37 °C, 5% CO_2). The digestion was neutralized with PBS supplemented with 20% fetal calf serum (FCS; Biochrom GmbH) and the cell-vessel suspension was incubated for 5 min at 37 °C. After removal of fat supernatant, the remaining cell-vessel suspension was filtered through a 500 μm mesh (pluriStrainer; pluriSelect Life Science, Leipzig, Germany) and centrifuged for 5 min at 600 × g to obtain a pellet.

Seeding of Integra.
Dermal substitutes (diameter: 8 mm) were cut out of Integra Dermal Regeneration Template (Integra Life Sciences, Ratingen, Germany) with a biopsy punch. For each recipient mouse, a pellet containing ~ 40,000 GFP[+] ad-MVF isolated from 1 mL fat tissue was mixed with 20 μL 0.9% NaCl and was seeded on the collagen-glycosaminoglycan surface of Integra with a 20 μL precision pipette (Eppendorf, Wesseling-Berzdorf, Germany). The same procedure without ad-MVF was performed for non-seeded implants of the control group.

Full-thickness skin defect model.
CD1 nu/nu mice were anesthetized by intraperitoneal injection of ketamine (75 mg/kg; Ursotamin, Serumwerk Bernburg AG, Bernburg, Germany) and xylazine (15 mg/kg; Rompun, Bayer, Leverkusen, Germany) and were placed under a stereomicroscope (Leica M651, Wetzlar, Germany). Subsequently, a skin defect on the crown of the skull was prepared using an 8 mm biopsy punch and the periosteum was resected with microsurgical instruments. A titanized mesh (TiMesh; pfm medical AG, Köln, Germany) was placed on the bone overlapping the wound edges. Next, non-seeded and prevascularized Integra matrices were implanted and secured with interrupted 6/0 monofilament. Postoperative analgesia was provided for 3 days with tramalhydrochloride (40 mg/100 mL drinking water; Grünenthal GmbH, Aachen, Germany).

For the transplantation experiments, full-thickness skin grafts were excised from the right groin of anesthetized CD1 nu/nu mice and defatted under a stereomicroscope. The STSG were transplanted onto the Integra matrices and secured with interrupted 6/0 monofilament. Finally, a sterile plastic dressing and a second titanized mesh were fixed to the previously implanted mesh with interrupted 5/0 monofilament.

Ultrasound and photo-acoustic imaging. Ultrasound and photo-acoustic imaging using a Vevo LAZR system (FUJIFILM VisualSonics Inc., Toronto, ON, Canada) and a real-time microvisualization LZ550 linear-array transducer (FUJIFILM VisualSonics Inc.) with a center frequency of 40 MHz was performed to detect hemoglobin oxygen saturation (sO_2) within non-seeded and prevascularized Integra. Twenty-one days after implantation, the animals were anesthetized with 1.5% isoflurane and positioned in prone position on a heated stage. Sterile ultrasound gel was applied to avoid air interference with ultrasound coupling into the animal.

For three-dimensional high-resolution B-mode ultrasound and OxyHemo-mode photo-acoustic imaging, the scanhead was driven over the entire implant by a linear motor to acquire two-dimensional images at parallel and uniformly spaced, 150 μm-sized intervals. Oxy-Hemo-mode photo-acoustic images were recorded at 750 nm and 850 nm with a two-dimensional gain of 40 dB to detect sO_2 within the samples[41,42]. Values were computed using the Vevo LAB 1.7.2. software (FUJIFILM VisualSonics Inc.).

Trans- and epi-illumination stereomicroscopy. The implants and the surrounding skin were excised at day 21, placed under the stereomicroscope and digital images in TIF format were recorded. Using the software package ImageJ[43] the background was subtracted and the images were converted into binary black and white images allowing the quantification of the vascular network. The vascularization (given in %) was defined as (vascularized area/total implant area) ∗ 100.

Planimetric analyses based on repetitive *in vivo* epi-illumination microscopy were performed to quantify the survival of the skin grafts. For this purpose, the anesthetized mice were placed under the stereomicroscope and digital images in TIF format were recorded. Using ImageJ, the survival of the skin grafts (given in %) was evaluated as follows: (Vital skin graft area/total skin graft area) ∗ 100.

Experimental protocol. Ad-MVF of 8 GFP[+] donor mice were isolated and seeded onto 8 Integra matrices. The matrices were implanted for 21 days into full-thickness skin defects on the skull of CD1 nu/nu mice. Eight non-seeded implants served as controls. *In vivo* imaging of the matrices was performed using epi-illumination stereomicroscopy (day 0, 3, 7, 14 and 21) and ultrasound/photo-acoustic imaging (day 21). At day 21, the animals were sacrificed and trans-illumination stereomicroscopy was performed. Finally, the specimen were processed for histological and immunohistochemical analyses.

In additional experiments, ad-MVF of 6 GFP[+] donor mice were seeded onto Integra and the dermal substitutes were covered with STSG 10 days after implantation into skin defects of CD1 nu/nu mice. Six non-seeded, STSG-covered implants served as controls. The grafts were assessed by epi-illumination stereomicroscopy directly after implantation and at day 5. The animals were killed and the specimen were processed for histological and immunohistochemical analyses.

Histology and immunohistochemistry. Formalin-fixed tissue samples were embedded in paraffin and cut into 3-mm thick sections. Sections were stained with hematoxylin and eosin (HE) or Sirius red for the visualization of mature collagen fibers (type I)[44]. With a BX60 microscope (Olympus, Hamburg, Germany) and the imaging software cellSens Dimension 1.11 (Olympus), the collagen content in relation to normal skin was assessed in 3 regions of interest (ROIs) of each sample.

Additional sections were stained with a monoclonal rat anti-mouse antibody against CD31 (1:100; dianova GmbH, Hamburg, Germany) and a polyclonal rabbit antibody against lymphatic vessel endothelial hyaluronan receptor-1 (LYVE-1; 1:200; Abcam, Cambridge, UK). A goat anti-rat IgG-Alexa555 antibody (1:100; Molecular Probes, Eugene, OR, USA) and a goat anti-rabbit IgG-Alexa555 antibody (1:200; Molecular Probes) served as secondary antibodies. Cell nuclei were stained with Hoechst 33342 (2 μg/mL; Sigma-Aldrich, Taufkirchen, Germany). The density of CD31^{+} blood and LYVE-1^{+} lymphatic vessels (given in mm^{−2}) and the fraction of CD31^{+}/GFP^{+} blood and LYVE-1^{+}/GFP^{+} lymphatic vessels (given in %) were assessed within 5 ROIs of each implant.

To differentiate between GFP^{+} and GFP[-] blood and lymphatic vessels, sections were stained with the mentioned primary and secondary antibodies against CD31 and LYVE-1 and with a polyclonal goat anti-GFP antibody (1:100; Rockland, Limerick, PA) to enhance GFP fluorescence. A biotin-labeled donkey anti-goat IgG antibody (1:15; Jackson ImmunoResearch, Baltimore, MD) was used as secondary antibody and was detected by fluorescein labeled-streptavidin (1:50; Vector Labs, Burlingame, CA). For this purpose, sections were placed in Coplin jars with 0.05% citraconic anhydride solution (pH 7.4) for 1 h at 98 °C and incubated overnight at 4 °C with the primary antibody, followed by the secondary antibody at 37 °C for 2 h. Finally, the fraction of GFP[+] and GFP[-] blood and lymphatic vessels was assessed.

For the immunohistochemical assessment of STSG epithelialization, sections were stained with a polyclonal rabbit antibody against cytokeratin (1:100; Abcam). As secondary antibody a biotinylated goat anti-rabbit IgG antibody (ready-to-use; Abcam) was used, which was detected by peroxidase-labeled-streptavidin (1:50; Sigma-Aldrich). 3-Amino-9-ethylcarbazole (Abcam) was used as chromogen. The sections were counterstained with Mayer's hemalum solution (Merck, Darmstadt, Germany).

Statistics. Data were tested for normal distribution and equal variance. Differences between groups were analyzed using the unpaired Student *t* test (SigmaPlot; Systat Software Inc, San Jose, CA, USA). All values are expressed as mean ± standard error of the mean (SEM). Statistical significance was accepted for values of $P < 0.05$.

Data availability.   The datasets generated and/or analyzed during the current study are available from the corresponding author on reasonable request.

References

1. Eming, S. A., Martin, P. & Tomic-Canic, M. Wound repair and regeneration: mechanisms, signaling, and translation. *Sci. Transl. Med.* **6**, 265sr6 (2014).
2. Sen, C. K. *et al.* Human skin wounds: a major and snowballing threat to public health and the economy. *Wound Repair Regen.* **17**, 763–771 (2009).
3. Shevchenko, R. V., James, S. L. & James, S. E. A review of tissue-engineered skin bioconstructs available for skin reconstruction. *J. R. Soc. Interface.* **7**, 229–258 (2010).
4. Burke, J. F. *et al.* Successful use of a physiologically acceptable artificial skin in the treatment of extensive burn injury. *Ann. Surg.* **194**, 413–428 (1981).
5. Debels, H., Hamdi, M., Abberton, K. & Morrison, W. Dermal matrices and bioengineered skin substitutes: a critical review of current options. *Plast. Reconstr. Surg. Glob. Open* **3**, e284 (2015).
6. Ruszczak, Z. Effect of collagen matrices on dermal wound healing. *Adv. Drug. Deliv. Rev.* **55**, 1595–1611 (2003).
7. Frueh, F. S., Menger, M. D., Lindenblatt, N., Giovanoli, P. & Laschke, M. W. Current and emerging vascularization strategies in skin tissue engineering. *Crit. Rev. Biotechnol.* **37**, 613–625 (2017).
8. Laschke, M. W. & Menger, M. D. Adipose tissue-derived microvascular fragments: natural vascularization units for regenerative medicine. *Trends Biotechnol.* **33**, 442–448 (2015).
9. Laschke, M. W. & Menger, M. D. Prevascularization in tissue engineering: Current concepts and future directions. *Biotechnol. Adv.* **34**, 112–121 (2016).
10. Laschke, M. W. *et al.* Vascularisation of porous scaffolds is improved by incorporation of adipose tissue-derived microvascular fragments. *Eur. Cell. Mater.* **24**, 266–277 (2012).
11. Frueh, F. S. *et al.* Adipose tissue-derived microvascular fragments improve vascularization, lymphangiogenesis, and integration of dermal skin substitutes. *J. Invest. Dermatol.* **137**, 217–227 (2017).
12. Frueh, F.S., Später, T., Scheuer, C., Menger, M.D. & Laschke, M.W. Isolation of murine adipose tissue-derived microvascular fragments as vascularization units for tissue engineering. *J. Vis. Exp.* **122** (2017).
13. Kim, I., Mogford, J. E., Chao, J. D. & Mustoe, T. A. Wound epithelialization deficits in the transforming growth factor-alpha knockout mouse. *Wound. Repair. Regen.* **9**, 386–390 (2001).
14. Reid, R. R., Said, H. K., Mogford, J. E. & Mustoe, T. A. The future of wound healing: pursuing surgical models in transgenic and knockout mice. *J. Am. Coll. Surg.* **199**, 578–585 (2004).
15. Schenck, T. L. *et al.* A full skin defect model to evaluate vascularization of biomaterials *in vivo*. *J. Vis. Exp.* **90** (2014).
16. Tenenhaus, M. & Rennekampff, H. O. Current concepts in tissue engineering: Skin and wound. *Plast. Reconstr. Surg.* **138**, 42S–50S (2016).
17. Skardal, A. *et al.* Bioprinted amniotic fluid-derived stem cells accelerate healing of large skin wounds. *Stem. Cells. Transl. Med.* **1**, 792–802 (2012).
18. Marino, D., Luginbühl, J., Scola, S., Meuli, M. & Reichmann, E. Bioengineering dermo-epidermal skin grafts with blood and lymphatic capillaries. *Sci. Transl. Med.* **6**, 221ra14 (2014).
19. da Silva, L. P. *et al.* Stem cell-containing hyaluronic acid-based spongy hydrogels for integrated diabetic wound healing. *J. Invest. Dermatol.* **137**, 1541–1551 (2017).
20. Griffin, D. R., Weaver, W. M., Scumpia, P. O., Di Carlo, D. & Segura, T. Accelerated wound healing by injectable microporous gel scaffolds assembled from annealed building blocks. *Nat. Mater.* **14**, 737–744 (2015).
21. Cerqueira, M. T. *et al.* Cell sheet technology-driven re-epithelialization and neovascularization of skin wounds. *Acta. Biomater.* **10**, 3145–3155 (2014).
22. Chen, L. *et al.* Pre-vascularization enhances therapeutic effects of human mesenchymal stem cell sheets in full thickness skin wound repair. *Theranostics.* **7**, 117–131 (2017).
23. Jameson, J. *et al.* A role for skin γδ T cells in wound repair. *Science.* **296**, 747–749 (2002).
24. Gay, D. *et al.* Fgf9 from dermal γδ T cells induces hair follicle neogenesis after wounding. *Nat. Med.* **19**, 916–923 (2013).
25. Keyes, B. E. *et al.* Impaired Epidermal to Dendritic T Cell Signaling Slows Wound Repair in Aged Skin. *Cell.* **167**, 1323–1338.e14 (2016).
26. Haertel, E., Joshi, N., Hiebert, P., Kopf, M. & Werner, S. Regulatory T cells are required for normal and activin-promoted wound repair in mice. *Eur. J. Immunol.* **48**, 1001–1013 (2018).
27. Havran, W. L. & Jameson, J. M. Epidermal T cells and wound healing. *J. Immunol.* **184**, 5423–5428 (2010).
28. Toulon, A. *et al.* A role for human skin-resident T cells in wound healing. *J. Exp. Med.* **206**, 743–750 (2009).
29. Fang, R. C. & Mustoe, T. A. Animal models of wound healing: utility in transgenic mice. *J. Biomater. Sci. Polym. Ed.* **19**, 989–1005 (2008).
30. Später, T., Frueh, F. S., Menger, M. D. & Laschke, M. W. Potentials and limitations of Integra® flowable wound matrix seeded with adipose tissue-derived microvascular fragments. *Eur. Cell. Mater.* **33**, 268–278 (2017).
31. Später, T. *et al.* Seeding density is a crucial determinant for the *in vivo* vascularisation capacity of adipose tissue-derived microvascular fragments. *Eur. Cell. Mater.* **34**, 55–69 (2017).
32. Lindenblatt, N. *et al.* A new model for studying the revascularization of skin grafts *in vivo*: the role of angiogenesis. *Plast. Reconstr. Surg.* **122**, 1669–1680 (2008).
33. Lindenblatt, N. *et al.* Temporary angiogenic transformation of the skin graft vasculature after reperfusion. *Plast. Reconstr. Surg.* **126**, 61–70 (2010).
34. McDaniel, J. S., Pilia, M., Ward, C. L., Pollot, B. E. & Rathbone, C. R. Characterization and multilineage potential of cells derived from isolated microvascular fragments. *J. Surg. Res.* **192**, 214–222 (2014).
35. Hendrickx, B. *et al.* Integration of blood outgrowth endothelial cells in dermal fibroblast sheets promotes full thickness wound healing. *Stem Cells.* **28**, 1165–1177 (2010).
36. Laschke, M. W., Vollmar, B. & Menger, M. D. Inosculation: connecting the life-sustaining pipelines. *Tissue. Eng. Part. B. Rev.* **15**, 455–465 (2009).
37. Skobe, M. & Detmar, M. Structure, function, and molecular control of the skin lymphatic system. *J. Investig. Dermatol. Symp. Proc.* **5**, 14–9 (2000).
38. Strassburg, S., Torio-Padron, N., Finkenzeller, G., Frankenschmidt, A. & Stark, G. B. Adipose-derived stem cells support lymphangiogenic parameters *in vitro*. *J. Cell. Biochem.* **117**, 2620–2629 (2016).
39. Yan, A. *et al.* Adipose-derived stem cells promote lymphangiogenesis in response to VEGF-C stimulation or TGF-β1 inhibition. *Future Oncol.* **7**, 1457–1473 (2011).
40. Okabe, M., Ikawa, M., Kominami, K., Nakanishi, T. & Nishimune, Y. 'Green mice' as a source of ubiquitous green cells. *FEBS Lett.* **407**, 313–319 (1997).
41. Mallidi, S., Watanabe, K., Timerman, D., Schoenfeld, D. & Hasan, T. Prediction of tumor recurrence and therapy monitoring using ultrasound-guided photoacoustic imaging. *Theranostics.* **5**, 289–301 (2015).

42. Rich, L. J. & Seshadri, M. Photoacoustic imaging of vascular hemodynamics: validation with blood oxygenation level-dependent MR imaging. *Radiology.* **275**, 110–118 (2015).
43. Rasband, W. S. ImageJ, U. S. National Institutes of Health, Bethesda, Maryland, USA. Available at, http://imagej.nih.gov/ij/ (1997–2016).
44. Junqueira, L. C., Bignolas, G. & Bretani, R. R. Picrosirius staining plus polarization microscopy, a specific method for collagen detection in tissue sections. *Histochem. J.* **11**, 447e55 (1979).

Acknowledgements

Author Contributions

F.S.F.: idea and study design, surgery, data analysis, manuscript and figure preparation. T.S.: surgery, histological analysis. C.K.: photo-acoustic imaging, data analysis, manuscript preparation. C.S.: MVF isolation, data analysis, manuscript preparation. A.C.S.: surgery, histological analysis. N.L. and P.G.: study design, critical manuscript revision. M.D.M.: study design, data analysis, critical manuscript revision. M.W.L.: idea and study design, data analysis, critical manuscript revision. All authors reviewed and approved the final version of the manuscript.

Additional Information

Competing Interests: The authors declare no competing interests.

Publisher's note: Springer Nature remains neutral with regard to jurisdictional claims in published maps and institutional affiliations.

6. Discussion

6.1 Discussion of Material and Methods

6.1.1 Isolation of ad-MVF

After the first description in rats in 1972 [WAGNER et al., 1972; WAGNER and MATTHEWS, 1975], the isolation of ad-MVF from murine adipose tissue has only recently been introduced in tissue engineering. Mouse ad-MVF are more versatile when compared with rat isolates, because the use of different transgenic strains may allow insights into molecular mechanisms after ad-MVF transplantation. The enzymatic isolation of ad-MVF from mouse epididymal fat pads is a straightforward procedure with a few critical steps. The murine body exhibits several extra- and intraabdominal fat deposits. In the present thesis the epididymal fat was chosen as adipose source, because it exhibits several important advantages when compared to subcutaneous fat deposits: First, the epididymal fat pads are bigger and better definable when compared to the more diffuse subcutaneous fat layer. Second, they are characterized by a homogeneous tissue structure and lack larger blood vessels, which reduces the contamination with fibrotic tissue. Finally, the axillary and inguinal subcutaneous fat also contains numerous lymphatic structures, such as lymphatic collectors and lymph nodes that represent an additional source for ad-MVF contamination. However, the harvest of epididymal fat pads is invasive and requires a laparotomy. The procedure should be performed under magnification by means of surgical loops or a stereomicroscope for a reliable identification of the adipose tissue, the epididymis and the testes. It is crucial to preserve a safety margin of a few mm between the epididymal fat and the spermatic structures to prevent sample contamination by accidental excision of the epididymis. Another source of contamination is the abdominal fur. To ensure sterility, the abdominal skin should be dissected free of the underlying muscles prior to the laparotomy. The total time required for the simple surgical procedure is ~ 20 min. The subsequent isolation of ad-MVF consists of mechanical mincing, enzymatic digestion, filtration and, finally, centrifugation and can be performed within 90 - 120 min. The most crucial step of the *in vitro* procedure is to judge whether the enzymatic digestion can be stopped. The microscopic evaluation of the degradation requires experience with ad-MVF isolation and is based on a qualitative assessment of the cell-vessel suspension (**Figure 2**).
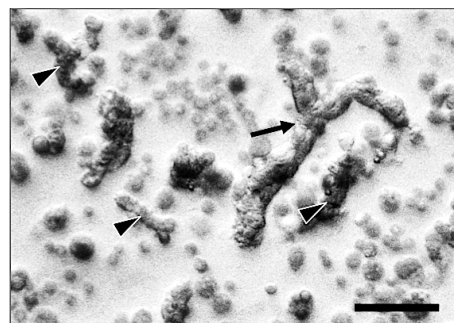
Figure 2. Isolation of ad-MVF. Microscopic image of a cell-vessel suspension during the ad-MVF isolation process. The enzymatic digestion should be stopped when the smear contains large (arrow), medium-sized and small (arrowheads) ad-MVF as well as single cells. Overdigestion with collagenase results in a single cell suspension without ad-MVF. Scale bar = 50 µm.

Too long exposition to collagenase results in ad-MVF destruction. Hence, the enzymatic digestion should not exceed 10 min. In the subsequent filtration and centrifugation steps, not all single cells are removed from the ad-MVF solution. Importantly, the fragments exhibit a markedly lower vascularization capacity after complete purification. This finding may be explained by the speculation that a "physiological environment" is critical for the vascularization potential of ad-MVF. ad-MVF contain a relevant fraction of mesenchymal stem cells, which are closely attached to their physiological niche to the fragments [McDaniel et al., 2014]. Hence, the ad-MVF isolation process should be as minimally invasive as possible to preserve the microvascular biology of the fragments.

One major advantage of ad-MVF isolation is the short enzymatic digestion time of only ~ 10 min. In contrast, freshly isolated single-cell isolates, such as the SVF, commonly require enzymatic digestion times of 60 - 90 min [Chen et al., 2016; Später et al., 2018]. Consequently, ad-MVF may be particularly suited for intraoperative one-step isolation and re-implantation procedures. However, to achieve this goal, their isolation will have to be facilitated by automated closed-system devices, which are already available for the preparation of stem cells, SVF or platelet-rich plasma in different fields of surgery [Donnenberg et al., 2011; Cohn et al., 2015; Tissiani and Alonso, 2016; Zimmermann et al., 2017].

6.1.2 Animal Models

6.1.2.1 Modified Dorsal Skinfold Chamber Model

The dorsal skinfold chamber model is a versatile tool, originally introduced for repetitive intravital microcirculatory analyses in hamsters [Endrich et al., 1980]. During the preparation, one layer of skin and subcutis including the panniculus carnosus muscle is completely removed within the circular area of the chamber's observation window [Menger et al., 2002]. Subsequently, the frames of the chamber are fixed with connecting screws with a frame-to-frame distance of 400 - 500 µm using stainless steel nuts as spacers to prevent compression of the supplying arterioles and the draining venules of the chamber tissue [Laschke et al., 2011]. Finally, the chamber window is hermetically closed with a cover glass providing


Figure 3. Dorsal skinfold chamber. *C57BL/6 mouse mounted with a dorsal skinfold chamber. The titanium chamber minimally affects animal behavior, such as feeding, ambulating or body hygiene. Note the slight tilting of the chamber to the right side. Chamber weight = ~ 2 g. Scale bar = 25 mm.*

access for microscopy. The chamber is well tolerated by rodents (**Figure 3**). However, the traditional preparation does not allow microcircular analyses of the surrounding skin.

SORG et al. [2007 and 2009] modified the dorsal skinfold chamber by creating a small circular defect with preserved surrounding skin for wound healing studies. This modified dorsal skinfold chamber was herein used for the implantation of prevascularized and non-seeded single layer Integra matrices for repetitive intravital fluorescence microscopic and planimetric analyses. Even though the surgical dissection is easy to learn and requires no more than 30 min once mastered, the model exhibits a few technical and biological pitfalls:

- *Loss of elasticity of the dorsal skinfold.* This phenomenon may compromise the experiments twofold. First, the chamber is prone to tilting (see also **Figure 3**), which finally jeopardizes the vascularization within the observation window. Second, the tissue within the chamber tends to vertical sliding during the 14-days observation period, particularly if the skin is sutured too tightly to the cranial chamber, which might result in skin necrosis with loss of fixation (**Figures 4A-C**). To prevent this complication, the chamber has to be mounted precisely in the midline of the dorsal skin (i.e., the skinfold) and the skin should be fixed with sufficient tissue and adequate sutures without excessive pressure.

- *Inadequate defect preparation.* It is crucial to dissect exactly 4 mm-sized defects because too large defects technically compromise the experiments in two ways. First,
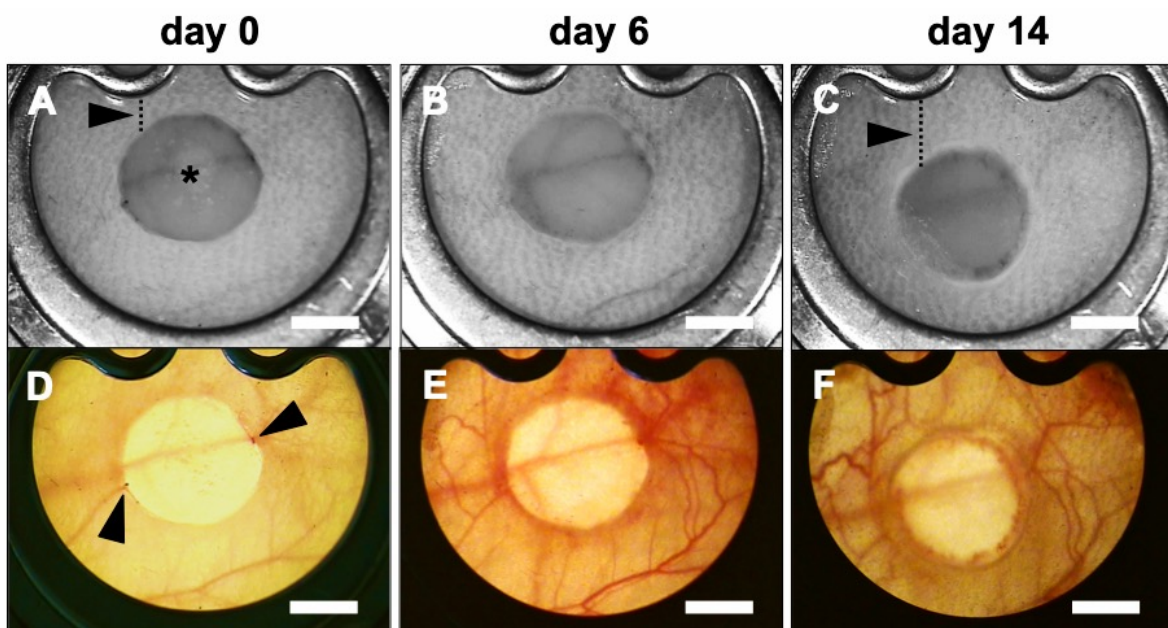
Figure 4. Technical pitfalls of the modified dorsal skinfold chamber. *Epi-illumination (**A-C**) and trans-illumination (**D-F**) stereomicroscopic images of a non-seeded single layer Integra (**A**, asterisk) immediately after implantation (**A** and **D**), at day 6 (**B** and **E**) as well as at the end of the 14-days observation period (**C** and **F**). Note the vertical sliding within the observation window throughout the course of the experiment (**A** and **C**, arrowheads). In non-seeded implants, transected subcutaneous vessels are only associated with minor implant-induced hemorrhages (**D**, arrowheads). Scale bars = 2 mm.*

the implanted skin substitute may not appropriately inosculate to the surrounding skin following hematoma or seroma formation between the wound edges and the implant. Second, the ingrowing epithelium may not cover the implanted Integra and, in rare cases, even result in an epithelial barrier between the wound bed and the implant. This problem was herein eliminated by careful microsurgical dissection of the circular defect. For a precise match of defect and implant size, sterile dermal punches were used. However, the defects should not be created using the punches alone because the mechanical trauma of punching may again compromise the vascularization of the wound. Hence, the punch is only used as a guiding mark for the microsurgical circular dissection.
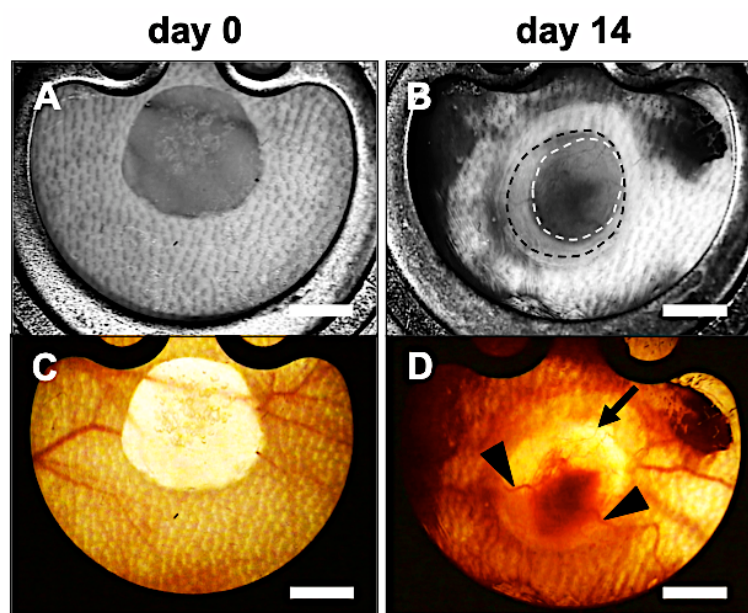
Figure 5. Biological pitfalls of the modified dorsal skinfold chamber. Epi-illumination (A and B) and trans-illumination (C and D) stereomicroscopic images of an ad-MVF-seeded single layer Integra immediately after implantation (A and C) and at the end of the 14-days observation period (B and D). B and D: Increased implant vascularization is associated with enhanced epithelial coverage, interfering with microcirculatory analyses. Epithelial layer = area between dashed black and white line in B. Note large (D, arrowheads) and smaller (D, arrow) vessels feeding the ad-MVF-derived microvascular network 14 days after implantation. Scale bars = 2 mm.

- *Epithelial coverage and microcirculatory analysis*. The main advantage of wound healing studies in the dorsal skinfold chamber is the possibility of intravital fluorescence microscopy. The analysis of the microcirculation requires an undisturbed access to the surface of the implant. In implants with increased vascularization, the epithelial coverage is significantly enhanced. Hence, the centripetally growing epithelium may interfere with microcirculatory analyses (**Figure 5**). With the present experimental design it was possible to image the microvasculature without restrictions

at day 0, 3, 6 and 10 after implantation. However, at day 14, intravital fluorescence microscopy was clearly limited in prevascularized matrices, which were mainly covered with an epithelial layer at this time point. A possible solution would be the dissection of bigger defects for future experiments.

- *Implant-induced bleeding and microcirculatory analysis*. The preparation of full-thickness skin defects includes the transection of large-caliber subcutaneous vessels. Excessive bleeding was encountered in the transection area of such vessels. However, in the majority of the experiments, only marginal hemorrhages were present in the contact zone of transected vessels and the implanted Integra (**Figure 4D**). Prevascularized Integra exhibits a higher risk for significant bleeding, which may jeopardize microcirculatory analyses. The highest risk for relevant hemorrhages was found at day 3 and 6 after implantation, i.e. immediately after inosculation to the host microvasculature. For the quantification of implant-induced hemorrhages, a semi-quantitative hemorrhagic score was introduced in subsequent studies [SPÄTER et al., 2017].

- *Age of experimental animals*. Microcirculatory analyses with the dorsal skinfold chamber are usually performed in mice exhibiting a body weight of 22 - 25 g. For the herein presented wound healing experiments, however, C57BL/6 mice with a body weight of 25 - 28 g are recommended. This detail may be important because significant difficulties were experienced using younger mice. Remarkably, after the preparation of full-thickness skin defects in young animals, it was not possible to implant Integra without a step-off to the surrounding skin. This subtle incongruence results in a delayed or absent epithelial coverage of the implants and is among the main biases of epithelialization studies using the dorsal skinfold chamber model. One reason could be a thinner skin or a thinner subcutaneous / muscular layer in younger animals.

- *Skin pigmentation of experimental animals*. C57BL/6 mice can exhibit large pigmented areas on their skin [CURTIS et al., 2011]. These "black dots" impair the quality of the intravital fluorescence microscopic analysis of the skin's microvasculature. Unfortunately, pigmentation is neither predictable nor visible through the black fur of the mice. Consequently, the back of the animals was depilated before anesthetizing them and pigmented animals were excluded from further experiments.

- *Excision of tissue specimens for in vitro analyses*. After the *in vivo* observation period, the Integra implants were excised for histological and immunohistochemical assessment. A common mistake is the interruption of the implant/epithelium interface by careless manipulation of the specimens. This can be avoided by excising the

specimens "en block", i.e. as a rectangular full-thickness excision including both the implant and the contralateral skinfold with a safety margin of at least 10 mm on each side of the implant. For further enhancement of the specimens, the animals can be bled out before killing them. This reduces the harvesting-associated bleeding with lower contamination of the specimens with erythrocytes before fixation.

Rodent wound healing experiments are often compromised by contraction of the panniculus carnosus muscle [DUNN et al., 2013; GRIFFIN et al., 2015]. This problem is mainly avoided in the dorsal skinfold chamber model by fixation of the skin between the two titanium frames. Moreover, the implants are protected from exsiccation and manipulation by the animal in the closed chamber [MICHAEL et al., 2013]. Consequently, it is not necessary to regularly change wound dressings, which may influence the healing process. In summary, the modified dorsal skinfold chamber is an extremely versatile tool for the study of vascularization and epithelialization of dermal skin substitutes in murine full-thickness skin defects. It represents a quick and cost-effective experimental approach and allows dynamic insights into the microvascular pathophysiology of healing wounds.

6.1.2.2 Autologous Skin Graft Model

In clinical skin reconstruction, Integra is commonly used in a staged procedure with STSG coverage after revascularization of the dermal skin substitute. To address this fact, a novel mouse wound model was developed in the present thesis for a proof-of-concept study using ad-MVF-prevascularized bilayer Integra. For this purpose, two established mouse models were combined: The head punch model, which has been widely used for wound healing studies [KIM et al., 2001; REID et al., 2004] and a model described by SCHENCK et al. [2014], who used a subcutaneous titanized mesh to prevent wound contraction after Integra implantation on the back of mice. In the initial stage of this experiment, bilayer Integra was implanted into 8 mm-sized full-thickness skin defects on the skull of CD1 nu/nu mice without additional fixation. However, after a few days, the implants were lost due to loosening. This problem was solved by placing a titanized mesh underneath the implants directly on the bone and slightly overlapping the wound edges. Technically, the mesh is not fixed on the bone, but it is critical that the securing sutures incorporate the skin, the Integra as well as the titanized mesh. The bilayer Integra is well protected against exsiccation and additional bandages on the wounds were not necessary. The animals tolerated the implants well and showed normal behavior throughout the 21 days of the experiment. However, the construct is not entirely resistant against external manipulation and the animals should be housed alone and without litter, which significantly contaminates the implanted Integra. In contrast to the dorsal skinfold chamber, *in vivo* analyses of the implants' vascularization are challenging using the skull model. Photo-acoustic imaging was herein established for the assessment of tissue

oxygenation within implanted Integra. The results of this analysis were used as a surrogate parameter for the vascularization of the dermal skin substitutes. For a reliable and reproducible investigation, the anesthetized mice needed to be kept warm and carefully fixed.

In the second part of this study, STSG coverage was performed 10 days after the implantation of prevascularized and non-seeded Integra. In the pertinent literature, the harvest of STSG in mice is thought to be extremely difficult due to the loose and thin skin of the animals. Accordingly, murine investigations on skin transplants were commonly performed using full-thickness skin grafts [LINDENBLATT et al., 2008 and 2010]. In the present thesis, a simple technique is introduced that allows the harvest of STSG in mice. For this purpose, full-thickness skin grafts are excised from the groin of anesthetized CD1 nu/nu mice. The skin grafts are secured with needles on a sterile cork plate (**Figure 6A**). Next, the adjacent adipose tissue and the deep dermal layer including a rich vascular plexus is microsurgically removed using a stereomicroscope (**Figure 6B**). In the meantime, the groin wounds are closed with interrupted sutures and the silicone pseudoepidermis of the bilayer Integra is carefully removed after surgical disinfection (**Figure 6C**). Finally, the STSG is secured with interrupted sutures and an additional titanized mesh, as described by FRUEH et al. [2018b]. Overall, the procedure is technically feasible and, once mastered, can be performed within 30 min. As indicated by histology, the skin grafts harvested using this technique exhibit typical STSG configuration. One critical step of this operation is the adequate positioning of the 8 mm-sized defects on the small skull of the mice. It should be placed exactly on the midline with a distance to the eyelids of ≥ 3 mm (**Figure 6D**). If the wound-eyelid distance is too small, the tension of the suture may lead to incomplete lid closure with subsequent ocular complications. After transplantation the STSG are easily accessible for stereomicroscopic imaging, allowing the planimetric quantification of STSG survival at the end of the experiments.
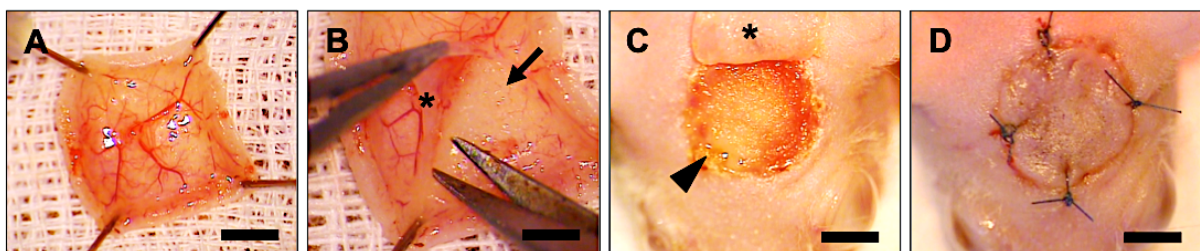
Figure 6. Skin graft model. A Full-thickness skin graft after excision from the groin of a CD1 nu/nu mouse. **B** Microsurgical defatting and removal of the deep dermis (asterisk) to harvest a STSG (arrow). **C** Removal of the silicone pseudoepidermis (asterisk) 10 days after bilayer Integra (arrowhead) implantation on the skull of a CD1 nu/nu mouse. **D** STSG in situ. Scale bars: **A, C** and **D** = 4 mm, **B** = 2.5 mm.

The CD1 nu/nu mice used for this experiment exhibit advantages for the investigation of prevascularized dermal skin substitutes. First, they are hairless, which facilitates repetitive

intravital stereomicroscopic and photo-acoustic imaging. Particularly for photo-acoustic imaging, the thick and often pigmented skin of C57BL/6 mice has been shown to prevent a reliable quantification of tissue oxygenation. Second, the immunoincompetent recipient strain allows the transplantation of GFP[+] ad-MVF harvested from transgenic C57BL/6 mice without inducing a rejection reaction. On the other hand, it has to be considered that CD1 nu/nu mice lack a thymus and, thus, are unable to produce T-cells. This may give rise to concerns about their eligibility to study implanted biomaterials and, in particular, wound healing, because inflammatory processes are essentially involved in the regulation of vascularization and lymphangiogenesis. In fact, epidermal and dermal T-cells are critically involved in the regulation of wound healing in mice by local production of growth factors and inflammatory cytokines [JAMESON et al., 2002; KEYES et al., 2016; HAERTEL et al., 2018]. This limitation should be taken into account when planning and executing wound healing experiments with this immunoincompetent animal strain. In conclusion, the herein introduced autologous skin graft model is a promising and minimally invasive tool to analyze the fate of STSG in mice.

6.2 Discussion of Results

6.2.1 Characterization of ad-MVF

One prerequisite for the successful prevascularization of Integra using ad-MVF is a penetration of the seeded fragments into the dermal skin substitute's pores. This may crucially depend from the size of individual ad-MVF. Therefore, in the first study of this thesis, the length distribution of freshly isolated ad-MVF was assessed by means of microscopic analyses. The mean length of isolated ad-MVF was 42 ± 1 µm with the majority of ad-MVF sized between 20 - 80 µm. Integra exhibits pore sizes between 20 - 125 µm and immediately after the seeding process, only a few ad-MVF were found in the inner structure of the matrices. However, 14 and 21 days following implantation into full-thickness skin defects, GFP[+] ad-MVF were homogeneously distributed within the Integra implants, indicating a fast ingrowth of the ad-MVF-derived microvascular network. Moreover, microscopic analyses revealed that ad-MVF retain their mature microvascular morphology with hierarchical microvessel segments. It was further shown that ad-MVF include arterioles, capillaries and venules, as indicated by immunohistochemical staining of the endothelial cell marker CD31 and the perivascular cell marker α-SMA. To assess the cellular composition of freshly isolated ad-MVF, additional flow cytometric analyses were performed. They showed that ad-MVF contain 26 ± 2 % CD31^{+} endothelial cells, 17 ± 2 % α-SMA^{+} perivascular cells as well as 9 ± 1 % cells positive for the mesenchymal stem cell marker CD117. In conclusion, these findings indicate that the isolation process of ad-MVF does not significantly impair their

microvessel morphology. This may be the main reason for an intriguing vascularization capacity, which is markedly higher when compared to the adipose tissue-derived SVF under comparable conditions [SPÄTER et al., 2018].

6.2.2 Vascularization of Integra

In the present thesis, ad-MVF are introduced as a novel prevascularization strategy for the dermal skin substitute Integra. A fast revascularization is the key challenge for engineered tissues. Therefore, the vascularization of Integra was analyzed using different experimental approaches.

Repetitive intravital fluorescence microscopy was performed at day 0, 3, 6, 10 and 14 after implantation of prevascularized and non-seeded single layer Integra into the dorsal skinfold chamber. Importantly, this technique allowed assessing the angiogenic activation of the host microvasculature as well as the formation and maturation of ad-MVF-derived microvessels. Three days after the implantation of non-seeded Integra, the host microvasculature showed angiogenic budding and capillary widening towards the implant (**Figure 7A**). However, throughout the course of the 14-days experiment, significant implant vascularization was not observed, as indicated by a low functional microvessel density and only a few blood-perfused regions of interest. In contrast, ad-MVF-seeded Integra revealed onset of blood perfusion as early as 6 days after implantation. Fluorescence microscopy allowed documenting the inosculation of ad-MVF-derived immature microvessels with ingrowing microvessels from the surrounding host skin (**Figure 7B**). This finding is important and proofs that the ad-MVF-induced microvascular network is functional and able to provide the center of the implants with oxygen. Moreover, it supports the generally accepted theory that skin substitutes are primarily revascularized through internal inosculation, i.e. the ingrowth of host microvessels [LASCHKE et al., 2009; FRUEH et al., 2018a]. Even though a few implants exhibited inosculation already at day 3, it was not possible to objectify blood flow within these implants at that time point. Hence, it may be speculated that the formation of the ad-MVF-derived
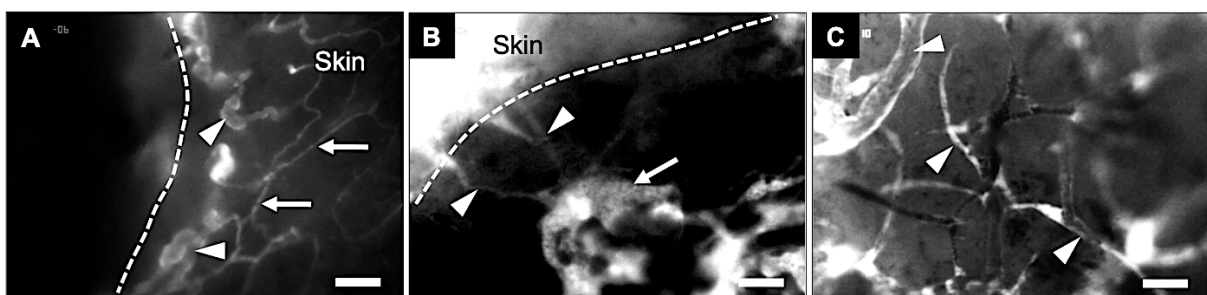
Figure 7. Intravital fluorescence microscopy A Non-seeded single layer Integra 6 days after implantation with host microvessels (arrows) and angiogenic budding (arrowheads) towards the implant's border. B ad-MVF-seeded Integra 6 days after implantation with ingrowing host microvessels (arrowheads), which inosculate with the ad-MVF-derived microvessels (arrow). Note the large diameter of the immature ad-MVF-derived microvasculature. C Hierarchical microvascular network 10 days after implantation of an ad-MVF-seeded Integra. Arrowheads = blood-perfused microvessels. Blue light epi-illumination intravital microscopy with 5 % FITC-labeled dextran. Dashed lines = implant border. Scale bars: A and B = 120 µm, C = 60 µm.

microvascular network requires at least 72 hours. Indeed, implants with inosculation at day 3 showed a tendency to more severe bleeding, which may be due to the premature microvascular network. After inosculation, the implants' vascularization rapidly increased and ~ 80 % blood-perfused regions of interest were already found at day 10 with a functional microvessel density of > 80 cm/cm^2. In line with these findings, the maturation of the ad-MVF-derived microvasculature was associated with decreasing microvessel diameters and an increase of the centerline red blood cell velocity over time. Moreover, it was possible to visualize the development of a highly hierarchical microvascular network, as indicated by fluorescence microscopy 10 days after implantation (**Figure 7C**).

Histological and immunohistochemical analyses of Integra implants at day 14 confirmed the intravital microscopic findings. The collagen-glycosaminoglycan matrix of ad-MVF seeded Integra was homogeneously filled with a well-vascularized granulation tissue whereas non-seeded implants were only invaded by single cells. Accordingly, a > 3 times higher density of CD31$^+$ microvessels was found in prevascularized implants. Importantly, > 95 % of these microvessels stained positive for GFP, hence originated from the ad-MVF. Suprisingly, 47 ± 9 % GFP$^+$/CD31$^+$ microvessels were also detected in the skin surrounding the implants. This is remarkable and indicates that the ad-MVF-derived microvasculature not only vascularized the Integra but also invaded the surrounding skin. Consequently, it may be assumed that ad-MVF-seeded Integra is additionally revascularized by external inosculation, i.e. the connection of outgrowing microvessels with the host microvasculature. The reason for the high growth activity of transplanted ad-MVF remains elusive. One possible explanation could be a strong hypoxic stimulation prior to inosculation with subsequent angiogenic growth factor expression.

The aim of the second *in vivo* experiment was to confirm the promising results of the dorsal skinfold chamber in an experimental model closer to human translation. For this purpose, ad-MVF-seeded and non-seeded double layer Integra were implanted in bradytrophic full-thickness skin defects on the skull of CD1 nu/nu mice for 21 days. The vascularization of the implants was assessed by means of photo-acoustic imaging, trans-illumination stereomicroscopy and immunohistochemistry. Photo-acoustic imaging revealed a ~ 4 times higher oxygen saturation of prevascularized Integra compared with non-seeded implants. Accordingly, trans-illumination stereomicroscopy showed a markedly higher vascularized area in prevascularized Integra. Finally, immunohistochemical analyses confirmed markedly higher microvessel densities in ad-MVF-seeded implants when compared to controls. Again, > 95 % of the microvessels within the implants were GFP$^+$, i.e. originated from the transplanted ad-MVF, most probably because in the skull model the surrounding skin represents the only site for inosculation with the host microvasculature. Moreover, the defects were markedly bigger (8 mm). Furthermore, the double layer Integra was used.

Hence, the ad-MVF had to be seeded on the bottom side of the matrices and were implanted in direct contact with the bradytrophic bone of the mouse skull. The findings of this study should be understood as further evidence that ad-MVF survive in an initially hypoxic environment and rapidly reassemble into a microvascular network even when seeded on the bottom side of implanted Integra. This is especially noteworthy, because in the clinical setting the commonly used double layer Integra would also have to be seeded on the "bottom" of the implant.

In conclusion, the analyses of both mouse models indicate that ad-MVF-seeding is a highly effective strategy to prevascularize Integra, leading to a functional microvascular network within ~ 10 days after implantation of the dermal skin substitute.

6.2.3 Integration and Epithelialization of Integra

A stable reconstruction of skin defects crucially depends on the integration of a dermal skin substitute. The collagen content of skin substitutes is an accepted parameter for tissue integration. Therefore, the total collagen content of implanted single layer Integra was herein quantified using Sirius red staining and polarized light microscopy. Due to birefringence, mature type I collagen fibers exhibit a reddish color under polarized light [JUNQUEIRA et al., 1979]. The collagen fiber density was evaluated in relation to the adjacent healthy skin. In line with the improved vascularization, ad-MVF-seeded Integra exhibited markedly higher amounts of collagen fibers when compared to non-seeded controls. However, the prevascularized implants only showed a low density of type I collagen in comparison to normal skin. These results are comparable to analyses of ADSC-seeded Integra in a rat model [MERUANE et al., 2012]. Obviously, and despite ad-MVF-enhanced vascularization, the loose collagen-glycosaminoglycan matrix of the dermal skin substitute may not provide sufficient stability after 14 - 21 days. Consequently, the neodermis is still remarkably fragile and should be protected from excessive mechanical stress.

Beside integration, the restoration of the epithelial barrier is critical for the outcome of reconstructed skin. In previous rodent experiments, increased vascularization of the dermal support enhanced wound re-epithelialization by *in situ* delivery of epidermal keratinocytes [LUGO et al., 2011]. Hence, a faster epithelialization of the ad-MVF-seeded Integra implants was expected in the present study. In fact, repetitive planimetric measurements of the epithelialized implant surface area revealed a significantly higher epithelialization of the prevascularized Integra at day 10 and 14. Because planimetry of the thin epithelial coverage is prone to inter-observer variability, additional immunohistochemical analyses were performed after the *in vivo* experiment. The cytokeratin[+] multi-layered epithelium covered 58

± 7 % of the diameter of ad-MVF-seeded Integra, which was significantly greater compared with 36 ± 5 % in the control group. Interestingly, the results of the immunohistochemical analyses were comparable to the planimetric assessment, indicating an acceptable accuracy of the latter. Taken together, it was hereby shown that 4 mm-sized defects, even though rather small for wound healing studies in mice, are appropriate for the evaluation of epithelial regeneration in the dorsal skinfold chamber and throughout an observation period of 14 days.

6.2.4 Early Skin Grafting of Integra

For final testing of the ad-MVF-based prevascularization strategy, STSG coverage of ad-MVF-seeded and non-seeded bilayer Integra was performed 10 days after implantation into full-thickness skin defects on the skull of CD1 nu/nu mice. The successful transplantation of skin grafts requires an intact microvascular network at the recipient site, supplying the avascular skin with oxygen. It is therefore not surprising that pilot experiments with one-staged Integra implantation and STSG coverage resulted in complete graft necrosis. Based on the previous experiments in the dorsal skinfold chamber model and on histological analyses of the prevascularized matrices, it was hypothesized that the vascularization as well as the integration of the neodermis should allow STSG coverage ~ 10 days after implantation of prevascularized Integra. Indeed, STSG coverage of ad-MVF-seeded Integra at this time point resulted in a survival rate of 40 ± 11 %, as indicated by planimetric analyses. In contrast, skin grafting of non-seeded implants was associated with a statistically significantly lower survival rate of 5 ± 5 %. Moreover, STSG on prevascularized Integra mainly exhibited an intact epidermal and dermal structure, whereas skin grafts on non-seeded implants were histopathologically characterized by tissue necrosis. Remarkably, the surviving STSG were primarily revascularized in the center of the implants. Moreover, the necrotic area was located in the grafts' periphery in all specimens. This finding is coherent with the pertinent literature on skin graft revascularization [O'CEALLAIGH et al., 2006; CAPLA et al., 2009; LINDENBLATT et al., 2010]. However, these previous experiments were performed without dermal skin substitutes and the authors speculated that central graft revascularization may be due to a i) faster ingrowth of host microvessels from the wound bed "underneath" the skin graft and ii) higher expression of angiogenic growth factors in the central area of the grafts, where oxygen is scarcely delivered through diffusion. Importantly, in the present wound model with ad-MVF-derived microvascular networks, the first argument may not hold true, because the newly forming microvessels may have exhibited less inosculation potential when compared to physiological vessels. This, however, might have even aggravated the hypoxic stress and subsequent growth factor expression within the center of the STSG.

Consequently, after inosculation to the surrounding host microvasculature, the angiogenic activity within the grafts may have been particularly high in the hypoxic center. This speculation is supported by the fact that only single GFP$^+$ cells integrated in STSG microvessels were found but no entirely GFP$^+$ vascular structures. Hence, the prevascularized Integra might have rather provided the STSG with oxygen through diffusion than through early inosculation. Taken together, it was possible to show that the prevascularization of Integra using ad-MVF allows STSG coverage as early as 10 days after implantation onto bradytrophic scalp defects in mice.

6.2.5 ad-MVF and Lymphangiogenesis

The lymphatic system is critically involved in the regulation of fundamental biological processes, such as the immune response and immunomodulation, the intestinal absorption of lipids and the maintenance of tissue fluid homeostasis [ALITALO et al., 2005; CUENI and DETMAR, 2008; ROCKSON, 2010]. Thin-walled capillaries represent the smallest unit of the cutaneous lymphatic system, which drains protein-rich lymph fluid from the extra-cellular spaces of the skin [HIRAKAWA and DETMAR, 2004]. Even though the cutaneous lymphatic and blood vascular systems are intimately related in terms of embryology and anatomy, the role of lymphangiogenesis for wound healing has been neglected for decades, mainly due to a lack of sophisticated lymphatic imaging techniques as well as lymph-specific histological markers [FRUEH et al., 2018a]. This is remarkable, because PAAVONEN et al. [2000] demonstrated almost 20 years ago that lymphangiogenesis, i.e. the growth of new lymphatic vessels, is an integral part of wound healing. Furthermore, subsequent experimental studies revealed that lymphangiogenic growth factor treatment enhances lymphatic regeneration across incisional wounds [SAARISTO et al., 2004] as well as in diabetic wounds [SAARISTO et al., 2006]. The consequence of these findings is the incorporation of the lymphatic system into artificial skin. Indeed, engineered skin substitutes including both blood and lymphatic vessels have recently been introduced [MARINO et al., 2014; KLAR et al., 2014; MATSUSAKI et al., 2015]. For this purpose, the lymphatic vasculature was engineered by co-culturing angiogenic cells, such as HDMEC or human umbilical vein endothelial cells, with fibroblasts and keratinocytes. Based on these results, it was hypothesized in the present thesis that ad-MVF-prevascularization may also stimulate the formation of a lymphatic vascular network within implanted Integra.

For the quantification of lymphangiogenesis in the dorsal skinfold chamber experiment, lymphatic vessel endothelial hyaluronan receptor (LYVE)-1$^+$ lymphatic vessels were detected in the implants and the surrounding skin by means of immunohistochemistry. Importantly,

both prevascularized and non-seeded Integra contained lymphatic vessels at day 14 after implantation. However, ad-MVF-seeded Integra exhibited a significantly higher lymphatic vessel density (21 ± 6 mm^{-2}) compared with control implants (2 ± 1 mm^{-2}).

It was further shown that 68 % of the lymphatic vasculature in prevascularized Integra was GFP$^+$, hence originated from the transplanted ad-MVF (**Figure 8A-C**). In contrast, only 10 % of the lymphatic vessels in the surrounding skin exhibited a GFP$^+$ endothelium. Remarkably, the GFP$^+$ lymphatic vessels invading the host skin tissue were mainly localized close to GFP$^-$ lymphatic vessels (**Figure 8D-F**). However, it was not possible to identify lympho-lymphatic anastomoses by means of immunohistochemistry. Nonetheless, it can be assumed that the outgrowing ad-MVF-derived lymphatic vessels connected to the lymphatic system of the host. The analysis of lymphangiogenesis in the skin graft model revealed similar results. ad-MVF-seeded bilayer Integra exhibited significantly more lymphatic vessels when compared to non-seeded control implants. In this study, an even higher percentage of GFP$^+$ lymphatic vessels was found in prevascularized implants (88 ± 1 %). Additional analyses were performed for the detection of LYVE-1$^+$/GFP$^+$ lymphatic vessels in the STSG 5 days after implantation onto prevascularized and non-seeded Integra. Even though a few LYVE-1$^+$/GFP$^+$ single cells were found within the STSG, these cells were not integrated into the endothelium of the skin grafts' lymphatic vasculature. This finding may be explained by the fact that lymphangiogenesis is a slower biological process when compared to angiogenesis
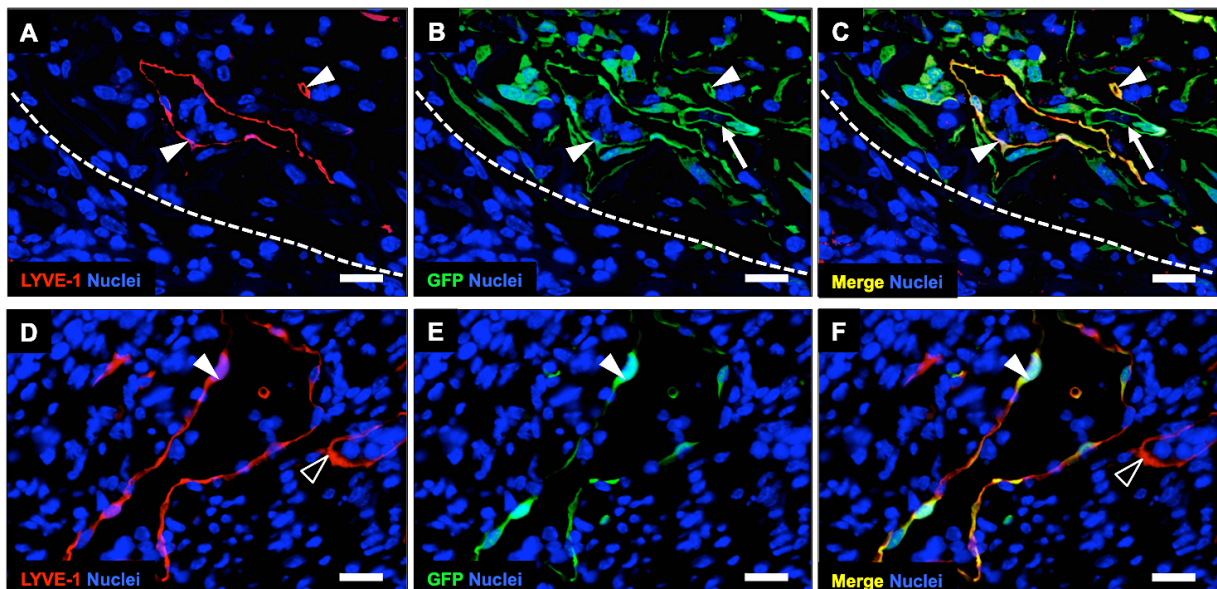
Figure 8. ad-MVF-derived lymphatic vascular network. *Immunohistochemical detection of LYVE-1$^+$ lymphatic vessels in ad-MVF-seeded bilayer Integra (**A**-**C**) and surrounding skin (**D**-**F**) 14 days after implantation into the dorsal skinfold chamber of a C57BL/6 mouse. **A**-**C** ad-MVF-derived LYVE-1$^+$/GFP$^+$ lymphatic vessels (arrowheads) and LYVE$^-$/GFP$^+$ blood vessel (**B** and **C**, arrow) in prevascularized Integra. Dashed line = skin/Integra border. **D**-**F** ad-MVF-derived LYVE-1$^+$/GFP$^+$ lymphatic vessel (arrowhead) invading the surrounding skin. Note the LYVE-1$^+$/GFP$^-$ host lymphatic vessel (**D** and **F** empty arrowhead) in close vicinity to the ad-MV-derived lymphatic vessel. Scale bars = 50 µm.*

and lympho-lymphatic anastomoses are only expected > 10 days after implantation into skin defects [MARINO et al., 2014].

These results represent the first sophisticated assessment of the lymphatic vasculature in Integra and probably are the most interesting finding of this thesis. The fact that ad-MVF are not only intriguing vascularization units but also promote lymphatic regeneration should be discussed in detail. As indicated by flow cytometric analyses, ad-MVF contain ~ 30 % endothelial cells. The epididymal fat pads also contain lymphatic vessels and, therefore, ad-MVF may also be characterized by a significant fraction of lymphatic vessel fragments and lymphatic endothelial cells. In analogy to blood vessel fragments, these lymphatic vessel fragments may rapidly reconnect with each other after transplantation and contribute to the formation of an ad-MVF-derived lymphatic network. Moreover, it may be speculated that the fragment-associated mesenchymal stem cell fraction is capable of differentiating into lymphatic endothelial cells and contributes to lymphatic vessel formation after transplantation. According to this assumption, ADSC have shown potential to promote lymphangiogenesis both *in vitro* [STRASSBURG et al., 2016] and *in vivo* [YAN et al., 2011]. Taken together, ad-MVF not only exhibit a high angiogenic activity but also represent exciting building blocks for the restoration of the lymphatic system. Based on the findings of the present thesis, novel experiments investigating the value of ad-MVF transplantation in lymphatic tissue engineering have already been initiated.

6.2.6 Conclusion

In the present thesis, ad-MVF-seeding has been introduced as a novel and promising prevascularization strategy for the dermal skin substitute Integra. The microvascular fragments enhance the vascularization and lymphangiogenesis of Integra and also result in a faster integration and epithelialization of the implant. This prevascularization strategy might also be suitable to enhance the performance of other engineered skin substitutes. Key advantages of ad-MVF prevascularization are the short isolation time of the microvascular fragments and their intact microvascular characteristics, which are prerequisites for an intraoperative one-staged application. However, the isolation process will have to be markedly facilitated by means of automate closed-system devices. Moreover, it has to be proven that ad-MVF harvested from subcutaneous adipose tissue of humans exhibit an equally high vascularization capacity compared with murine ad-MVF. If these hurdles are mastered, ad-MVF may soon be taken from bench to bedside. From the clinician's perspective, they are indeed a promising strategy to enhance the vascularization and lymphangiogenesis of engineered tissue substitutes.

7. References

1. **Akhtar S, Hasham S, Abela C, Phipps AR**. The use of Integra in necrotizing fasciitis. *Burns* 32: 251-254, 2006.

2. **Alitalo K, Tammela T, Petrova TV**. Lymphangiogenesis in development and human disease. *Nature* 438: 946-953, 2005.

3. **Baroni A, Buommino E, De Gregorio V, Ruocco E, Ruocco V, Wolf R**. Structure and function of the epidermis related to barrier properties. *Clin Dermatol* 30: 257-262, 2012.

4. **Burke JF, Yannas IV, Quinby WC Jr, Bondoc CC, Jung WK**. Successful use of a physiologically acceptable artificial skin in the treatment of extensive burn injury. *Ann Surg* 194: 413-428, 1981.

5. **Capla JM, Ceradini DJ, Tepper OM, Callaghan MJ, Bhatt KA, Galiano RD, Levine JP, Gurtner GC.** Skin graft vascularization involves precisely regulated regression and replacement of endothelial cells through both angiogenesis and vasculogenesis. *Plast Reconstr Surg* 117: 836-844, 2006.

6. **Chen YJ, Liu HY, Chang YT, Cheng YH, Mersmann HJ, Kuo WH, Ding ST**. Isolation and differentiation of adipose-derived stem cells from porcine subcutaneous adipose tissues. *J Vis Exp* 109: e53886, 2016.

7. **Cherubino M, Valdatta L, Balzaretti R, Pellegatta I, Rossi F, Protasoni M, Tedeschi A, Accolla RS, Bernardini G, Gornati R**. Human adipose-derived stem cells promote vascularization of collagen-based scaffolds transplanted into nude mice. *Regen Med* 11: 261-271, 2016.

8. **Cohn CS, Lockhart E, McCullough JJ**. The use of autologous platelet-rich plasma in the orthopedic setting. *Transfusion* 55: 1812-1820, 2015.

9. **Cueni LN, Detmar M**. New insights into the molecular control of the lymphatic vascular system and its role in disease. *J Invest Dermatol* 126: 2167-2177, 2006.

10. **Cueni LN, Detmar M**. The lymphatic system in health and disease. *Lymphat Res Biol* 6: 109-122, 2008.

11. **Curtis A, Calabro K, Galarneau JR, Bigio IJ, Krucker T**. Temporal variations of skin pigmentation in C57BL/6 mice affect optical bioluminescence quantitation. *Mol Imaging Biol* 13: 1114-1123, 2011.

12. **Donnenberg AD, Donnenberg VS, Griffin DL, Moore LR, Tekinturhan F, Kormos RL**. Intra-operative preparation of autologous bone marrow-derived CD34-enriched cellular products for cardiac therapy. *Cytotherapy* 13: 441-448, 2011.

13. **Dunn L, Prosser HC, Tan JT, Vanags LZ, Ng MK, Bursill CA**. Murine model of wound healing. *J Vis Exp* 75: e50265, 2013.

14. **Endrich B, Asaishi K, Götz A, Messmer K**. Technical report - A new chamber technique for microvascular studies in unanesthetized hamsters. *Res Exp Med (Berl)* 177: 125-134, 1980.

15. **Foubert P, Barillas S, Gonzalez AD, Alfonso Z, Zhao S, Hakim I, Meschter C, Tenenhaus M, Fraser JK**. Uncultured adipose-derived regenerative cells (ADRCs) seeded in collagen scaffold improves dermal regeneration, enhancing early vascularization and structural organization following thermal burns. *Burns* 41: 1504-1516, 2015.

16. **Frueh FS, Calcagni M, Giesen T, Giovanoli P, Harder Y**. Das Management von Weichteilverletzungen im Extremitätentrauma: Die Rolle der Plastischen Chirurgie. *Praxis (Bern 1994)* 105: 1493-1501, 2016.

17. **Frueh FS, Menger MD, Lindenblatt N, Giovanoli P, Laschke MW**. Current and emerging vascularization strategies in skin tissue engineering. *Crit Rev Biotechnol* 37: 613-625, 2017a.

18. **Frueh FS, Später T, Lindenblatt N, Calcagni M, Giovanoli P, Scheuer C, Menger MD, Laschke MW**. Adipose tissue-derived microvascular fragments improve vascularization, lymphangiogenesis, and integration of dermal skin substitutes. *J Invest Dermatol* 137: 217-227, 2017b.

19. **Frueh FS, Später T, Scheuer C, Menger MD, Laschke MW**. Isolation of murine adipose tissue-derived microvascular fragments as vascularization units for tissue engineering. *J Vis Exp* 122, 2017c.

20. **Frueh FS, Sanchez-Macedo N, Calcagni M, Giovanoli P, Lindenblatt N**. The crucial role of vascularization and lymphangiogenesis in skin reconstruction. *Eur Surg Res* 59: 242-254, 2018a.

21. **Frueh FS, Später T, Körbel C, Scheuer C, Simson AC, Lindenblatt N, Giovanoli P, Menger MD, Laschke MW**. Prevascularization of dermal substitutes with adipose tissue-derived microvascular fragments enhances early skin grafting. *Sci Rep* 8: 10977, 2018b.

22. **Gallico GG 3rd, O'Connor NE, Compton CC, Kehinde O, Green H**. Permanent coverage of large burn wounds with autologous cultured human epithelium. *N Engl J Med* 311: 448-451, 1984.

23. **Griffin DR, Weaver WM, Scumpia PO, Di Carlo D, Segura T**. Accelerated wound healing by injectable microporous gel scaffolds assembled from annealed building blocks. *Nat Mater* 14: 737-744, 2015.

24. **Haertel E, Joshi N, Hiebert P, Kopf M, Werner S**. Regulatory T cells are required for normal and activin-promoted wound repair in mice. *Eur J Immunol* 48: 1001-1013, 2018.

25. **Havran WL, Jameson JM**. Epidermal T cells and wound healing. *J Immunol* 184: 5423-5428, 2010.

26. **Hendrickx B, Vranckx JJ, Luttun A**. Cell-based vascularization strategies for skin tissue engineering. *Tissue Eng Part B Rev* 17: 13-24, 2011.

27. **Hirakawa S, Detmar M**. New insights into the biology and pathology of the cutaneous lymphatic system. *J Dermatol Sci* 35: 1-8, 2004.

28. **Hiscox AM, Stone AL, Limesand S, Hoying JB, Williams SK**. An islet-stabilizing implant constructed using a preformed vasculature. *Tissue Eng Part A* 14: 433-440, 2008.

29. **Hoying JB, Boswell CA, Williams SK**. Angiogenic potential of microvessel fragments established in three-dimensional collagen gels. *In Vitro Cell Dev Biol Anim* 32: 409-419, 1996.

30. **Hussain SH, Limthongkul B, Humphreys TR**. The biomechanical properties of the skin. *Dermatol Surg* 39: 193-203, 2013.

31. **Jameson J, Ugarte K, Chen N, Yachi P, Fuchs E, Boismenu R, Havran WL**. A role for skin gammadelta T cells in wound repair. *Science* 296: 747-749, 2002.

32. **Junqueira LC, Bignolas G, Brentani RR**. Picrosirius staining plus polarization microscopy, a specific method for collagen detection in tissue sections. *Histochem J* 11: 447-455, 1979.

33. **Kamel RA, Ong JF, Eriksson E, Junker JP, Caterson EJ**. Tissue engineering of skin. *J Am Coll Surg* 217: 533-555. 2013.

34. **Keyes BE, Liu S, Asare A, Naik S, Levorse J, Polak L, Lu CP, Nikolova M, Pasolli HA, Fuchs E**. Impaired epidermal to dendritic T cell signaling slows wound repair in aged skin. *Cell* 167: 1323-1338, 2016.

35. **Khademhosseini A, Vacanti JP, Langer R**. Progress in tissue engineering. *Sci Am* 300: 64-71, 2009.

36. **Kim I, Mogford JE, Chao JD, Mustoe TA**. Wound epithelialization deficits in the transforming growth factor-alpha knockout mouse. *Wound Repair Regen* 9: 386-390, 2001.

37. **Klar AS, Böttcher-Haberzeth S, Biedermann T, Schiestl C, Reichmann E, Meuli M**. Analysis of blood and lymph vascularization patterns in tissue-engineered human dermo-epidermal skin analogs of different pigmentation. *Pediatr Surg Int* 30: 223-231, 2014.

38. **Klar AS, Zimoch J, Biedermann T**. Skin tissue engineering: Application of adipose-derived stem cells. *Biomed Res Int* 2017: 9747010, 2017.

39. **Langer R, Vacanti JP**. Tissue engineering. *Science* 260: 920-926, 1993.

40. **Laschke MW, Harder Y, Amon M, Martin I, Farhadi J, Ring A, Torio-Padron N, Schramm R, Rücker M, Junker D, Häufel JM, Carvalho C, Heberer M, Germann G, Vollmar B, Menger MD**. Angiogenesis in tissue engineering: breathing life into constructed tissue substitutes. *Tissue Eng* 12: 2093-2104, 2006.

41. **Laschke MW, Vollmar B, Menger MD**. Inosculation: connecting the life-sustaining pipelines. *Tissue Eng Part B Rev* 15: 455-465, 2009.

42. **Laschke MW, Vollmar B, Menger MD**. The dorsal skinfold chamber: window into the dynamic interaction of biomaterials with their surrounding host tissue. *Eur Cell Mater* 22: 147-164, 2011.

43. **Laschke MW, Kleer S, Scheuer C, Schuler S, Garcia P, Eglin D, Alini M, Menger MD**. Vascularisation of porous scaffolds is improved by incorporation of adipose tissue-derived microvascular fragments. *Eur Cell Mater* 24: 266-277, 2012.

44. **Laschke MW, Grässer C, Kleer S, Scheuer C, Eglin D, Alini M, Menger MD**. Adipose tissue-derived microvascular fragments from aged donors exhibit an impaired vascularisation capacity. *Eur Cell Mater* 28: 287-298, 2014.

45. **Laschke MW, Menger MD**. Adipose tissue-derived microvascular fragments: natural vascularization units for regenerative medicine. *Trends Biotechnol* 33: 442-448, 2015.

46. **Laschke MW, Menger MD**. Prevascularization in tissue engineering: Current concepts and future directions. *Biotechnol Adv 34*: 112-121, 2016a.

47. **Laschke MW, Menger MD**. The dorsal skinfold chamber: A versatile tool for preclinical research in tissue engineering and regenerative medicine. *Eur Cell Mater* 32: 202-215, 2016b.

48. **Lindenblatt N, Calcagni M, Contaldo C, Menger MD, Giovanoli P, Vollmar B**. A new model for studying the revascularization of skin grafts in vivo: the role of angiogenesis. *Plast Reconstr Surg* 122: 1669-1680, 2008.

49. **Lindenblatt N, Platz U, Althaus M, Hegland N, Schmidt CA, Contaldo C, Vollmar B, Giovanoli P, Calcagni M.** Temporary angiogenic transformation of the skin graft vasculature after reperfusion. *Plast Reconstr Surg* 126: 61-70, 2010.

50. **Lugo LM, Lei P, Andreadis ST**. Vascularization of the dermal support enhances wound re-epithelialization by in situ delivery of epidermal keratinocytes. *Tissue Eng Part A* 17: 665-675, 2011.

51. **MacNeil S**. Progress and opportunities for tissue-engineered skin. *Nature* 445: 874-880, 2007.

52. **Marino D, Luginbühl J, Scola S, Meuli M, Reichmann E**. Bioengineering dermo-epidermal skin grafts with blood and lymphatic capillaries. *Sci Transl Med* 6: 221ra14, 2014.

53. **Margolis DJ, Cromblehome T, Herlyn M, Cross P, Weinberg L, Filip J, Propert K**. Clinical protocol. Phase I trial to evaluate the safety of H5.020CMV.PDGF-b and limb compression bandage for the treatment of venous leg ulcer: trial A. *Hum Gene Ther* 15: 1003-1019, 2004.

54. **Matsusaki M, Fujimoto K, Shirakata Y, Hirakawa S, Hashimoto K, Akashi M**. Development of full-thickness human skin equivalents with blood and lymph-like capillary networks by cell coating technology. *J Biomed Mater Res A* 103: 3386-3396, 2015.

55. **McDaniel JS, Pilia M, Ward CL, Pollot BE, Rathbone CR**. Characterization and multilineage potential of cells derived from isolated microvascular fragments. *J Surg Res* 192: 214-222, 2014.

56. **Menger MD, Laschke MW, Vollmar B**. Viewing the microcirculation through the window: Some twenty years experience with the hamster dorsal skinfold chamber. *Eur Surg Res* 34: 83-91, 2002.

57. **Meruane MA, Rojas M, Marcelain K**. The use of adipose tissue-derived stem cells within a dermal substitute improves skin regeneration by increasing neoangiogenesis and collagen synthesis. *Plast Reconstr Surg* 130: 53-63, 2012.

58. **Michael S, Sorg H, Peck CT, Reimers K, Vogt PM**. The mouse dorsal skin fold chamber as a means for the analysis of tissue engineered skin. *Burns* 39: 82-88, 2013.

59. **Nakano M, Nakajima Y, Kudo S, Tsuchida Y, Nakamura H, Fukuda O**. Effect of autotransplantation of microvessel fragments on experimental random-pattern flaps in the rat. *Eur Surg Res* 30: 149-160, 1998.

60. **Nakano M, Nakajima Y, Kudo S, Tsuchida Y, Nakamura H, Fukuda O**. Successful autotransplantation of microvessel fragments into the rat heart. *Eur Surg Res* 31: 240-248, 1999.

61. **Nestle FO, Di Meglio P, Qin JZ, Nickoloff BJ**. Skin immune sentinels in health and disease. *Nat Rev Immunol* 9: 679-691, 2009.

62. **Novosel EC, Kleinhans C, Kluger PJ**. Vascularization is the key challenge in tissue engineering. *Adv Drug Deliv Rev* 63: 300-311, 2011.

63. **Nunes SS, Greer KA, Stiening CM, Chen HY, Kidd KR, Schwartz MA, Sullivan CJ, Rekapally H, Hoying JB**. Implanted microvessels progress through distinct neovascularization phenotypes. *Microvasc Res* 79: 10-20, 2010.

64. **O'Ceallaigh S, Herrick SE, Bluff JE, McGrouther DA, Ferguson MW**. Quantification of total and perfused blood vessels in murine skin autografts using a fluorescent double-labeling technique. *Plast Reconstr Surg* 117: 140-151, 2006.

65. **Okabe M, Ikawa M, Kominami K, Nakanishi T, Nishimune Y**. 'Green mice' as a source of ubiquitous green cells. *FEBS Lett* 407: 313-319, 1997.

66. **Paavonen K, Puolakkainen P, Jussila L, Jahkola T, Alitalo K**. Vascular endothelial growth factor receptor-3 in lymphangiogenesis in wound healing. *Am J Pathol* 156: 1499-1504, 2000.

67. **Pham C, Greenwood J, Cleland H, Woodruff P, Maddern G**. Bioengineered skin substitutes for the management of burns: a systematic review. *Burns* 33: 946-957, 2007.

68. **Pilia M, McDaniel JS, Guda T, Chen XK, Rhoads RP, Allen RE, Corona BT, Rathbone CR**. Transplantation and perfusion of microvascular fragments in a rodent model of volumetric muscle loss injury. *Eur Cell Mater* 28: 11-23, 2014.

69. **Reid RR, Said HK, Mogford JE, Mustoe TA**. The future of wound healing: pursuing surgical models in transgenic and knockout mice. *J Am Coll Surg* 199: 578-585, 2004.

70. **Reverdin JL**. Greffe epidermique. *Bull Soc Imperiale Chir Paris* 14: 493, 1869.

71. **Reckhenrich AK, Hopfner U, Krötz F, Zhang Z, Koch C, Kremer M, Machens HG, Plank C, Egaña JT**. Bioactivation of dermal scaffolds with a non-viral copolymer-protected gene vector. *Biomaterials* 32: 1996-2003, 2011.

72. **Ring A, Langer S, Schaffran A, Stricker I, Awakowicz P, Steinau HU, Hauser J**. Enhanced neovascularization of dermis substitutes via low-pressure plasma-mediated surface activation. *Burns* 36: 1222-1227, 2010.

73. **Rockson SG**. Current concepts and future directions in the diagnosis and management of lymphatic vascular disease. *Vasc Med* 15: 223-231, 2010.

74. **Romanovsky AA**. Skin temperature: its role in thermoregulation. *Acta Physiol (Oxf)* 210: 498-507, 2014.

75. **Rowan MP, Cancio LC, Elster EA, Burmeister DM, Rose LF, Natesan S, Chan RK, Christy RJ, Chung KK**. Burn wound healing and treatment: review and advancements. *Crit Care* 19: 243, 2015.

76. **Saaristo A, Tammela T, Timonen J, Yla-Herttuala S, Tukiainen E, Asko-Seljavaara S, Alitalo K**. Vascular endothelial growth factor-C gene therapy restores lymphatic flow across incision wounds. *FASEB J* 18: 1707-1709, 2004.

77. **Saaristo A, Tammela T, Farkkilā A, Kärkkäinen M, Suominen E, Yla-Herttuala S, Alitalo K**. Vascular endothelial growth factor-C accelerates diabetic wound healing. *Am J Pathol* 169: 1080-1087, 2006.

78. **Schneider J, Biedermann T, Widmer D, Montano I, Meuli M, Reichmann E, Schiestl C**. Matriderm versus Integra: a comparative experimental study. *Burns* 35: 51-57, 2009.

79. **Schenck TL, Chávez MN, Condurache AP, Hopfner U, Rezaeian F, Machens HG, Egaña JT**. A full skin defect model to evaluate vascularization of biomaterials in vivo. *J Vis Exp* 90, 2014.

80. **Shepherd BR, Chen HY, Smith CM, Gruionu G, Williams SK, Hoying JB**. Rapid perfusion and network remodeling in a microvascular construct after implantation. *Arterioscler Thromb Vasc Biol* 24: 898-904, 2004.

81. **Shepherd BR, Hoying JB, Williams SK**. Microvascular transplantation after acute myocardial infarction. *Tissue Eng* 13: 2871-2879, 2007.

82. **Shevchenko RV, James SL, James SE**. A review of tissue-engineered skin bioconstructs available for skin reconstruction. *J R Soc Interface* 7: 229-258, 2010.

83. **Sen CK, Gordillo GM, Roy S, Kirsner R, Lambert L, Hunt TK, Gottrup F, Gurtner GC, Longaker MT**. Human skin wounds: a major and snowballing threat to public health and the economy. *Wound Repair Regen* 17: 763-771, 2009.

84. **Sorg H, Krueger C, Vollmar B**. Intravital insights in skin wound healing using the mouse dorsal skin fold chamber. *J Anat* 211: 810-818, 2007.

85. **Sorg H, Krueger C, Schulz T, Menger MD, Schmitz F, Vollmar B**. Effects of erythropoietin in skin wound healing are dose related. *FASEB J* 23: 3049-3058, 2009.

86. **Später T, Körbel C, Frueh FS, Nickels RM, Menger MD, Laschke MW**. Seeding density is a crucial determinant for the in vivo vascularisation capacity of adipose tissue-derived microvascular fragments. *Eur Cell Mater* 34: 55-69, 2017.

87. **Später T, Frueh FS, Nickels RM, Menger MD, Laschke MW**. Prevascularization of collagen-glycosaminoglycan scaffolds: Stromal vascular fraction versus adipose tissue-derived microvascular fragments. *J Biol Eng* 12: 24, 2018.

88. **Strassburg S, Torio-Padron N, Finkenzeller G, Frankenschmidt A, Stark GB**. Adipose-derived stem cells support lymphangiogenic parameters in vitro. *J Cell Biochem* 117: 2620-2629, 2016.

89. **Tissiani LA, Alonso N**. A Prospective and controlled clinical trial on stromal vascular fraction enriched fat grafts in secondary breast reconstruction. *Stem Cells Int* 2016: 2636454, 2016.

90. **Toulon A, Breton L, Taylor KR, Tenenhaus M, Bhavsar D, Lanigan C, Rudolph R, Jameson J, Havran WL**. A role for human skin-resident T cells in wound healing. *J Exp Med* 206: 743-750, 2009.

91. **Tufaro AP, Buck DW 2nd, Fischer AC**. The use of artificial dermis in the reconstruction of oncologic surgical defects. *Plast Reconstr Surg* 120: 638-646, 2007.

92. **Utzinger U, Baggett B, Weiss JA, Hoying JB, Edgar LT**. Large-scale time series microscopy of neovessel growth during angiogenesis. *Angiogenesis* 18: 219-232, 2015.

93. **Wagner RC, Kreiner P, Barrnett RJ, Bitensky MW**. Biochemical characterization and cytochemical localization of a catecholamine-sensitive adenylate cyclase in isolated capillary endothelium. *Proc Natl Acad Sci U S A* 69: 3175-3179, 1972.

94. **Wagner RC, Matthews MA**. The isolation and culture of capillary endothelium from epididymal fat. *Microvasc Res* 10: 286-297, 1975.

95. **Wang X, You C, Hu X, Zheng Y, Li Q, Feng Z, Sun H, Gao C, Han C**. The roles of knitted mesh-reinforced collagen-chitosan hybrid scaffold in the one-step repair of full-thickness skin defects in rats. *Acta Biomater* 9: 7822-7832, 2013.

96. **Yan A, Avraham T, Zampell JC, Haviv YS, Weitman E, Mehrara BJ**. Adipose-derived stem cells promote lymphangiogenesis in response to VEGF-C stimulation or TGF-β1 inhibition. *Future Oncol* 7: 1457-1473, 2011.

97. **Zhao S, Li L, Wang H, Zhang Y, Cheng X, Zhou N, Rahaman MN, Liu Z, Huang W, Zhang C**. Wound dressings composed of copper-doped borate bioactive glass microfibers stimulate angiogenesis and heal full-thickness skin defects in a rodent model. *Biomaterials* 53: 379-391, 2015.

98. **Zimmermann S, Fakin RM, Giesen T, Giovanoli P, Calcagni M**. Stromal vascular fraction-enriched fat grafting for the treatment of symptomatic end-neuromata. *J Vis Exp* 129, 2017.

8. Acknowledgement

I would like to thank everyone who contributed to this work.

First, Professor Michael Menger and Professor Matthias Laschke for the unique opportunity to join their research group. Their constant support and input made my MD-PhD fellowship an outstanding experience with a significant impact on both professional and personal development. In particular, I would like to thank Professor Matthias Laschke for the ongoing collaboration. His extraordinary intellectual and personal skills have been the prerequisite for the present work and inspired me for many other research projects.

Furthermore, Thomas Später M.Sc. for the cooperation and friendship. His tireless effort in ad-MVF isolation and analysis of histological sections was indispensable.

Moreover, Doctor Emmanuel Ampofo and Doctor Nadine Wilhelm for interesting scientific discussions, hospitality and friendship, which made my Saarland experience unforgettable.

I would also like to thank Doctor Christina Körbel for photoacoustic imaging, Doctor Claudia Scheuer and Julia Parakenings for ad-MVF isolation, Alexander Hess for helping with intravital microscopic analyses, Ruth Nickels for flow cytometry and preparation of histological samples, Janine Becker and Caroline Bickelmann for the preparation of histological samples as well as all the co-workers of the animal facility for taking great care of my animals.

I would also like to thank my clinical mentors Professor Pietro Giovanoli, Privatdozent Maurizio Calcagni and Professor Nicole Lindenblatt for introducing me to the Homburg group and for training in hand surgery and reconstructive microsurgery.

Special thanks go to my friends Jonas Bühler, Doctor Pascal Ducommun, Doctor Thomas Wälchli and Doctor Philipp Honigmann who supported me during the research fellowship.

Finally, I would like to thank my parents Ruth and Hans-Peter, my sisters Stephanie and Seraina, my brothers-in-law Christian and Gert and my wife Anna for endless support during this project. Without their motivation and love I would not have been able to realize it.

9. Publications

9.1 Original Articles

Frueh FS, Kunz VS, Gravestock IJ, Held L, Haefeli M, Giovanoli P, Calcagni M. Primary flexor tendon repair in zones 1 and 2: Early passive mobilization versus controlled active motion. *J Hand Surg Am* 39: 1344-1350, 2014. (IF = 1.67)

Frueh FS, Palma AF, Raptis DA, Graf CP, Giovanoli P, Calcagni M. Carpal tunnel syndrome: Analysis of online patient information with the EQIP tool. *Chir Main* 34: 113-121, 2015. (IF = 0.44)

Braun BJ, Veith NT, **Frueh FS**, Klein M, Knopp W, Pohlemann T. [Salvage procedure for painful proximalisation of the 1st metacarpal after trapeziectomy using the Mini TightRope®]. *Handchir Mikrochir Plast Chir* 48: 300-305, 2016. (IF = 0.69)

Palma AF, Zuk G, Raptis DA, Franck S, Eylert G, **Frueh FS**, Guggenheim M, Shafighi M. Quality of information for women seeking breast augmentation in the Internet. *J Plast Surg Hand Surg* 50: 262-271, 2016. (IF = 0.79)

Frueh FS, Körbel C, Gassert L, Müller A, Gousopoulos E, Lindenblatt N, Giovanoli P, Laschke MW, Menger MD. High-resolution 3D volumetry versus conventional measuring techniques for the assessment of experimental lymphedema in the mouse hindlimb. *Sci Rep* 6: 34673, 2016. (IF = 4.26)

Frueh FS, Später T, Lindenblatt N, Calcagni M, Giovanoli P, Scheuer C, Menger MD, Laschke MW. Adipose tissue-derived microvascular fragments improve vascularization, lymphangiogenesis, and integration of dermal skin substitutes. *J Invest Dermatol* 137: 217-227, 2017. (IF = 6.45)

Frueh FS, Ho M, Schiller A, Ducommun P, Manoliu A, Andreisek G, Calcagni M, Giovanoli P. Magnetic resonance neurographic and clinical long-term results after Oberlin's transfer for adult brachial plexus injuries. *Ann Plast Surg* 78: 67-72, 2017. (IF = 1.54)

Später T, **Frueh FS**, Menger MD, Laschke MW. Potentials and limitations of Integra® flowable wound matrix seeded with adipose tissue-derived microvascular fragments. *Eur Cell Mater* 33: 268-278, 2017. (IF = 3.67)

Frueh FS, Später T, Scheuer C, Menger MD, Laschke MW. Isolation of murine adipose tissue-derived microvascular fragments as vascularization units for tissue engineering. *J Vis Exp* 122, 2017. (IF = 1.18)

Später T, Körbel C, **Frueh FS**, Nickels RM, Menger MD, Laschke MW. Seeding density is a crucial determinant for the in vivo vascularisation capacity of adipose tissue-derived microvascular fragments. *Eur Cell Mater* 34: 55-69, 2017. (IF = 3.67)

Müller A, Fries P, Jelvani B, Lux F, Rübe CE, Kremp S, Giovanoli P, Buecker A, Menger MD, Laschke MW, **Frueh FS**. Magnetic resonance lymphography at 9.4 T using a Gadolinium-based nanoparticle in rats: Investigations in healthy animals and in a hindlimb lymphedema model. *Invest Radiol* 52: 725-733, 2017. (IF = 6.22)

Später T, **Frueh FS**, Karschnia P, Menger MD, Laschke MW. Enoxaparin does not affect network formation of adipose tissue-derived microvascular fragments. *Wound Repair Regen* 26: 36-45, 2018. (IF = 2.95)

Später T, **Frueh FS**, Metzger W, Menger MD, Laschke MW. In vivo biocompatibility, vascularization, and incorporation of Integra® dermal regenerative template and flowable wound matrix. *J Biomed Mater Res B Appl Biomater* 106: 52-60, 2018. (IF = 3.19)

Frueh FS, Später T, Körbel C, Scheuer C, Simson AC, Lindenblatt N, Giovanoli P, Menger MD, Laschke MW. Prevascularization of dermal substitutes with adipose tissue-derived microvascular fragments enhances early skin grafting. *Sci Rep* 8: 10977, 2018. (IF = 4.12)

Später T, **Frueh FS**, Nickels RM, Menger MD, Laschke MW. Prevascularization of collagen-glycosaminoglycan scaffolds: Stromal vascular fraction versus adipose tissue-derived microvascular fragments. *J Biol Eng* 12: 24, 2018. (IF = 5.26)

9.2 Review Articles

Frueh FS, Calcagni M. [Collagenase - A revolution of Dupuytren's therapy]. *Ther Umsch* 71: 379-384, 2014.

Frueh FS, Calcagni M, Lindenblatt N. The hemi-hamate autograft arthroplasty in proximal interphalangeal joint reconstruction: A systematic review. *J Hand Surg Eur Vol* 40: 24-32, 2015. (IF = 2.04)

Frueh FS, Calcagni M, Giesen T, Giovanoli P, Harder Y. Das Management von Weichteilverletzungen im Extremitätentrauma: Die Rolle der Plastischen Chirurgie. *Praxis (Bern 1994)* 105: 1493-1501, 2016.

Frueh FS, Gousopoulos E, Rezaeian F, Menger MD, Lindenblatt N, Giovanoli P. Animal models in surgical lymphedema research - a systematic review. *J Surg Res* 200: 208-220, 2016. (IF = 2.19)

Frueh FS, Menger MD, Lindenblatt N, Giovanoli P, Laschke MW. Current and emerging vascularization strategies in skin tissue engineering. *Crit Rev Biotechnol* 37: 613-625, 2017. (IF = 5.24)

Frueh FS, Vogel P, Honigmann P. Irreducible dislocations of the proximal interphalangeal joint: Algorithm for open reduction and soft-tissue repair. *Plast Reconstr Surg Glob Open* 6: e1729, 2018.

Frueh FS, Sanchez-Macedo N, Calcagni M, Giovanoli P, Lindenblatt N. The crucial role of vascularization and lymphangiogenesis in skin reconstruction. *Eur Surg Res* 59: 242-254, 2018. (IF = 1.34)

9.3 Case Reports / Letters

Frueh FS, Vuille-dit-Bille RN, Raptis DA, Notter H, Muff BS. Perforated sigmoid diverticulitis in a lumbar hernia after iliac crest bone graft - a case report. *BMC Surg* 14: 46, 2014. (IF = 1.47)

Honigmann P, **Frueh FS**. Letter about a published paper. *J Hand Surg Eur* 43: 451, 2018. (IF = 2.65)

9.4 Citable Abstracts

Frueh FS, Kunz VS, Gravestock IJ, Held L, Haefeli M, Giovanoli P, Calcagni M. Outcome results of primary flexor tendon repair in Zone 1 and 2: Early passive mobilisation versus controlled active motion (CAM). *J Hand Surg Eur* 43: S21-S22, 2014. (IF = 2.04)

Palma AF, **Frueh FS**, Haefeli M, Graf C, Raptis DA, Guggenheim M, Giovanoli P, Calcagni M. Carpal Tunnel Syndrome - Is the Internet providing comprehensive patient information? *J Hand Surg Eur Vol* 43: S11-S12, 2014. (IF = 2.04)

Palma AF, **Frueh FS**, Raptis DA, Graf C, Calcagni M. Carpal Tunnel Syndrome - Is the Internet providing comprehensive patient information? *Swiss Med Wkly* 145: Supplementum 210, 2015. (IF = 1.55)

Frueh FS, Später T, Lindenblatt N, Calcagni M, Giovanoli P, Scheuer C, Menger MD, Laschke MW. Adipose tissue-derived microvascular fragments improve vascularization, lymphangiogenesis, and integration of dermal skin substitutes. *Eur Surg Res* 57: 330-331, 2016. (IF = 1.38)

Gassert L, **Frueh FS**, Körbel C, Müller A, Gousopoulos E, Lindenblatt N, Giovanoli P, Laschke MW, Menger MD. 3D volumetry versus conventional volumetry techniques for the assessment of experimental lymphedema in the mouse hindlimb. *Eur Surg Res* 57: 308-309, 2016. (IF = 1.38)

Später T, **Frueh FS**, Metzger W, Menger MD, Laschke MW. In vivo biocompatibility, vascularization, and incorporation of Integra® dermal regenerative template and flowable wound matrix. *Eur Surg Res* 57: 321, 2016. (IF = 1.38)

Später T, Körbel C, **Frueh FS**, Nickels RM, Menger MD, Laschke MW. Seeding density is a crucial determinant for the in vivo vascularization capacity of adipose tissue-derived microvascular fragments. *Eur Surg Res* 58: 322, 2017. (IF = 1.34)

Fritz T, Ducommun P, Hug U, Pohlemann T, Calcagni M, Menger MD, Metzger W, **Frueh FS**. Histological, immunohistochemical and microstructural assessment of flexor tendon grafts for pulley reconstruction: A cadaver study. *J Hand Surg Eur Vol* 43: SS169-SS170, 2018. (IF = 2.65)

Fries P, Müller A, Lux F, Tillement O, **Frueh FS**, Kremp S, Bücker A. Experimentelle MR-Lymphografie mittels eines Gd-basierten Nanopartikels – Ergebnisse einer präklinischen Machbarkeitsstudie. *Fortschr Röntgenstr* 190: S6-S7, 2018. (IF = 1.64)

9.5 Non-citable Abstracts

Frueh FS, Kunz VS, Gravestock IJ, Held L, Haefeli M, Giovanoli P, Calcagni M. Primary flexor tendon repair in zones 1 and 2: Early passive mobilization versus controlled active motion. *47. Jahreskongress Schweizerische Gesellschaft für Handchirurgie*, Biel (CH), 2013.

Frueh FS, Palma AF, Raptis DA, Graf CP, Giovanoli P, Calcagni M. Carpal Tunnel Syndrome - Is the Internet providing comprehensive patient information? *48. Jahreskongress Schweizerische Gesellschaft für Handchirurgie*, Thun (CH), 2014.

Frueh FS, Calcagni M, Lindenblatt N. The hemi-hamate autograft arthroplasty in proximal interphalangeal joint reconstruction: A systematic review. *48. Jahreskongress Schweizerische Gesellschaft für Handchirurgie*, Thun (CH), 2014.

Frueh FS, Giesen T, Giovanoli P, Calcagni M. Arterialisierung des venösen Systems als Ultima Ratio bei ischämischen Händen von Sklerodermie-Patienten. *56. Symposium Deutschsprachige Arbeitsgemeinschaft für Handchirurgie*, Aarau (CH), 2015.

Frueh FS, Ho M, Schiller A, Ducommun P, Manoliu A, Andreisek G, Calcagni M, Giovanoli P. Magnetic resonance neurographic and clinical long-term results after Oberlin's transfer for adult brachial plexus injuries. *49. Jahreskongress Schweizerische Gesellschaft für Handchirurgie*, Fribourg (CH), 2015.

Frueh FS, Später T, Lindenblatt N, Calcagni M, Giovanoli P, Scheuer C, Menger MD, Laschke MW. Adipose tissue-derived microvascular fragments improve vascularization, lymphangiogenesis, and integration of dermal skin substitutes. *50. Jahreskongress Schweizerische Gesellschaft für Handchirurgie*, Genf (CH), 2016.

Frueh FS, Später T, Lindenblatt N, Calcagni M, Giovanoli P, Scheuer C, Menger MD, Laschke MW. Adipose tissue-derived microvascular fragments improve vascularization, lymphangiogenesis, and integration of dermal skin substitutes. *25. Wissenschaftliche Jahrestagung der Saarländischen Chirurgenvereinigung*, Kirkel (D), 2017.

Frueh FS, Später T, Körbel C, Scheuer C, Simson AC, Lindenblatt N, Giovanoli P, Menger MD, Laschke MW. Prevascularization of Integra® with adipose tissue-derived microvascular fragments enhances early skin grafting. *53. Jahrestagung der Schweizerischen Gesellschaft für Plastische, Rekonstruktive und Ästhetische Chirurgie*, St. Moritz (CH), 2017.

Müller A, Fries P, Jelvani B, Lux F, Rübe CE, Kremp S, Giovanoli P, Buecker A, Menger MD, Laschke MW, **Frueh FS**. Magnetic resonance lymphography at 9.4 T using a Gadolinium-based nanoparticle in rats: Investigations in healthy animals and in a hindlimb lymphedema model. *53. Jahrestagung der Schweizerischen Gesellschaft für Plastische, Rekonstruktive und Ästhetische Chirurgie*, St. Moritz (CH), 2017.

Frueh FS, Körbel C, Gassert L, Müller A, Gousopoulos E, Lux F, Rübe CE, Kremp S, Jelvani B, Lindenblatt N, Giovanoli P, Laschke MW, Menger MD. Experimentelles Lymphödem im Nagermodell - Analyse von Volumetriemethoden und Nanopartikel-basierter interstitieller MR-Lymphographie. *41. Jahreskongress der Deutschen Lymphologie-Gesellschaften*, Bad Soden (D), 2017.

Frueh FS, Körbel C, Häfeli M, Honigmann P. Systematic review and outcome analyses of computer-assisted corrective osteotomy in hand surgery. *51. Jahreskongress Schweizerische Gesellschaft für Handchirurgie*, Thun (CH), 2017.

Frueh FS, Vogel P, Honigmann P. Irreducible dislocations of the proximal interphalangeal joint: Algorithm for open reduction and soft-tissue repair. *51. Jahreskongress Schweizerische Gesellschaft für Handchirurgie*, Thun (CH), 2017.

Frueh FS, Vogel P, Honigmann P. Irreducible dislocations of the proximal interphalangeal joint: Algorithm for open reduction and soft-tissue repair. *53. Annual Meeting Société Française de Chirurgie de la Main*, Paris (F), 2017.

Frueh FS, Jelvani B, Körbel C, Scheuer C, Lindenblatt N, Giovanoli P, Harder Y, Menger MD, Laschke MW. Analyse des lymphangiogenen Potentials vaskularisierter Lymphknotenlappen in einem axillären Ischämie-Reperfusions-Modell an Ratten. *2. Forschungsakademie Deutschsprachige Arbeitsgemeinschaft für Mikrochirurgie*, Erlangen (D), 2018.

Frueh FS, Später T, Körbel C, Scheuer C, Simson AC, Lindenblatt N, Giovanoli P, Menger MD, Laschke MW. Prevascularization of dermal substitutes with adipose tissue-derived microvascular fragments enhances early skin grafting. *27. Meeting European Association of Plastic Surgeons*, Madrid (E), 2018.

Später T, **Frueh FS**, Karschnia P, Menger MD, Laschke MW. Enoxaparin does not affect network formation of adipose tissue-derived microvascular fragments. *26. Wissenschaftliche Jahrestagung der Saarländischen Chirurgenvereinigung*, Kirkel (D), 2018.

Frueh FS, Jelvani B, Körbel C, Scheuer C, Lindenblatt N, Giovanoli P, Harder Y, Menger MD, Laschke MW. Analyse des lymphangiogenen Potentials vaskularisierter Lymphknotenlappen in einem axillären Ischämie-Reperfusions-Modell an Ratten. *40. Jahrestagung Deutschsprachige Arbeitsgemeinschaft für Mikrochirurgie*, Lugano (CH), 2018.

Frueh FS, Ducommun P, Hug U, Pohlemann T, Calcagni M, Menger MD, Metzger W, Fritz T. Histological and microstructural assessment of tendon grafts for pulley reconstruction - a cadaver study. *52. Jahreskongress Schweizerische Gesellschaft für Handchirurgie*, St. Gallen (CH), 2018.

9.6 Awards

2016   Greatest Future Clinical Application - Award Schweizerische Gesellschaft für Handchirurgie (SGH)

for the paper "Adipose tissue-derived microvascular fragments improve vascularization, lymphangiogenesis, and integration of dermal skin substitutes"

2018   Wissenschaftspreis Deutschsprachige Arbeitsgemeinschaft für Mikrochirurgie (DAM)

for the paper "Analyse des lymphangiogenen Potentials vaskularisierter Lymphknotenlappen in einem axillären Ischämie-Reperfusions-Modell an Ratten"

2019   Travel Award Federation of European Societies for Surgery of the Hand (FESSH)

10. Curriculum Vitae

Personal Data

Name
Florian Samuel Früh, MD

Date of Birth
May 31st 1983

Education

Medical School	University of Zürich	2003 - 2009
Hand Surgery Specialist (FMH)	**Bülach Hospital** **University Hospital Zürich** **Cantonal Hospital Baselland**	2010 - 2017

Postgraduate

Resident General Surgery	**Bülach Hospital** Brigitte Muff, MD	2010 - 2012
Resident Plastic Surgery Hand Surgery	**University Hospital Zürich** Pietro Giovanoli, MD Maurizio Calcagni, MD	2012 - 2015
MD-PhD - Fellowship Experimental Surgery	**Saarland University** Michael D. Menger, MD Matthias W. Laschke, MD PhD	2015 - 2019
Faculty Hand Surgery	**Cantonal Hospital Baselland** Philipp Honigmann, MD	2017 - 2018
Faculty Plastic Surgery Hand Surgery	**University Hospital Zürich** Pietro Giovanoli, MD Maurizio Calcagni, MD	2018 - present

Certificates

MD	Zürich, Switzerland	2010
EBHS (FESSH)	Brescia, Italy	2015
ECFMG (USMLE)	Los Angeles, USA	2017